“The cuprizone model and multiple sclerosis: disparities and similarities“

Von der Fakultät für Mathematik, Informatik und Naturwissenschaften

der RWTH Aachen University zur Erlangung des akademischen Grades eines

Doktors der Naturwissenschaften genehmigte Dissertation

vorgelegt von

Priv. Doz. Dr. med. Markus Kipp

aus Oberndorf am Neckar

Berichter: Universitätsprofessor Dipl. Ing. Dr. Werner Baumgartner

Universitätsprofessor Dr. hum. biol. Cordian Beyer

Tag der mündlichen Prüfung: 22. August 2011

Diese Dissertation ist auf den Internetseiten der Hochschulbibliothek online verfügbar.

SUMMARY 5

(ENGLISH) 5
(GERMAN) 6

GENERAL INTRODUCTION 9

1. MULTIPLE SCLEROSIS 9
1.1 GENERAL REMARKS 9
1.2 CLINICAL ASPECTS OF THE DISEASE 9
1.3 AETIOLOGY 9
1.4 THERAPEUTIC OPTIONS 10
1.5 RELEVANT ANIMALS MODELS IN MS RESEARCH 10
1.6 NEUROPATHOLOGY 11
1.7 GREY MATTER PATHOLOGY IN MULTIPLE SCLEROSIS 13
2. THE TOXIC CUPRIZONE DEMYELINATION MODEL 14
3. REMYELINATION IN MULTIPLE SCLEROSIS 15
4. AIMS AND SCOPE OF THE STUDY 16

MATERIALS AND METHODS 17

1. ANIMALS AND DISEASE INDUCTION 17
2. TISSUE PREPARATION 17
3. MULTIPLE SCLEROSIS MATERIAL 17
4. IMMUNOHISTOCHEMISTRY 18
5. HISTOCHEMISTRY 18
6. ELECTRON-MICROSCOPY AND SEMI-THIN SECTIONS 19
7. IMMUNOFLOURESCENCE DOUBLE LABELLING 19
8. SCORING OF DEMYELINATION AND QUANTIFICATION OF CELL NUMBER 19
9. GENE EXPRESSION ANALYSIS 20
10. AFFYMETRIX GENECHIP® 22
11. TRANSFECTION EXPERIMENTS 23
12. WESTERN BLOT ANALYSIS 23
13. STATISTICAL ANALYSIS 23

RESULTS 24

CHAPTER 1: THE HIPPOCAMPUS AND BASAL-GANGLIA COMPLEX ARE AFFECTED IN THE CUPRIZONE MODEL AND MULTIPLE SCLEROSIS 24
1.1 CUPRIZONE-TREATMENT INDUCES DEMYELINATION OF THE HIPPOCAMPUS 24
1.2 INFLAMMATION IS MOST PRONOUNCED IN DEMYELINATED HIPPOCAMPAL WHITE MATTER STRUCTURES 26
1.3 COMPARISON OF HIPPOCAMPAL LESIONS IN THE CUPRIZONE MODEL AND MULTIPLE SCLEROSIS 27
1.4 BASALGANGLIA DEMYELINATION AND INFLAMMATION 28
CHAPTER 2: REGION-SPECIFIC LOCAL BRAIN RESPONSES ACCOUNT FOR REGIONAL DIFFERENCES IN CUPRIZONE-INDUCED DEMYELINATION 30
2.1 THE HIPPOCAMPAL FIMBRIA REGION IS RESISTANT TO CUPRIZONE INTOXICATION DESPITE MICROGLIOSIS 30
2.2 REGION SPECIFIC INFLAMMATION DETERMINES DEMYELINATION IN THE CUPRIZONE MODEL 30
CHAPTER 3: INFLAMMATORY RESPONSE DEPENDS ON EXTEND OF MYELIN LOSS IN EXPERIMENTAL DEMYELINATION AND MULTIPLE SCLEROSIS TYPE 1 LESIONS 33
3.1 CORTICAL GREY MATTER DEMYELINATION IS PROMINENT IN THE CUPRIZONE MODEL 33

3.2 MAGNITUDE OF MYELIN LOSS WITHIN THE CORTICAL GREY MATTER OF CUPRIZONE-TREATED MICE 33
3.3 DEMYELINATION IS PARALLELED BY OLIGODENDROCYTE LOSS 35
3.4 MICROGLIA AND ASTROCYTE RESPONSE ARE MAINLY DETERMINED BY MYELIN DEBRIS 35
3.5 MAGNITUDE OF MICROGLIA ACTIVATION IN TYPE 1 MULTIPLE SCLEROSIS LESIONS DEPENDS ON LESION ACTIVITY 38
CHAPTER 4: BRAIN LIPID BINDING PROTEIN EXPRESSION IN ACTIVATED ASTROCYTES: POTENTIAL TARGET FOR REMYELINATION THERAPY 42
4.1 REMYELINATION IS LIMITED AFTER PROLONGED CUPRIZONE EXPOSURE DESPITE THE PRESENCE OF OLIGODENDROCYTE PROGENITOR CELLS 43
4.2 REMYELINATION APPEARS TO BE LIMITED DUE TO THE ABSENCE OF PRO-MYELINATION FACTORS 43
4.3 INFLAMMATORY RESPONSE IS CRITICAL FOR ENDOGENOUS REMYELINATION 45
4.4 VALIDATION OF AFFYMETRIX GENECHIP® ANALYSIS 48
4.5 INFLAMMATORY CELL COMPOSITION DIFFERS BETWEEN ACUTE AND CHRONIC LESIONS 49
4.6 $GFAP^+$ ASTROCYTES STRONGLY EXPRESS THE RADIAL GLIA CELL MARKER BLBP IN ACUTELY BUT NOT CHRONICALLY DEMYELINATED LESIONS 51
4.7 EXPRESSION OF BLBP IN ACTIVATED $GFAP^+$ ASTROCYTES STRONGLY CORRELATES WITH THE PRESENCE OF $OLIG2^{STRONG+}$ OLIGODENDROCYTE PROGENITOR CELLS IN THE CUPRIZONE MODEL 53
4.9 NUMBER OF BLBP-EXPRESSING ASTROCYTES IN HUMAN MS LESIONS DECLINES WITH DISEASE DURATION 56
4.10 EXPRESSION OF BLBP IN U87 ASTROCYTOMA CELLS REGULATES FGF2, PDGF-AA AND SPP1 BUT NOT IGF1 MRNA EXPRESSION 59

DISCUSSION 60

1. THE CUPRIZONE MODEL AS A TOOL TO STUDY DEMYELINATION 60
2. MECHANISM OF CUPRIZONE-INDUCED DEMYELINATION 62
3. WHAT DETERMINES MICROGLIA ACTIVATION? 62
4. THE CUPRIZONE MODEL AS A TOOL TO STUDY REMYELINATION 64
5. IDENTIFICATION OF ONGOING REMYELINATION 65
6. RELEVANCE OF INFLAMMATION FOR REMYELINATION 66
7. ASTROGLIA: GENERAL REMARKS 67
8. BLBP EXPRESSION IN ASTROCYTES 68
9. POSSIBLE ROLE OF BLBP FOR ASTROCYTE-MEDIATED OLIGODENDROCYTE MATURATION 69

REFERENCES 70

LIST OF PUBLICATIONS 75

RESEARCH ARTICLES 75
REVIEW ARTICLES 77

CURRICULUM VITAE (DEUTSCH) 78

APPENDIX 79

APPENDIX 1: TRANSCARDIAL PERFUSION OF MICE 79
APPENDIX 2: PARAFFIN-EMBEDDING OF MICE TISSUE SAMPLES 79
APPENDIX 3: IMMUNOHISTOCHEMISTRY 80
APPENDIX TABLE 1: CLINICAL DETAILS OF PATIENTS (CHAPTER 3) 81
APPENDIX TABLE 2: CLINICAL DETAILS OF PATIENTS (CHAPTER 4) 82
APPENDIX TABLE 3: LIST OF ANTIBODIES 83
APPENDIX TABLE 4: LIST OF PRIMERS 84

Summary

(English)

Multiple sclerosis (MS) is a chronic, inflammatory and demyelinating disorder of the central nervous system. Although demyelination is still a characteristic entity, it has become increasingly apparent in recent years that substantial axonal destruction and neuronal loss are equally important features. The frequent involvement of grey matter structures has received new impetus. Studies on the pathogenesis of grey matter lesions suggest that its underlying disease mechanisms are unique. Less marked microglia activation in grey compared to white matter lesions is obvious but underlying mechanisms are poorly understood. Adequate animal models are a likewise powerful and irreplaceable tool to study disease pathogenesis. In order to serve as a useful model, it should be similar in its aetiology or phenotype. The recognition of the importance of grey matter pathology in MS did lead to the desire for animal models that display grey matter damage. Within the scope of the presented thesis, I characterized the toxic cuprizone model with a special focus on grey matter pathology. This work is not confined to descriptive changes but makes a comparison between the model itself and MS. In recent years the contribution of innate immune cells in mediating MS pathogenesis is being appreciated. We were able to show that histopathological hallmarks of MS are closely mirrored by the cuprizone model. Furthermore, our studies clearly demonstrate that the magnitude of microglia activation is related to the amount of myelin debris during a demyelination event. Thus, the lower inflammatory infiltrate of grey matter lesion is not related to a unique grey matter cytoarchitecture that makes it more resistant to inflammation. Differences in myelination account for observed regional differences.

The second part of this thesis deals with one of the most effective repair mechanisms in the central nervous system, i.e. remyelination. A better understanding of the remyelination processes in MS and possible reasons for its failure is required. We created lesions with either robust or impaired endogenous remyelination capacity. Lesions were analyzed for mRNA expression levels by gene-chip arrays. One finding was the predominance of immune and stress response factors in the group of genes which were classified as remyelination-supporting factors. We further demonstrate that lesions with impaired remyelination capacity show weak expression of the radial-glia cell marker brain lipid binding protein (BLBP) whereas expression of this marker protein is high in lesions with marked remyelination. The expression of BLBP in activated astrocytes correlates with the presence of oligodendrocyte progenitor cells. Highest numbers of BLBP-expressing astrocytes were evident in lesions of early MS whereas significantly less are present in tissue samples from patients with long disease duration. Transfection experiments show that BLBP regulates growth factor expression in U87 astrocytoma cells. In conclusion, we provide evidence that expression of BLBP in activated astrocytes orchestrates remyelination.

(German)

Die Multiple Sklerose (MS) ist eine chronisch entzündliche Entmarkungserkrankung des Zentralen Nervensystems. Obwohl der Verlust der Myelinscheide auch heute noch ein zentraler Bestandteil der pathologischen Diagnosestellung darstellt zeigen sich auch Schäden im Bereich der grauen Substanz, die Nervenzellkörper enthält. Das Fortschreiten der Behinderung der Patienten hängt wesentlich von der Schädigung dieser grauen Substanz ab. Es wird vermutet, dass sich die zu Grunde liegenden Mechanismen der Gewebedestruktion in weißer und grauer Substanz unterscheiden. Die Entzündungsherde in der grauen Substanz sind meist weniger stark ausgeprägt.

Tiermodelle sind unersetzbare Werkzeuge zum erforschen neuer therapeutischer Ansätze. Vor allem der „graue" Aspekt der MS wurde bisher in Tiermodellen nur unzureichend untersucht. Im Rahmen der vorgelegten Arbeit charakterisierten wir das sog. „Cuprizone" MS Modell. Sowohl die Beteiligung der grauen Substanz als auch regionale Unterschiede der Mikroglia-Aktivierung standen im Mittelpunkt meiner Untersuchungen. Des Weiteren wurden vergleichende Studien zur humanen Pathologie durchgeführt. Wir können zeigen, dass wesentliche Aspekte bei MS durch das Cuprizone Tiermodell repräsentiert werden. Die gängige Vermutung, dass geringer ausgeprägte Entzündungsherde der grauen Substanz auf zytoarchitektonische Besonderheiten zurück zu führen sind konnten teilweise widerlegt werden. Die Menge an anfallenden Myelin Abbauprodukten im Rahmen einer akuten Demyelinisierung scheinen vielmehr eine wichtige Rolle zu spielen.

Zugrundeliegende Mechanismen des Wiederaufbaus von Markscheiden nach Demyelinisierung ist ein weiterer Schwerpunkt dieser Arbeit. Axonale Protektion ist eine der großen Herausforderungen bei der Behandlung demyelinisierender Erkrankungen, allen voran bei chronischen Verlausformen der MS. Remyelinisierung spielt in diesem Zusammenhang eine entscheidende Rolle. Es handelt sich hierbei um einen höchst effektiven Reparaturmechanismus des Zentralen Nervensystems der aus noch nicht geklärter Ursache bei MS Patienten im Krankheitsverlauf zum Erliegen kommt. In unseren Studien benutzten wird das toxische Cuprizone Demyelinisierungsmodell. Ein entscheidender Vorteil dieses Modells besteht in der Möglichkeit Läsionen mit und ohne endogener Remyelinisierungskapazität generieren zu können. Mit Hilfe der Affymetrix Array Technologie konnten wir etliche Faktoren identifizieren, die im Rahmen des Aufbaus entmarkter Axone von Bedeutung sind. Unsere Ergebnisse deuten darauf hin, dass ruhende Astrozyten im Rahmen der Demyelinisierung zu radialen-Glia ähnlichen Zellen de-differenzieren, um dann im Prozess der Remyelinisierung eine entscheidende Rolle zu spielen. Die Expression von Fettsäure-bindenden Proteinen wie BLBP scheint wichtig. Sowohl im Tiermodell als auch bei MS korreliert das BLBP Expressionsniveau positiv mit der Remyelinisierungspotenz. Durch stabile Transfektion konnten wir ausserdem aufzeigen, dass BLBP direkt an der Expression verschiedener Wachstumsfaktoren von Astrozyten beteiligt ist. Dieser Teil der vorgelegten Arbeit leistet einen wesentlichen Beitrag zu einem besseren Verständnis der Rolle von Astrozyten bei Remyelinisierung.

Abbreviations

AA	arachidonic acid
AD	Alexander disease
AQP4	aquaporin-4
BBB	blood-brain barrier
BCA	bicinchoninic acid
BLBP	brain lipid binding protein
CC	corpus callosum
CNPase	2',3'-cyclic nucleotide 3' phosphodiesterase
CNS	central nervous system
DHA	docosahexaenoic acid
EAE	experimental autoimmune encephalomyelitis
EBV	Epstein-Barr-Virus
FABP	fatty acid binding protein
FCS	fetal calf serum
FGF2	fibroblast growth factor 2
Fig(s)	figure(s)
GFAP	glial fibrillary acidic protein
H&E	hematoxylin and eosin
HLA	human leukocyte antigen
HPRT	hypoxanthine phosphoribosyltransferase 1
IHC	immunohistochemistry
LFB/PAS	Luxol Fast Blue and Periodic Acid Schiff
MAG	myelin-associated glycoprotein
MOBP	myelin-associated oligodendrocyte basic protein
MOG	myelin oligodendrocyte glycoprotein
MRI(s)	magnetic resonance imaging(s)
MS	multiple sclerosis
NAGM	normal-appearing grey matter
NAWM	normal-appearing white matter
NMO	neuromyelitis optica
OPC	oligodendrocyte progenitor cell
PDGFα	platelet-derived growth factor alpha polypeptide
PLP	proteolipid protein (myelin) 1
pMcx	primary somato-motor cortex
PPAR	peroxisome proliferator-activated receptor
PP-MS	primary progressive multiple sclerosis

PPWM	peri-plaque white matter
pScx	primary somato-sensory cortex
PUFA	polyunsaturated fatty acid
ROI	region of interest
RR-MS	relapsing-remitting multiple sclerosis
rtPCR	Reverse-transcription polymerase chain reaction
sec	seconds
SEM	standard error of the mean
SP-MS	secondary progressive multiple sclerosis
SPP1	osteopontin
TNFα	tumor necrosis factor-α
wks	weeks

General Introduction

1. Multiple sclerosis

1.1 General remarks

Multiple sclerosis (MS), a chronic inflammatory and demyelination disease, was first indentified as a separate neurological disorder by the French neurologist Jean-Martin Charcot, and is the most common disorder of the central nervous system (CNS) in young adults. Brain inflammation is associated with lesions appearing typically in plaques within the white matter. Recent histopathological studies, however, convincingly show that grey matter regions are equally affected. Women are affected more often than men [1]. The disease typically becomes clinically apparent between the ages of 20 and 40 years, although, it can begin either earlier or later in life. In Canada, Europe and the United States the prevalence ranges from 100-200 cases per 100,000 population. MS classically starts with visual problems or tingling sensations, however, due to the chronic nature of this disease, many patients develop other deficiencies such as impairment of motor functions, impairment of cognitive functions or an imbalance of the autonomic nervous system [2].

1.2 Clinical aspects of the disease

MS appears in several courses with new symptoms either in discrete episodes (relapsing remitting form) or slowly accumulating over time (progressive form). Most patients are first diagnosed with relapsing–remitting MS (RR-MS). This disease stage is characterized by self-limited attacks of neurological dysfunction. Attacks develop acutely, evolving over days to weeks. Over the next several weeks to months, the majority of patients experience a recovery of function that is often, but not always, complete. In between attacks the patient is neurologically and symptomatically stable. At later disease stages, most patients enter the secondary-progressive stage. This second clinical course, secondary progressive MS (SP-MS), begins as RR-MS but, at some point, the attack rate is reduced and the course becomes characterized by a steady deterioration in function, unrelated to acute attacks. This type of MS, which ultimately develops in approximately 80% of RR-MS patients, causes the greatest amount of irreversible neurological disability. Primary progressive MS (PP-MS) affects about 15% of people diagnosed with MS. It is called this because from the first (primary) symptoms it is progressive. Symptoms gradually get worse over time, rather than appearing as sudden attacks (relapses) [1-3].

1.3 Aetiology

Although the actual cause of MS remains to be elucidated, it is thought that genetic environmental factors contribute to the development of the disease. The genetic contribution is mainly restricted to the human leukocyte antigen (HLA) region. Heterozygosity or homozygosity for the HLA-

DRB1*1501 allele, for example, increase the susceptibility of MS by 3.4-fold or 7.5-fold respectively [4]. Non-HLA genetic risk factors are polymorphisms in the interleukin-7 receptor gene [5], in the interleukin-2 receptor gene [6] or in the 3' untranslated region of the interleukin-23 gene [7]. Another important factor appears to be certain environmental factors such as sunlight exposure, infections and smoking. The higher incidence of MS in countries more distant from the equator supports the idea that sunlight somehow influences the development of MS. In addition, studies with identical twins showed that higher exposure during childhood decreases the risk of getting MS [8]. This effect might be attributed to vitamin D. As shown by Munger et al. and others, high circulating levels of vitamin D were associated with a lower risk of MS [9, 10]. Another environmental factor that has been implicated in the aetiology of MS is the exposure to microbial or viral infections, such as Epstein-Barr virus (EBV). Almost all MS patients are seropositive for EBV and the risk to develop MS is higher in persons with a symptomatic EBV-infection or in people with high titres of anti-EBV antibody [11]. The idea that an infection agent could be linked to MS pathogenesis arose from studies where researchers have discovered epidemics of MS. There were four outbreaks in the Faroe Islands over a 40 year period after World War II. Interestingly, there were almost no reported cases of MS among residents of the Faroe Islands before 1943. Since the islands were occupied by British troops, researchers believe the soldiers unknowingly brought a virus or bacteria with them during their occupation. But this theory has not been definitely proven, just like no other virus has been proven to cause MS.

1.4 Therapeutic options

For a long period, MS therapy was restricted to the acute treatment of severe relapses using immunosuppressive drugs, basically the corticosteroide (methyl)-prednisolone. Corticosteroids can decrease the inflammatory response by dampening the inflammatory cytokine cascade, inhibiting the activation of T cells, decreasing the extravasation of immune cells into the CNS, facilitating the apoptosis of activated immune cells, and, indirectly, by decreasing the cytotoxic effects of nitric oxide and tumor necrosis factor-α (TNFα) [12]. Other therapeutic options in MS are the so called "disease-modifying agents". These drugs are prescribed to decrease the amount of clinical-detectable relapses during the relapsing phase of the disease and thus "modify" the clinical disease course. It is noteworthy that while the disease modifying therapies help RR-MS patients they are not effective for PP-MS patients [13], suggesting that in progressive disease, irrespective of being SP-MS or PP-MS, autoimmunity plays a minor role.

1.5 Relevant animals models in MS research

Animal models play an important role in the investigation of fundamental disease mechanism as well as in testing the efficacy of novel compounds or therapeutic regimens for use in MS. Since the histopathological hallmark of MS is loss of the nerve's myelin sheath, i.e. demyelination, destruction

of myelin and oligodendrocyte loss are key features of most animal models used in the context of MS research. Demyelination in the CNS can be induced by viruses [14], chemicals [3, 15], or by sensitization with certain CNS proteins resulting in experimental autoimmune encephalomyelitis (EAE). Recently, spontaneous EAE models have become available by generating transgenic mice with myelin-specific T cell receptors and/or immunoglobulins directed against myelin antigens [16].

1.6 Neuropathology

Post-mortem tissue is widely used to study which molecular and cellular mechanisms are involved in the development of MS lesions. The histopathological hallmarks of the lesion are inflammation, demyelination and axonal degeneration. Using general histological methods such as haematoxylin and eosin (H&E) or Kluver-Barrera/luxol fast blue (LFB) stain in combination with immunohistochemistry (IHC) for myelin and human leukocyte antigen (HLA)-DR antigens (such as anti-LN3 antibodies), lesions can be classified into several stages. The lesion classification used in this thesis is that of Bö and Trapp, modified by De Groot and van der Valk [17]. According to the distribution of inflammatory cells and the presence or absence of myelin, five lesion stages can be discriminated:

- Pre-active: the white matter contains activated microglial cells (strongly positive for HLA-DR), however, there is no demyelination (figs. 1A/B).
- Active demyelinating: the white matter area is hypercellular due to macrophages and/or microglia which are phagocytosing myelin sheaths, giving them a so called “foamy” appearance (fig. 1D). The presence of granules within macrophages that stain positive for particular myelin antigens, such as myelin associated glycoprotein (MAG) or proteolipid protein (PLP), or stain positive for chemical stains, such as LFB, indicate recent phagocytosis.
- Chronic active: the lesion contains a hypocellular centre (fig. 1G) and a hypercellular rim (fig. 1F) with myelin-containing macrophages indicating ongoing demyelination at the lesion edge and complete demyelination with cessation of inflammatory processes in the centre of the lesion.
- Chronic inactive: the lesion is hypocellular although some residual inflammatory activity might be present at the borders of the lesion (not shown).

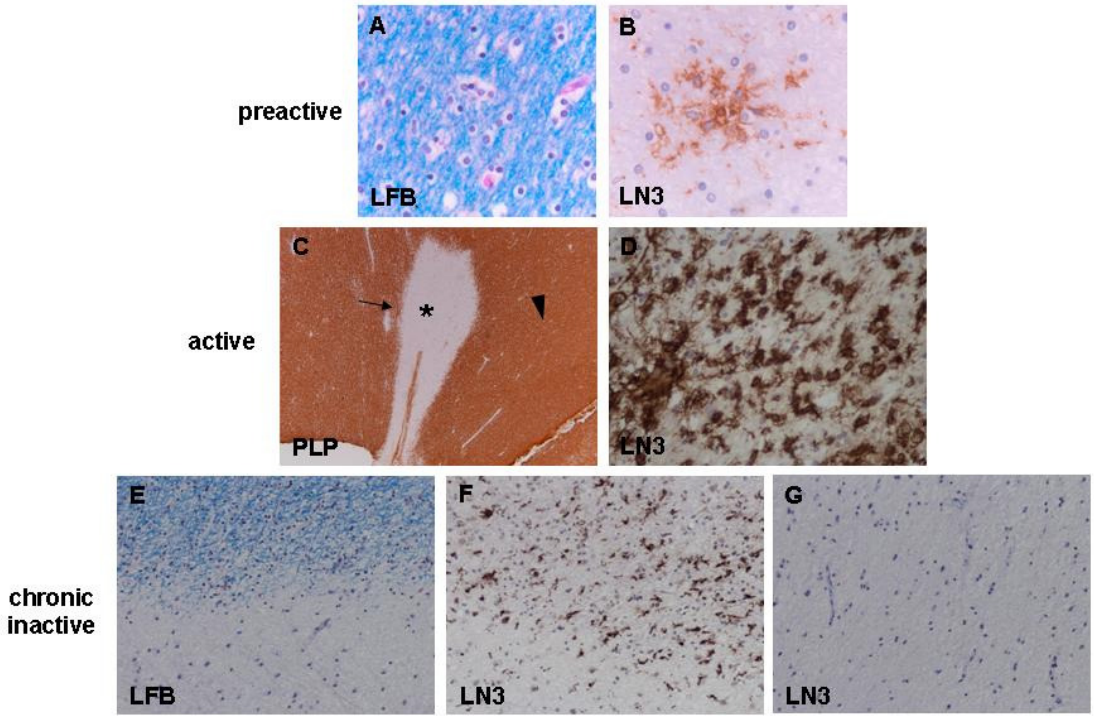


Figure 1

Appearance of preactive, active and chronic-active lesion in LFB, anti-PLP and anti-LN3 stained sections is presented. Note focal accumulation of LN3-expressing microglia (B) in the normal appearing white matter tissue (A), characteristic for preactive lesions. (C) shows focal loss of PLP-immunoreactivity. The lesion centre is indicated by a star, the lesion rim by the arrow. Arrowhead indicates the so called "periplaque white matter" with a normal appearance in routine myelin stains. (D) shows many activated so called "foamy" macrophages in the active lesion centre. (E) delineates the rim of a chronic-active lesion. The upper part still contains some blue-stained myelinated axons whereas the lower part of the picture is devoid of myelin. Characteristic for chronic-active lesions is the presence of activated microglia/macrophages at the lesion border (F). In contrast, microglia/macrophage numbers are low within the centre of the lesion (G).

So called normal appearing white matter (NAWM) of MS patients is often used as control reference tissue, however some pathology is present in those areas as well [18, 19].

Only little is known about demyelinating lesions in early MS. Lucchinetti and co-workers addressed this interesting issue by studying both autopsy and biopsy tissues from early RR-MS cases [20]. Despite the similarities in the inflammatory reaction (inflammatory infiltrates composed mainly of T cells and macrophages), the investigated lesions can be segregated into four distinct patterns with the common hallmark of myelin destruction. Pattern I lesions can be considered as sites of active demyelination associated with a T cell- and macrophage dominated inflammation. Pattern II lesions additionally display deposition of immunoglobulin and activated complement at sites of active myelin destruction. Both lesion types are typically centred by small veins or venules and show sharply demarcated edges. Loss of different myelin proteins, such as MAG, myelin oligodendrocyte protein

(MOG), PLP, or 2',3'-cyclic nucleotide 3' phosphodiesterase (CNPase) occurs to the same extent. Pattern III lesions also contain an inflammatory infiltrate, composed mainly of T cells and macrophages/microglia, but there is no deposition of immunoglobulin or complement. Furthermore, lesions are not centred by veins but preservation of a rim of myelin is frequently observed around an inflamed vessel within the demyelinated plaque. Within pattern III lesions, myelin-forming oligodendrocytes show nuclear condensation and fragmentation which are typical signs of apoptosis. Pattern IV lesions contain microglia/macrophages and T cells (as pattern I lesions) but display significant cell death in the periplaque white matter. Pattern II is most frequently observed in MS cases, followed in the order of magnitude by pattern III, pattern I, and pattern IV. Interestingly, pattern III lesions were mainly found in patients with less than 2 months duration of disease before biopsy or autopsy [3].

The concept of heterogeneity among lesions remains somewhat controversial. While different patterns of demyelination may exist early in the disease, this is probably not the case in patients with longer disease duration. In a recent study using an unselected pool of autopsy material from patients with a disease duration ranging from 7-51 years, lesion heterogeneity was not detected [21]. This study strongly suggests that, in contrast to early disease, there is a common mechanism of demyelination in established MS.

1.7 Grey matter pathology in multiple sclerosis

In MS, brain inflammation is associated with lesions appearing typically in plaques within the white matter (see fig. 1). Recent histopathological studies, however, convincingly show that grey matter regions, such as the forebrain cortex, are equally affected. Cortical demyelination can be widespread and was found to be most prominent in patients with either primary or secondary progressive MS, being rare or even absent in the acute or relapsing disease stage [22]. Cortical lesions can be classified in relation to their location. Lesions that extend across both white matter and grey matter are termed Type 1 lesions whereas lesions within the cerebral cortex that do not extend to the surface of the brain or to the subcortical white matter are classified as Type 2. The most common cortical lesion types are so called “subpial” Type 3 lesions. A common appearance of Type 3 lesions is that of long ribbons of subpial demyelination, often affecting several adjacent gyri. Type 4 lesions extend throughout the full width of the cerebral cortex, but do not reach into the subcortical white matter [23, 24].

The pathology of grey matter lesions differs from that of white matter lesions in several aspects, such as less pronounced lymphocyte infiltration, macrophage activity, complement composition or blood brain barrier alterations [21, 24-26]. The observed differences could be due to differences of the blood brain barrier or other elements of the cytoarchitecture of the cerebral cortex that make it more resistant to inflammation [25]. Given the extensive cortical involvement in patients with chronic MS, little T- and B cell infiltration in chronic cortical lesions, and extensive white matter demyelination in most MS patients, cortical MS lesions have been proposed to be degenerative in origin. However, whether

or not the development of cortical demyelinated lesions in MS displays a separate identity remains to be clarified.

2. The toxic cuprizone demyelination model

Cuprizone ingestion in mice induces a highly reproducible demyelination of certain brain regions, among them the corpus callosum (CC). This commissural white matter tract represents the most frequently investigated region in this animal model [3]. After 5–6 weeks (wks) of cuprizone treatment, the CC is almost completely demyelinated, a process called ‘‘acute demyelination’’. Acute demyelination is followed by spontaneous remyelination during subsequent weeks when mice are fed normal chow. In contrast, remyelination is highly impaired/delayed when cuprizone administration is prolonged (12-13 weeks or even longer), a process called ‘‘chronic demyelination’’. During late stages of acute demyelination, spontaneous remyelination occurs partially but fails under a continued cuprizone challenge [3].

First experiments using cuprizone as a toxic compound date back to the late 1960s and were conducted by Carlton [27]. He reported that oxalic biscyclohexylidenehydrazide, a chelator used as a reagent for copper analysis, induces microscopic lesions in the brain accompanied by oedema, hydrocephalus, demyelination and astrogliosis. He administered different doses of cuprizone mixed in basic chow ranging from 0.2 to 0.5%. Mice fed cuprizone showed signs of growth retardation in a dose-dependent manner. At higher concentrations (0.5%), cuprizone caused high mortality especially when introduced in the chow early during development. The mortality in 4-week-old mice was 100%, whereas mortality declined to 20% in 8-week-old mice. In parallel, development of a severe hydrocephalus was more frequent in younger animals [28]. Based on these early findings, most laboratories use 6- to 9-week-old mice feeding a diet containing 0.2–0.3% cuprizone. To assure proper demyelination in aged animals, the cuprizone concentration needs to be increased [29]. Furthermore, a strain-dependent susceptibility to cuprizone has to be considered. For example, it has been shown that SJL mice display a unique pattern of demyelination that does not follow the profile that is described in C57BL/6 mice. SJL mice do not readily demyelinate at the midline within the CC but show greater demyelination directly lateral to midline [30]. In our own studies, we continuously use C57BL/6 mice.

As mentioned, cuprizone is a well-known copper-chelating agent, discovered and described in the early 1950s. The resulting copper–cuprizone complex is characterized by a very intense and unusual absorption band in the visible region, centred at 595 nm [31]. Due to the highly chromogenic reaction of cuprizone with copper (II) ions, cuprizone was largely exploited for the quantitative determination of copper in various samples. Starting from the early 1970s, a lot of interest focused again on cuprizone, mainly within the biomedical scientific community, as this compound was reported to possess unique neurotoxic properties and, therefore, to serve as a valuable pharmacological tool for CNS demyelination and spongiosis in various laboratory animals [3, 15]. The underlying mechanisms of cuprizone-induced oligodendrocyte cell death are not fully understood. It is well known that feeding of cuprizone causes the formation of mega-mitochondria in the liver. Liver tissue from cuprizone-fed

animals was studied with respect to mitochondrial dysfunction [32]. Since cuprizone induces alterations of mitochondrial morphology [3], it is speculated that the neurotoxic properties of this copper-chelating compound are due to a disturbance of cellular respiration, a key function of mitochondria. Since cuprizone-induced copper deficit might be detrimental to mitochondrial function in the brain [33] it has been assumed that it is a disturbance of energy metabolism in oligodendroglia and cell function that leads to demyelination [3, 15]. Why oligodendroglia should be preferentially susceptible to copper deficit is not known, although an obvious hypothesis is that the perikaryon of this cell type has to maintain a vast expanse of myelin and this extraordinary metabolic demand places it in jeopardy if the demand cannot be met. I will point out later that this assumption is probably not correct.

3. Remyelination in multiple sclerosis

Demyelination is still a characteristic entity for the pathology of MS but it has become increasingly apparent in recent years that substantial axonal and neuronal loss are equal important features [34-36]. Remyelination is the best-documented and most robust example of tissue repair in the human CNS and is unequivocally neuroprotective in MS. Approximately 40% of *post-mortem* MS tissues demonstrate remyelination which can occur early and late during the course of MS [37-39]. Remyelination represents one of the most effective mechanisms to achieve axonal protection in demyelinating disorders. Remyelination is believed to restore the structural integrity of the axon-myelin unit and axonal conduction properties that are lost following demyelination [40, 41]. It is unresolved why in some patients remyelination is widespread while in others, it is sparse. The increasing importance of axonal damage and loss as the pathological basis for progressive loss of function in MS demands a better understanding of the remyelination processes in MS and possible reasons for its failure. Several mechanisms have been suggested that may result in a blockade of remyelination. The loss and destruction of oligodendrocyte progenitor cells within the lesions in the course of repeated de- and remyelination might play an important role [42, 43]. In some lesions, however, progenitor cells are abundantly present [44-47], but remyelination still fails either because axons are not permissive for remyelination [48] or the maturation of progenitor cells is inhibited [49].

Cell types involved in endogenous remyelination might be local brain-resident cells such as astrocytes and microglia, or inflammatory cells from the peripheral vascular system such as leukocytes. Several factors have been described to be important for proper endogenous remyelination such as TNFα, interleukin 1β [50, 51] and hormones, i.e. oestradiol, progesterone and thyroxin [1, 52, 53]. On the other hand, recent studies identified additional factors which might contribute to remyelination failure such as the axon-derived polysialylated form of the neural cell adhesion molecule NCAM [48], LINGO-1 [54], myelin debris [55], or astroglial hyaluronan [56]. It is still not clear whether the lack of pro-myelinating factors or the presence of active remyelination inhibitors accounts for remyelination failure in MS lesions.

4. Aims and scope of the study

Animal models are an irreplaceable tool for the development of new therapeutic strategies and options. A detailed understanding of MS pathology is of particular importance as is a detailed characterisation of the currently used animal models. Within my thesis, I characterized the toxic cuprizone model in detail. While many studies either investigate human ***or*** animal pathology and/or pathogenesis, translational research (i.e. a ***direct*** comparison of animal models with the disease presentation in humans) is necessary. One aim of my thesis was this essential step in MS research.

Besides regional differences in cuprizone-induced demyelination, a better understanding of endogenous remyelination processes was a major objective of my studies. It is possible that the persistent expression of only one or two key inhibitors of remyelination (alternatively the restricted expression of inducers of remyelination) might act as ‘‘master regulators’’ of this process, thus preventing remyelination. However, it is more likely that non-remyelinating lesions result from an abnormal regulation of multiple steps during the remyelination process, resulting in a failure of the normal coordinated repair response after a demyelinating event. By using state of the art techniques (i.e. gene chip array analysis) we aimed to identify those factors and to investigate underlying mechanisms on the molecular level. Microglia cells as brain resident macrophages have been in the focus during demyelinating processes whereas the function of astroglia during tissue repair is highlighted in the remyelination phase. A better understanding of both cell populations will certainly broaden our knowledge of CNS disorders in general and, particularly, of MS.

Materials and Methods

1. Animals and disease induction

Mice (Charles River or Harlan Winkelmann, both Germany) were bred and maintained in a pathogen-free environment. Animals underwent routine cage maintenance once a week and microbiological monitoring according to the Federation of European Laboratory Animal Science Associations recommendations. Food and water were available *ad libitum*. Research and animal care procedures were approved by the Review Board for the Care of Animal Subjects of the district government (North Rhine-Westphalia, Germany). Toxic demyelination was induced by feeding male C57BL6 mice (19-21 g) a diet containing 0.2% cuprizone (Sigma-Aldrich, Germany) mixed into a ground standard rodent chow (Sniff, Germany) for 5 wks. The mixture was prepared fresh twice a week and stored at 4 °C. For experimental autoimmune encephalomyelitis (EAE) experiments, female SJL/J mice (6–8 wks; 20 g body weight; Janvier, France) were immunized by subcutaneous injection of 250 µg of PLP peptide p139–151 (purity >95%; Pepceuticals, UK) in a 0.2 ml emulsion consisting of equal volumes of phosphate-buffered saline (PBS) and complete Freund's adjuvant (CFA, Difco, USA) containing 6 mg/ml Mycobacterium tuberculosis H37Ra (Difco, USA). Bordetella pertussis toxin (200 ng; List Biological Laboratories, Canada) was administered by intraperitoneal injection at days 0 and 2. Mice were scored as follows: 0, no disease; 1, tail weakness; 2, paraparesis; 3, paraplegia; 4, paraplegia with forelimb weakness; 5, moribund or dead.

2. Tissue preparation

For histological and immunohistochemical studies, mice were transcardially perfused with 2% paraformaldehyde containing saturated picric acid (pH 7.4). After overnight post-fixation in the same fixative, brains were dissected, embedded, and then coronary sectioned into 5 µm sections from the levels 205 to 275 according to the mouse brain atlas by Sidman et al. (http://www.hms.harvard.edu/research/brain/atlas.html). Spinal cord sections were prepared from the lumbar part. A detailed protocol for the transcardial fixation is given in ***Appendix 1***. The protocol for paraffin-embedding is given in ***Appendix 2***. For gene or protein expression analysis, mice were transcardially perfused with ice-cold PBS, brains quickly removed, and the entire corpus callosum and the adjacent cortex separately dissected using a stereo-microscopic approach. Tissues were immediately frozen in liquid nitrogen and kept at -80°C until used.

3. Multiple sclerosis material

Paraffin-embedded *post-mortem* CNS tissues were obtained through a rapid autopsy protocol from subjects with mostly progressive MS (in collaboration with the Netherlands brain bank Amsterdam). Biopsy tissue from patients diagnosed with inflammatory demyelination of the CNS consistent with MS was obtained from neurosurgery centres in Germany via the Department of Neuropathology in Göttingen, Germany. The biopsies were performed for diagnostic reasons, for example, to exclude

neoplastic- or infectious diseases and sent to the Department of Neuropathology in Göttingen for a second opinion. The study was approved by the institutional ethics review board and all donors or their relatives provided written consent for the use of brain tissues and clinical information for research purposes. Microscopic analysis of *post-mortem* samples was performed by two blinded readers (Prof. Sandra Amor and Prof. Paul van der Valk). Staging of lesions was performed as reported previously [17].

For the study described in chapter 3, 167 tissue blocks from 21 *post-mortem* brains were included. The average age of patients was 66.48±13.0 (mean ± standard deviation). Average disease duration was 31.35±13.2. Detailed clinical information is given in ***Appendix table 1***. For the study described in chapter 4, six biopsies from 6 different patients and 25 tissue blocks from 7 *post-mortem* brains were included in the study. The average age of patients was 55.69±20.45. Detailed clinical information is given in ***Appendix table 2***.

4. Immunohistochemistry

For IHC, paraffin-embedded sections were de-waxed, rehydrated, epitopes if necessary unmasked by either Tris/EDTA-buffer (pH 9.0) or citrate buffer (pH 6.0) and heating in a customary microwave, washed in PBS, quenched in H_2O_2, again washed in PBS and incubated overnight with the primary antibody diluted in blocking solution (Immunologic, Netherlands). Unspecific binding during mouse-to-mouse protocols was minimized by incubating slides for 3h with blocking solution at room temperature (Immunologic, Netherlands). According to the manufacturer, the diluent contains complex proteins and non-protein mixtures which eliminate histostaining background by blocking Fc receptors and prevents non-specific protein-protein interactions. A complete list of antibodies used in the study, the applied concentrations as well as the performed heat-mediated antigen retrieval step is given in ***Appendix table 3.*** A detailed protocol for the entire IHC procedure is given in ***Appendix 3***. For the visualisation of epitope-primary antibody complexes we used either the VECTASTAIN® ABC (peroxidase) system (vectorlabs, USA) or EnVision® polymer secondary antibodies (Dako, Germany). The VECTASTAIN® ABC-kit employs biotinylated secondary antibodies that form Avidin: Biotinylated enzyme complexes. This method has been termed the "ABC" technique [57]. The Dako EnVision® polymer system is a two-step IHC staining technique. This system is based on an horseradish peroxidise-labelled polymer which is conjugated with secondary antibodies. The labelled polymer does not contain avidin or biotin. Consequently, nonspecific staining resulting from endogenous avidin-biotin activity is eliminated or significantly reduced.

5. Histochemistry

Luxol Fast Blue and Periodic Acid Schiff (LFB/PAS) stainings were performed for the detection of myelin as published [58]. Sections were deparaffinized in a series of xylene (3 × 5 min) and partially dehydrated in 100% ethanol and 96% ethanol. Then, sections were incubated with 0.1% LFB (Gurr, UK) at 60°C for 3 h. After this, sections were rinsed in 96% ethanol for 10 s and subsequently rinsed

in distilled water. Sections were differentiated in 0.1% lithium carbonate and after this in 70% ethanol. Then, sections were rinsed in distilled water and incubated with 0.8% periodic acid solution for 10 min. Thereafter, sections were rinsed in tap water and subsequently in distilled water. Sections were incubated with Schiff's solution (Merck, Germany) for 30 min. After a short rinse in tap water, sections were counterstained with haematoxylin for 5 min and intensely washed with tap water for 5 min.

6. Electron-microscopy and semi-thin sections

For electron microscopy, mice were anesthetized and perfused with PBS followed by solution containing 4% paraformaldehyde and 2.5% glutaraldehyde. Brains were sliced into 1 mm sections, further trimmed and reoriented to obtain cross sections. Thin sections were cut and subsequently stained with uranyl acetate and lead citrate. Electron microscopy pictures were digitally recorded. This procedure was performed in collaboration with Prof. W. Baumgartner (RWTH-Aachen University, Department of Cellular Neurobionics). Technically, the entire procedure was performed by Agnes Weth. Evaluation of the pictures was performed by my self.

7. Immunoflourescence double labelling

For immunofluorescence double labelling, sections were rehydrated, unmasked by citrate buffer and heating, blocked with PBS containing 2% heat-inactivated fetal calf serum (FCS) (Gibco, Germany) and 1% bovine serum albumin (Sigma-Aldrich, Germany), and incubated for 90 min with the indicated combination of primary antibodies diluted in blocking solution. After washing, sections were incubated with a combination of fluorescent anti-mouse secondary antibodies (Alexa Fluor 488 donkey IgG; Invitrogen, Germany) and fluorescent anti-rabbit secondary antibodies (Alexa Fluor 568 goat IgG; Invitrogen, Germany) both diluted in blocking solution. Sections were then incubated with Hoechst 33342 (Invitrogen, Germany; 1:1000) diluted in PBS for the staining of cell nuclei. In order to exclude unspecific binding of the fluorescent secondary antibodies to primary antibodies, appropriate negative controls were performed by first incubating sections with the primary antibodies of murine origin and subsequently incubating these sections with fluorescent anti-rabbit secondary antibody and *vice versa*. Unspecific secondary antibody binding to the tissue itself was excluded by performing negative controls by incubating sections with each of the fluorescent secondary antibodies alone. Stained and processed sections were documented with the microscope working station Zeiss LSM 7 Duo (Carl Zeiss AG, Germany).

8. Scoring of demyelination and quantification of cell number

In order to evaluate demyelination in PLP-stained sections of mice treated with cuprizone, we scored the CC between zero and three. A score of three is equivalent to the myelin status of a mouse not treated with cuprizone, whereas zero is equivalent to a totally demyelinated CC. A score of one or two corresponds to one-third or two-thirds fibre myelination of the CC, respectively. Loss of PLP immunoreactivity in PLP-induced EAE animals was quantified by measuring PLP-staining intensity

within the entire lumbar spinal cord using ImageJ (version 1.44h; Java 1.6.0_10). Results are expressed as percentage of entire spinal cord transverse section area. Loss of cortical PLP immunoreactivity in cuprizone-induced demyelination was quantified by measuring PLP-staining intensity within the region of interest (ROI) in binary-converted pictures using ImageJ (version 1.44h; Java 1.6.0_10). Results are expressed as percentage area of the entire ROI. A value of 100% represents a fully myelinated, 0% a fully demyelinated area. Quantification of astrocytes, oligodendrocytes, or microglia/macrophage numbers was done by manual counting the number of positive cells in the CC and lumbar spinal cord. Cell counting was performed using a Nikon Eclipse 55i (Nikon, Germany) and a 40x objective. Numbers are expressed as cells/mm^2.

9. Gene expression analysis

Isolation of total RNA was performed with the NucleoSpin kit (Macherey-Nagel, Germany). RNA concentration and purity were assessed by using OD260 and OD260/OD280 ratio, respectively determined by the NanoDrop 2000 (Thermo Scientific, Germany). 1 µg RNA was subsequently reverse transcribed using an Invitrogen M-MLV RT-kit and random hexanucleotide primers (Invitrogen, Germany). Successful generation of cDNA was checked by conventional PCR using hypoxanthine guanine phosphoribosyl transferase 1 (HPRT) primers. HPRT, which plays a central role in the generation of purine nucleotides through the purine salvage pathway, is abundantly expressed in mammalian cells and thus can be regarded as a "housekeeping gene". Housekeeping genes are typically required for the maintenance of basic cellular function, and are found in all cells of an organism. As illustrated in fig. 2, the applied mouse HPRT primer pair was designed as an intron/exon spanning oligonucleotide. The purpose of having primers that span at least one intron is to differentiate whether a band is amplified from genomic DNA or cDNA. If the isolated RNA is contaminated with genomic DNA and primers span one or more introns, one will get two bands with one from the cDNA and the other from genomic DNA. The "contaminated" genomic DNA band is longer, thus migrating slower during electrophoresis. In the given example, the specific cDNA amplicon should have a size of 248 base pair, the unspecific genomic DNA band of 1086 base pair, respectively. Thus, successful reverse transcription as well as lack of genomic DNA contamination was checked by one single PCR.
Thereafter, cDNA samples were diluted 1:10 in RNAse/DNAse free water (Invitrogen, Germany). Before diluting the cDNA, a certain amount of each cDNA sample was pooled and further diluted to create an internal standard curve. Reverse-transcription polymerase chain reactions (rtPCR) were carried out in a reaction mixture consisting of 2 µl diluted cDNA, 2 µl RNAse/DNAse free water, 5 µl SensiMix™ reagent (Bioline, Germany), and 0.5 µl of primer (10 pmol/µl; Invitrogen, Germany). Reactions were conducted in 96-well plate format using the MyIQ rtPCR Detection System (BioRad, Germany) under the following conditions: 10min enzyme activation at 95°C, 40 cycles of 15sec denaturation at 95°C, 30sec annealing at individual temperatures, 30sec amplification at 72°C, and 5sec fluorescence measurement at 80°C.

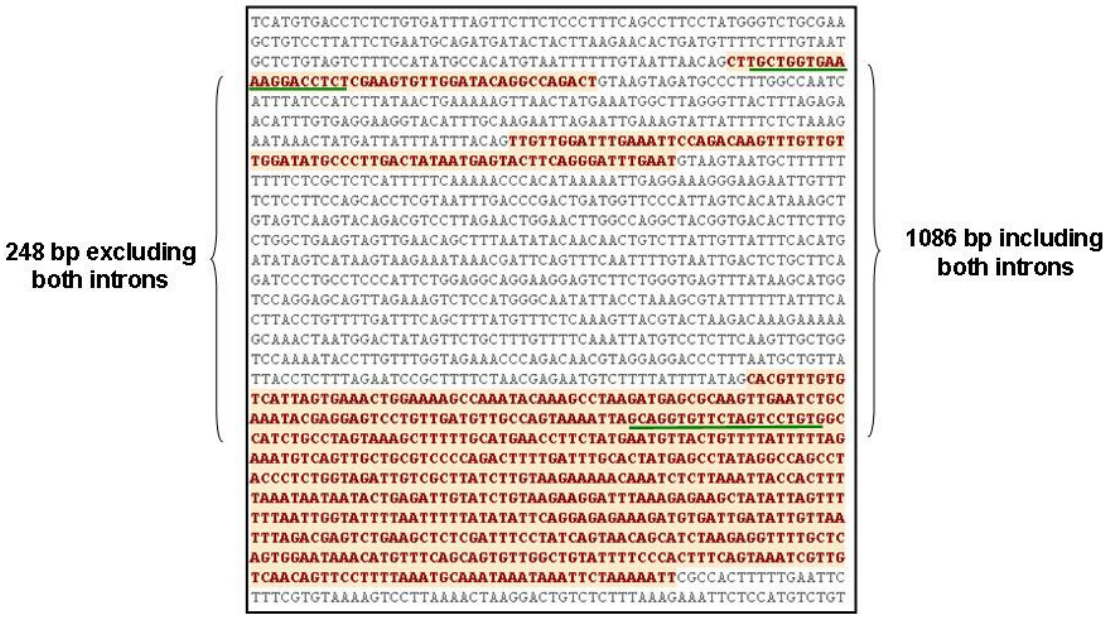


Figure 2

Organization of the HPRT1 mouse gene is illustrated. Exons are shown in brown characters. In between the exons, introns are shown in black characters. Green lines illustrate the positions of the forward and reverse oligonucleotide.

Primer sequences are given in ***Appendix table 4***. Relative quantification was performed by the ΔCt method, which results in ratios between target genes and a housekeeping reference gene (HPRT for mice tissue, 18s for human material). Because the validity of this method critically depends on the constant expression of the housekeeping gene, this prerequisite was tested for all treatment conditions. In each run, external standard curves were generated by several fold dilutions of target genes. The concentration of the target genes was calculated by comparing Ct values in each sample with Ct values of the internal standard curve. Finally, data were expressed as the ratio of the amount each transcript vs. the concentration of HPRT/18s. Melting curves and gel electrophoresis of the PCR products were routinely performed to determine the specificity of the PCR reaction. For each experiment, negative controls were performed in which 2 µl of RNAse/DNAse free water was added to the PCR reaction instead of cDNA. Positive controls using cDNA samples which were affirmed to contain the template to be amplified were performed as well.

For end-point PCR, RNA isolation, purity assessment and reverse transcription were performed as described above. rtPCR reactions were carried out using a commercial PCR Kit (Bioline, Germany) and 2 µl undiluted cDNA and 0.25 µl of primer (10 pmol/µl; Invitrogen, Germany). Reactions were

conducted in standard tubes using the Mastercycler epgradientS (Eppendorf, Germany) under following conditions: 3 min of initial denaturation at 95°, followed by 35 cycles of each 40 s of denaturation at 95 °C, 45 s of annealing at individual temperatures and 40 s of elongation at 72 °C. Negative and positive controls were performed as already described above. After PCR reaction, cDNA samples were applied on a 2% agarose gel containing ethidium bromide and separated by electrophoresis (Bio-Rad, Germany). Pictures of gels were taken using the Alpha Imager (AlphaInnotech, USA).

10. Affymetrix GeneChip®

Regulation of gene expression in different treatment groups was analyzed by Affymetrix GeneChip® as published previously [59, 60]. Total RNA (n=3) was isolated and the quality assessed using RNA NanoChips with the Agilent 2100 Bioanalyzer (Agilent, USA). Probes for the GeneChip® Mouse Gene 1.0 ST Arrays (Affymetrix, USA) were prepared and hybridized to the arrays according to the Affymetrix GeneChip® Whole Transcript (WT) Sense Target labelling Assay Manual. Briefly, for each sample, 300 ng of total RNA was reverse transcribed into cDNA using a random hexamer oligonucleotide tagged with a T7 promoter sequence. After second strand synthesis the double-stranded cDNA was used as the template for amplification with T7 RNA polymerase to create antisense cRNA. Random hexamers were then used to reverse transcribe the cRNA into single stranded sense strand cDNA. The sense cDNA was then fragmented by uracil DNA glycosylase (UDG) and apurinic/apyrimidic endonuclease 1. Fragment size was checked using a Bioanalyzer (Agilent, USA) with optimal fragment size in the 50-200 bp range. Fragmented sense cDNA was biotin-labelled with terminal deoxynucleotidyl transferase. The probes were then hybridized to the GeneChip® Human Mouse 1.0 ST Arrays at 45° C for 16 h, washed and stained on Fluidics Station 450 and finally scanned on a GeneChip® Scanner 3000 7G (Affymetrix, USA). The image data were analyzed with AGCC (Affymetrix, USA). Gene expression levels were pre-processed with RMA algorithm [61]. Only those genes which were expressed higher than 3 fold over negative control in at least one treatment condition were further analyzed. Four different expression patterns (see below) were screened; 2 fold changes were used as cut-off for up/down regulation. Patterns were mathematically defined as follows: E_{con}, $E_{5w,}$ E_{13w} are expression values in control, week 5, and week 13 animals, respectively. Pattern 1: $2x\ E_{con} \leq E_{5w} \geq E_{13w}$; Pattern 3: $E_{con} \geq 2x\ E_{5w} \leq E_{13w}$; Pattern 2: $E_{con} = E_{5w} \geq 2x\ E_{13w}$; Pattern 4: $E_{con} = E_{5w} \leq 0.5\ x\ E_{13w}$. Genes following pattern 1 were further ranked according to magnitude of expression differences between expression values E_{5w} and E_{13w}. The following mathematical definition was applied (compare figure 2B): $2x\ E_{con} \leq E_{5w} \geq E_{13w}\ x\ Y$, with Y=20/13 (30%); Y=20/14 (40%); Y=20/15 (50%); Y=20/16 (60%); Y=20/17 (70%); Y=20/18 (80%). Strictness of inclusion criteria increases with Y value. Genes in pattern 1 subgroup 50% (Y=20/15) were selected as candidate genes and analyzed for Gene Ontology enrichment with Bingo [62].

11. Transfection experiments

U87 cells were transfected with either the empty pREP4 vector (controls) or a pREP4-BLBP expression construct as published previously [63]. Cultures were maintained in DMEM containing 10 % FCS and antibiotics as published [64]. Selection of cultures was regularly performed in hygromycin (400 µg/mL, Invitrogen, Germany) for 48h. Transfected cells where kindly provided by our collaboration partner Prof. R. Godbout (University of Alberta, Department of Oncology, Edmonton, Canada).

12. Western Blot analysis

Protein isolation by homogenizing tissue samples in a RIPA lysis buffer composed of 150 mM NaCl, 50 mM Tris (pH 8.0), 5 mM EDTA and 1% (vol/vol) Nonidet P40 was performed following standard protocols [29, 65]. Protease Inhibitor Cocktail Tablets supplied in a glass vial from Roche Applied Science, Germany were added to avoid protein degradation. After the isolation procedure, protein concentration measurement was performed using the bicinchoninic acid (BCA) protein assay kit (Thermo Scientific, Germany). This kit combines the well-known reduction of Cu^{2+} to Cu^{1+} by protein in an alkaline medium with the highly sensitive and selective colorimetric detection of the cuprous cation (Cu^{1+}) by bicinchoninic acid. The BCA/copper complex was analyzed using a spectrometer at 562nm wavelength (Tecan, Switzerland). Equal amounts of proteins were separated by 10% SDS-PAGE, blotted onto nitrocellulose membranes (Amersham Hybond; GE Healthcare, Germany) and incubated with respective antibodies diluted in 5% milk TBS-Tween 0.01% over night (anti-GFAP, EnCor, USA). After washing and incubating with horseradish peroxidise conjugated anti-rabbit secondary antibody (goat IgG; Biorad, Germany), labelled proteins were visualized with ECL-reagent (GE Healthcare, Germany). After visualization, the antibodies were stripped from the nitrocellulose membrane by incubation with stripping buffer containing 50 mM Tris–HCl and 2% SDS at 70 °C for 30 min. After washing the membrane, antibody incubation and visualization steps using anti-β-actin antibody (rabbit IgG; Sigma, USA) were performed as described above.

13. Statistical analysis

At least six animals were included for gene expression analysis by rt RT-PCR or IHC. Five animals were included for western blotting analysis. Differences between groups were statistically tested by ANOVA followed by a Tukey's post-hoc multiple-range test using SPSS software (SPSS Inc., Chicago, IL, USA) except for differences between myelin scoring in cuprizone-treated animals. There, differences between groups were tested with the non-parametric Mann-Whitney-U-Test. All data are given as arithmetic means ± SEM. P values of the different analyses with $p<0.05$ were considered to be statistically different.

Results

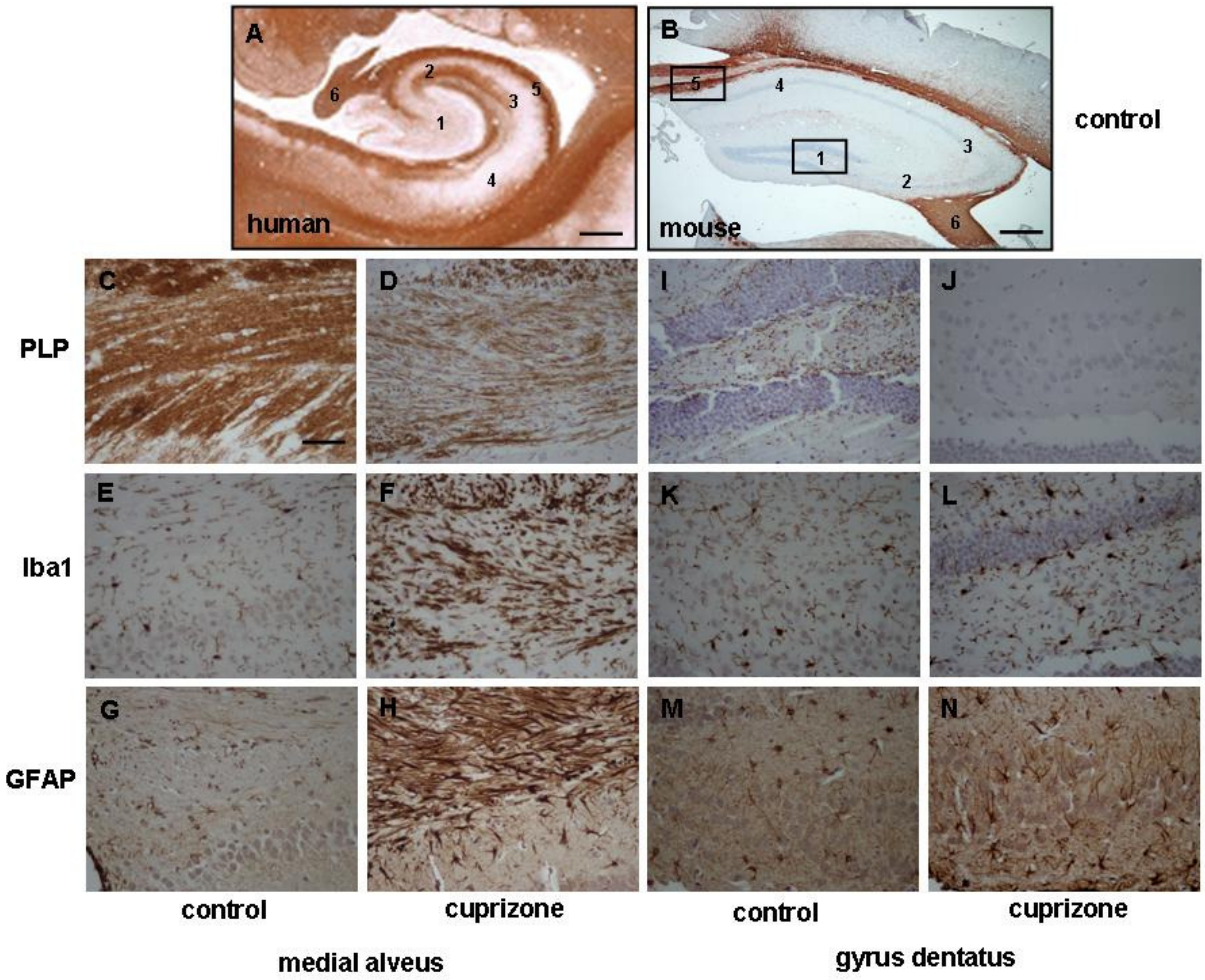
Chapter 1: The hippocampus and basal-ganglia complex are affected in the cuprizone model and multiple sclerosis

There are several models available to study MS pathology. The most frequently used is the EAE rodent model. In this model, demyelinating foci are induced by immunization against a specific myelin antigen, although there is no evidence that human MS is triggered by a similar mechanism. A detailed histopathological study conducted by Lucchinetti et al. has highlighted the profound heterogeneity in the pattern of demyelination among MS patients [20]. One histopathological hallmark of MS is lesion dissemination in space. One focus of my thesis work concerns regional differences of MS pathology. Cuprizone-induced demyelination was believed to predominantly affect the CC and superior cerebellar peduncles. Consequently, the CC was in the focus of most of the studies [15]. We have now shown that cuprizone provokes additional demyelination in other brain areas such as the hippocampus [29], cerebellum [66], caudate putamen, and ventral part of the caudate nucleus [67]. Interestingly, distinct grey matter sub-regions in the cortex, within the hippocampus formation, and the striatal complex are also affected.

In the following chapter, our most important findings are highlighted. Furthermore, I relate them to MS histopathology. As pointed out later, one important difference between white vs. grey matter pathology is the extend of microglia/macrophage activation.

1.1 Cuprizone-treatment induces demyelination of the hippocampus

Both, paraclinical and histopathological studies have shown that the hippocampus is affected in MS [68-70]. The hippocampus formation compromises one of the brain structures that seems to be crucial for long-term episodic memory performance, yet with a precise role that still remains elusive [71]. In line with the assumed hippocampal function in memory performance, a large number (40–65%) of patients with established MS experience cognitive deterioration of variable severity [72, 73]. Acute memory impairment has even been described as an initial distinct symptom in MS before the onset of well known and common sensomotoric impairment [74]. In the presented study, we have analyzed demyelination in distinct grey and white matter areas of the hippocampus in male mice [29]. The status of myelination and oligodendrocyte depletion was determined by histological staining and immunohistochemistry for proteolipoprotein (PLP). Ultrastructural changes were analyzed by electron microscopy. In addition, astrocyte and microglia responses were investigated in demyelinated hippocampus areas.



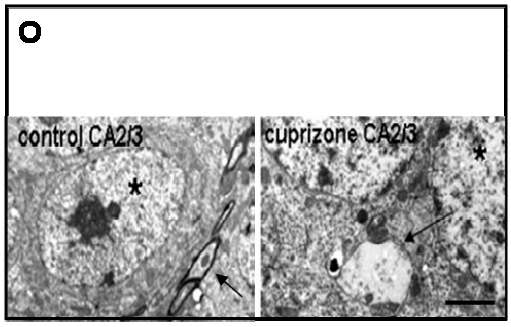


Figure 3

Effects of cuprizone (5wks, 0.2%) on rodent hippocampus white and grey matter myelination, microgliosis and astrocytosis is demonstrated by anti-PLP, anti-Iba1 and anti-GFAP IHC, respectively. A (human) and B (mouse): Overview of the regions (anti-PLP staining) included in the study. (1) hilus of gyrus dentatus, (2-4) cornu ammonis subregions, (5) medial alveus and (6) fimbria. Regions outlined by boxes in (B) are shown in (C-N) in higher magnification. (C-H): Higher magnification views of the medial alveus. (I-N): Higher magnification views of the hilus region. (O): Ultrastructure of axonal demyelination in the cornu ammonis 2/3 (CA2/3) sub-region. Stars in (O) indicate a neuronal nucleus. Arrows in (O) indicate myelinated (left side) and demyelinated (right side) axons. Note that the demyelinated axon has a swollen morphology. Scale bars: 1000µm in (A), 350µm in (B), 20µm in (C-N), 2.5µm in (O).

Figs. 3A/B show an overview of the principal regions included in the study. Control human (fig. 3A) and mouse brains (fig. 3B) show differing myelin intensities throughout the hippocampus formation as assessed by anti-PLP IHC. Whereas high myelin content is present in the alveus (5) and fimbria (6), it is significantly lower in other areas, such as the gyrus dentatus (1) or cornu ammonis subregions (2-4). Thus, distinct myelin rich white matter regions as well as grey matter regions with sparse myelin content can be distinguished within the human and rodent hippocampus formation. The administration of cuprizone induced a highly reproducible demyelination of distinct hippocampal subregions (see figs. 3 C-N. White matter demyelination was mainly observed in the medial part of the alveus (compare figs. 3C vs. 3D) and the adjacent dorsal hippocampal commissure. The fimbria region and the lateral orientated alveus were just moderately affected (see chapter 2). In contrast, all hippocampal grey matter regions appeared to be equally affected by the administration of cuprizone (5wks cuprizone). Exemplarily, the hilar region of the gyrus dentatus with the adjacent granule cell layer is presented. Low PLP-immunoreactivity is present within that region in control animals (fig. 3I) whereas myelinated fibres are absent after 5 wks cuprizone exposure (fig. 3J). In parallel, there is a significant reduction in mature oligodendrocyte cell bodies, as demonstrated by anti-APC and anti-Olig2 staining (data not shown) [29].

To obtain information about cuprizone-induced ultrastructural changes in the mouse hippocampus, electron microscopy studies were performed on control mice and animals treated with cuprizone. Exemplarily, the stratum pyramidale of the cornu ammonis is presented (fig. 3O). Several axons with normal appearing myelin sheets (arrow) can be detected in the vicinity of neuronal cell bodies (star) in the cornu ammonis of control animals. As demonstrated, myelin sheets of most axonal fibres are destroyed by cuprizone application. Furthermore, axonal neurofilament networks appeared impaired, as shown in fig. 1O (arrow), indicating neurodegenerative processes besides demyelination.

In summary,

1.2 Inflammation is most pronounced in demyelinated hippocampal white matter structures

Besides myelin and oligodendrocyte loss, we determined the brain-intrinsic inflammatory response i.e. astrocytosis and microgliosis within the affected white and grey matter of cuprizone-treated animals. IHC for Iba-1 to detect microglia/macrophages demonstrated a moderate, non-significant increase of microglia cell numbers in the affected grey matter (figs. 3K/L) after a 5 wks cuprizone challenge compared to controls. In contrast, a distinct increase in microglia cell number was clearly evident within the affected white matter area (figs. 3E/F). After 5 wks cuprizone exposure, higher numbers of GFAP-expressing astrocytes are seen within distinct hippocampal white (figs. 3G/H) and grey matter (figs. 3 M/N) sub-regions. In addition, the morphology of astrocytes revealed thin cells only possessing a few short processes under control conditions. In contrast, after cuprizone treatment, astrocytes became hypertrophic and multipolar. However, affected white matter areas clearly display more severe astrocytosis compared to the grey matter, respectively. In summary, our analysis revealed

that within the hippocampus formation, demyelinated white matter areas, such as the alveus or fimbria display a more severe inflammatory response compared to grey matter regions, respectively.

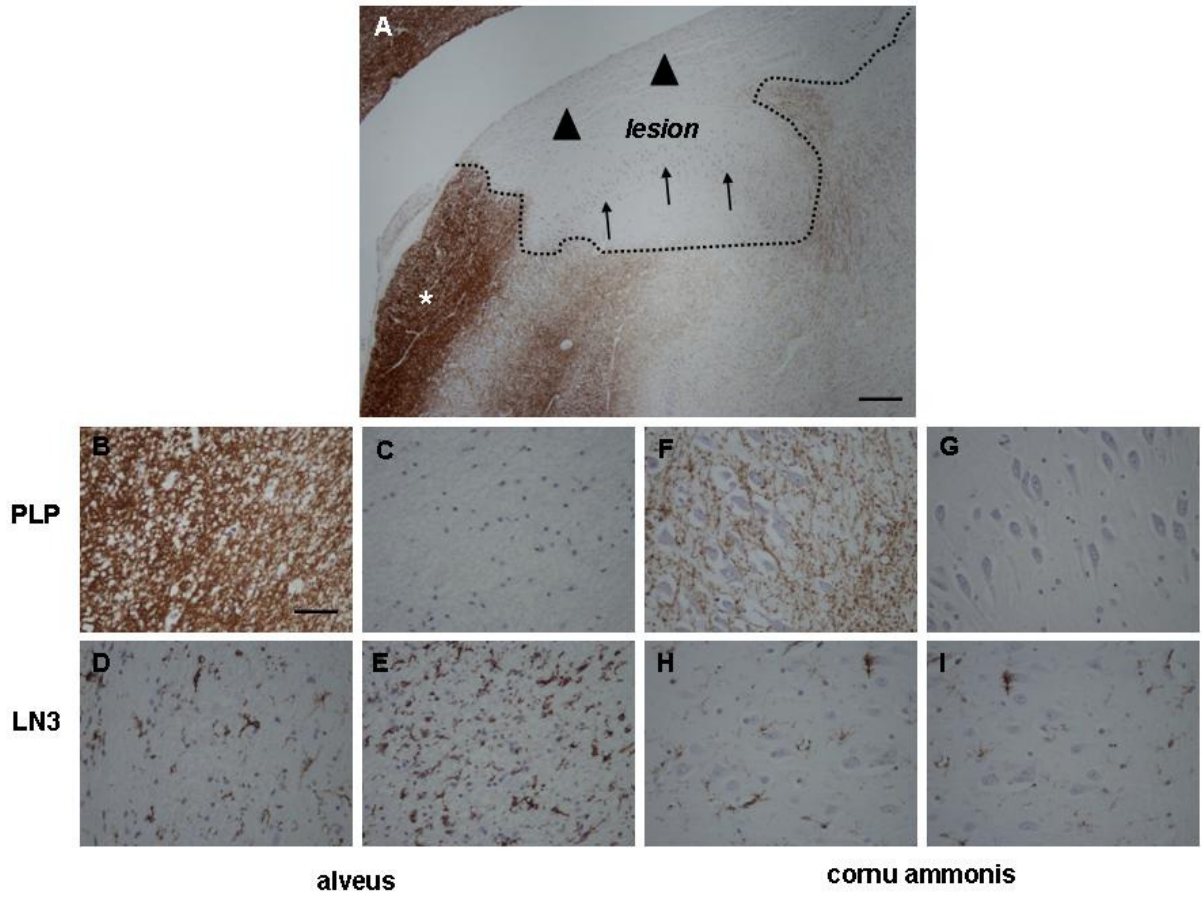


Figure 4

Human hippocampal white and grey matter demyelination and microgliosis is demonstrated by anti-PLP and anti-LN3 IHC, respectively. (A): Overview of a hippocampus mixed white and grey matter MS lesion (anti-PLP staining). Dotted line in (A) delineates the lesion, star the normal myelinated alveus, arrowheads the demyelinated part of the alveus, arrows the demyelinated cornu ammonis region. (B-E): Higher magnification views of the alveus. (F-I): Higher magnification views of the cornu ammonis region. Scale bars: 1000µm in (A) and 20µm in (B-I).

1.3 Comparison of hippocampal lesions in the cuprizone model and multiple sclerosis

As already reported by Geurts and colleagues [68], hippocampal lesions are a frequent phenomenon in MS. Lesions were either found solely within the hippocampus formation or involved both, hippocampal and para-hippocampal areas. We investigated the inflammatory response (i.e. microglia activation) within hippocampal white and grey matter regions of MS patients. Fig. 4A shows an MS plaque within the hippocampus formation (outlined by the dotted line). The star in fig. 4A marks the normal myelinated alveus region which is shown in fig. 4B in higher magnification. Within this normal appearing white matter part, just few LN3 (MHC class II)-expressing microglia/macrophages can be seen (fig. 4D). The demyelinated part of the alveus (marked in fig. 4A with arrowheads, shown in fig. 4C in higher magnification) contains several $LN3^+$ cells (fig. 4E). Fig. 4F shows anti-PLP

staining of the normal appearing grey matter within the cornu ammonis region. Myelinated axons are present there. Those fibres can not be seen within the demyelinated part of the cornu ammonis grey matter (marked in fig. 4A with arrows, shown in fig. 4G in higher magnification). In contrast to the demyelinated white matter, the affected hippocampal grey matter does not show prominent foci of LN3-expressing microglia/macrophages (figs. 4H/I).

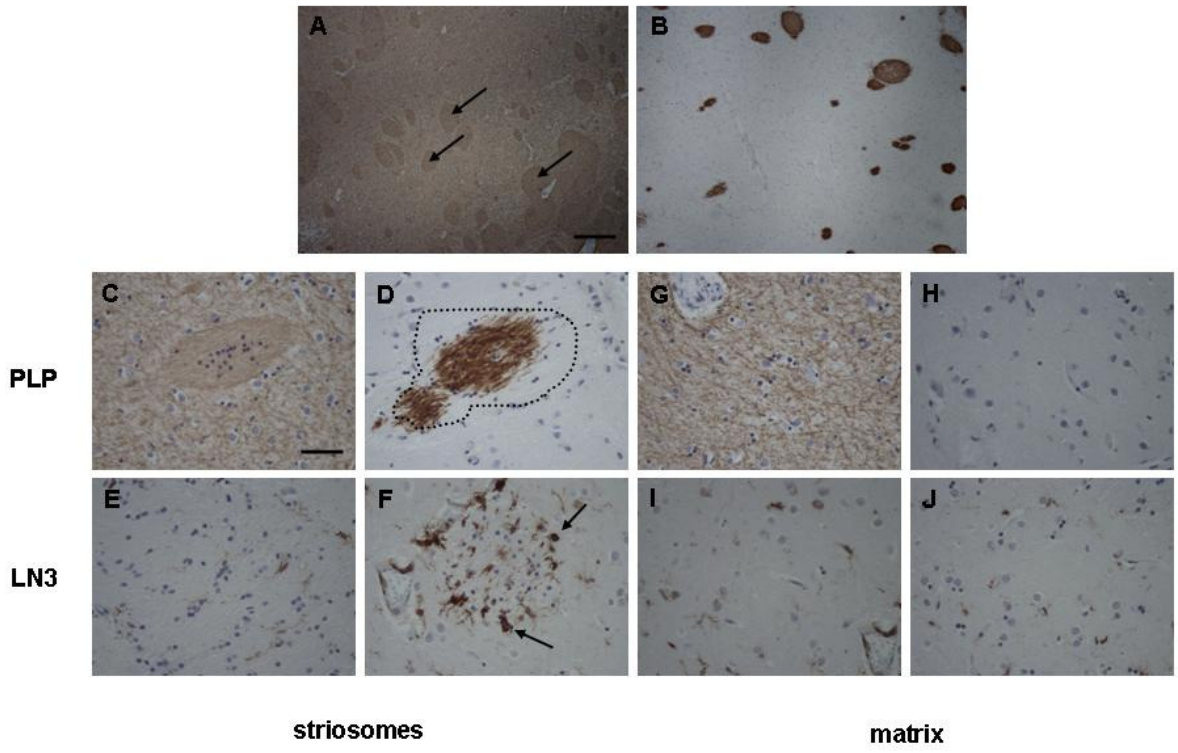


Figure 5

Human basal ganglia white and grey matter demyelination and microgliosis is demonstrated by anti-PLP and anti-LN3 IHC, respectively. (A): Overview of normal myelinated striatum (anti-PLP staining). Arrows indicate the white matter striosomes. (B): Striatal MS lesion (anti-PLP staining). (C-F): Higher magnification views of the striosomes. The original size of the striosome is delineated by the dotted line in (D). Arrows in (F) indicate LN3-expressing microglia/macrophages within the affected striosomes. (G-J): Higher magnification views of the grey matter matrix region. Scale bars: 800µm in (A/B) and 20µm in (C-J).

1.4 Basalganglia demyelination and inflammation

Involvement of basal ganglia in MS appears to be related to a set of symptoms such as fatigue, impaired cognition, and movement disturbance. We were recently able to show that the basal ganglia system is affected by cuprizone administration, as well [67]. White matter striosomes, located within the caudate-putamen and the ventral part of the caudate nucleus displayed intense demyelination, whereas those within the globus pallidus and the head of the caudate nucleus were not affected. The grey matter matrix region, however, was equally affected in the medial and lateral region. Besides

demyelination, we observed hypertrophic and hyperplastic astrocytosis and microglia cell invasion/local proliferation in the demyelinated areas.

To compare histopathological changes between the cuprizone model and MS lesions, 19 basal ganglia lesions were analyzed for the expression of myelin proteins and microglia/macrophages. Exemplarily, the striatum as a part of the basal ganglia system is presented in fig. 5. As demonstrated, described changes in the basal ganglia system of cuprizone-treated animals closely reflect histopathological changes observed in the human situation. 8 out of 19 analyzed human basal ganglia lesions displayed a partial or complete preservation of myelinated axons within the striosomal compartment (figs. 5C/D). In contrast, the grey matter matrix region is almost completely demyelinated, as demonstrated by a definite loss of PLP-immunoreactivity (figs. 5G/H). Similar to our observations in the hippocampus, white matter areas display a more severe inflammatory response compared to grey matter regions within the basal-ganglia complex. In non-affected white matter striosomes, just some LN3-expressing microglia/macrophages are detectable (fig. 5E). In contrast, many activated microglia/macrophages are evident within the partially demyelinated striosomes (fig. 5F). Microgliosis is not evident in the demyelinated matrix region (figs. 5I/J).

In summary we were able to show that feeding of cuprizone to young adult mice induces demyelination of different subcortical areas such as the hippocampus or the corpus striatum. Furthermore, we were able to demonstrate that within those regions, the brain-intrinsic inflammatory response (i.e. activation of microglia and astrocytes) is most severe in myelin rich areas. The same phenomenon was observed in respective regions of MS patients.

Chapter 2: Region-specific local brain responses account for regional differences in cuprizone-induced demyelination

Parts of this work have been published in Inflamm Res. 2011 Aug;60(8):723-6. Epub 2011 Apr 24

As pointed out above, regional differences can be observed in cuprizone-induced demyelination. Why some regions, such as the fimbria of the hippocampus, are resistant to the cuprizone challenge is not known. Interestingly, it has been shown by Hesse and colleagues that in early - but not in later - stages, dying oligodendrocytes express activated caspase 3, suggesting a switch from classical apoptotic pathways to caspase 3-independent mechanisms during the course of the cuprizone diet [75]. To understand more about selective regional vulnerability in this animal model we compared the cuprizone-resistant hippocampal fimbria with the cuprizone-vulnerable CC. We have focused on these two regions because both represent white matter areas, however, with a different vulnerability to the cuprizone challenge (see chapter 1 and Norkute et al. [29]).

2.1 The hippocampal fimbria region is resistant to cuprizone intoxication despite microgliosis

In a first set of experiments animals were fed cuprizone for 5 wks to induce acute demyelination of the CC. As already mentioned above, definite loss of PLP immunoreactivity can be observed in the CC (figs. 6B/E), whereas other regions appear unaffected such as the fimbria of the hippocampus (figs. 6C/F). Both regions included in the subsequent study are indicated by the arrow and star in fig. 6D. Quantitative measurement of PLP staining intensity confirmed our observational results. There was a significant decrease in PLP staining intensity in the CC (control mean 69.2 ± 6.8 SEM vs. 5 wks cuprizone 19.4 ± 4.4; $p<0.005$). This was not observed in the fimbria (control mean 65.3 ± 5.1 SEM vs. 5 wks cuprizone 61.0.4 ± 3.2; $p=0.49$). To further investigate both regions on the cellular levels, we visualized microglia by anti-Iba1 and (activated) astrocytes by anti-GFAP antibodies, respectively. The quantification of fimbrial $Iba1^+$ and $GFAP^+$ cell numbers after acute cuprizone-induced demyelination is presented in figure 6U. Microglia were uniformly distributed in the CC (fig. 6G) and fimbria (fig. 6I) of control animals while a sustained increase in $Iba1^+$ cell numbers was present in the demyelinated CC (fig. 6H) and, although to a lesser extend, in the fimbria (fig. 6J). After 5 weeks cuprizone, higher numbers of $GFAP^+$ astrocytes were seen within the CC (fig. 6L) compared to controls (fig. 6K) but not in the fimbria (figs. 6M/N).

2.2 Region specific inflammation determines demyelination in the cuprizone model

Due to our observation that definite microgliosis can be observed within the white matter fimbria after acute cuprizone-induced demyelination, we assumed that the fimbria is affected as the CC by the toxin *per se*, but does not develop to a "classically" demyelinated lesion. To test for this hypothesis, animals were fed cuprizone in a second experiment up to 5 wks and sacrificed on day 2, week 1, week 2 and week 5 after start of the cuprizone diet. Cells with morphological characteristics typical for apoptosis

such as condensed and/or fragmented nuclei were seen at week 1 in both regions included in the study (figs. 6O/P). Control animals fed with powdered food without cuprizone were lacking apoptotic cells (data not shown). In a previous study, IHC for detection of CNPase confirmed that these apoptotic cells are oligodendrocytes [75].

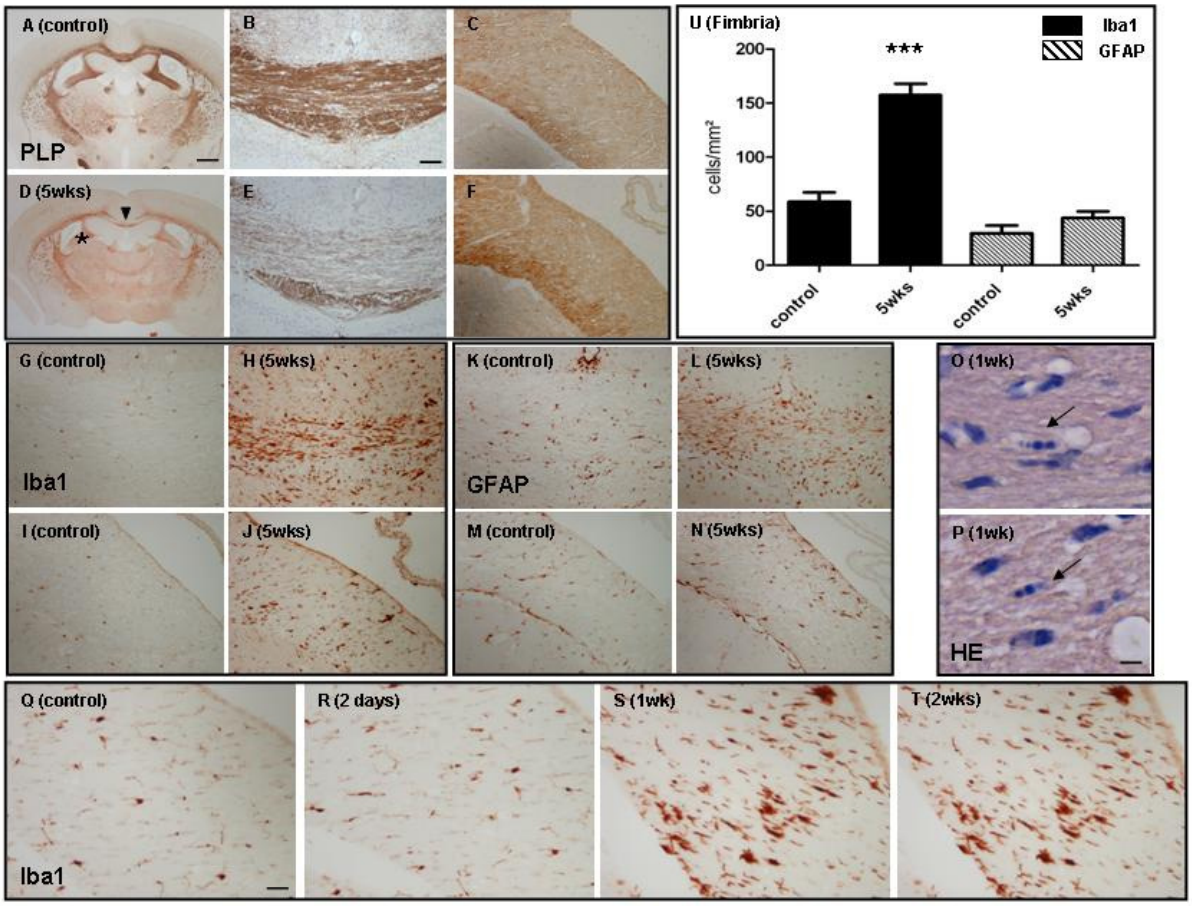


Figure 6

*Myelination and inflammatory cell composition in the medial corpus callosum (CC) and fimbria region of the hippocampus is presented. Anti-PLP antibodies were used to visualize intact myelin in sections of control and cuprizone treated animals (A-F). Anti-Iba1 and anti-GFAP antibodies were used to visualize microglia or astrocytes, respectively. Arrowhead in (D) indicates the medial part of the CC which is shown in (B/E, G/H, K/L and O) in higher magnification. The star in (D) indicates the fimbria region of the hippocampus which is shown in (C/F, I/J, M/N, P and Q-T) in higher magnification. Pictures (O/P) show H&E stained sections, illustrating apoptotic oligodendrocytes (arrows) within the CC and fimbria region. Quantification of Iba1$^+$ microglia and GFAP$^+$ astrocytes (fimbria region) in control and 5 weeks cuprizone treated animals is given in (U). Scale bars: 500µm (A/D); 50µm (B/C, E/F, G-N); 10µm (O/P); 8µm (Q-T); *p<0.05, **p<0.01, and ***p<0.001.*

Anti-Iba-1 IHC revealed that pronounced microgliosis is evident in both regions after week 1. In control animals, Iba1$^+$ cells displayed a typical ramified morphology indicating a resting state (fig. 6Q). At week 1 (fig. 6S), and week 2 (fig. 6T) processes of microglia cells within the fimbria appeared to be retracted and cell bodies were swollen which is frequently associated with microglia activation

[76]. Comparable morphological changes of microglia were evident in the CC at week 1 and 2. While the magnitude of microgliosis progressed in the CC until week 5 (fig. 6H), a reduction of microglia cell numbers could be observed in the fimbria. Only a moderate activation of fimbrial astrocytes was detectable at week 2 (increased number and swollen processes), whereas at all other time points included in the study, astrocytic cell parameters were the same as observed in the fimbria of control animals. Within the CC, astrocytosis started at week 2, however, in contrast to the fimbria progressed in the CC until week 5.

It might be feasible that regional differences exist in microglia function as previously suggested [77]. We assume that some intrinsic signalling contributes to a "switch" from an anti-inflammatory to a pro-inflammatory phenotype of microglia within the affected CC. The first phenotype is also called "M2 or alternatively activated", the later one "M1 or classically activated" [78, 79]. Therapeutic bolstering of this apparent regulation could, therefore, be effective in halting the formation of new destructive lesions in MS.

Chapter 3: Inflammatory response depends on extend of myelin loss in experimental demyelination and multiple sclerosis Type 1 lesions

Our results from chapter 2 strongly suggest that brain-intrinsic inflammation, among others microgliosis, is critical for MS lesion progression. In MS, the pathology of grey matter lesions differs from that of white matter lesions in several aspects, such as less pronounced lymphocyte infiltration, complement composition, blood brain barrier alterations or microglia/macrophage activity [21, 24-26]. The observed differences could be due to differences of the blood brain barrier *per se* or other elements of the cytoarchitecture of the cerebral cortex that make it more resistant to inflammation [25]. However, the reduced inflammatory response in grey matter lesions, especially microglia/macrophage activation, could simply be due to the lower grey matter myelin content and in consequence less myelin debris during a demyelinating event. In the present study we used the toxic cuprizone demyelination model [3] to study the relation between myelin debris and microgliosis/astrocytosis in the demyelinated forebrain white and grey matter. Our findings were opposed to human pathology.

3.1 Cortical grey matter demyelination is prominent in the cuprizone model

It has been recently reported that cortical demyelination is a prominent feature in the murine cuprizone model [80]. In a first set of experiments we reassessed extend and pattern of cortical demyelination after acute cuprizone-induced demyelination (5 wks). Fig. 7A shows a frontal sectioned mouse brain slice at the level of bregma zero indicating the two principal regions included in the study, i.e. the primary somato-motor (pMcx) and somato-sensory (pScx) area, respectively. Both cortical layers each contain a characteristic distribution of neuronal cell types and can thus be distinguished. The pMcx consists of five layers (termed agranular cortex) whereas the pScx of six layers (termed granular layer), respectively. A representative overview of PLP-stained control and cuprizone-treated brains is shown in figs. 7B/C. Figs. 7D/E show the pMcx and pScx of control animals in a higher magnification, whereas figs. 7F/G show respective regions of cuprizone-fed animals. As illustrated, cuprizone exposure resulted in a massive demyelination as detected by a loss of PLP-stained fibres in all cortex regions compared to controls. In control animals, myelinated axons are densely packed within the large areas of the cortex sparing the molecular layer 1. After 5 wks cuprizone treatment, many PLP^+ fibres can be detected within layer 6 of the pMcx, whereas layers 1 to 3 are almost completely demyelinated. The pScx displays a similar demyelination pattern however, some PLP^+ fibres are visible within layer 4 (arrows in fig. 7C).

3.2 Magnitude of myelin loss within the cortical grey matter of cuprizone-treated mice

Since the different cortical layers can be easily identified within the granular pScx compared to the agranular pMcx with rather blurry borders between the different layers, we were intended to quantify changes in PLP immunoreactivity within the pScx region (see fig. 8).

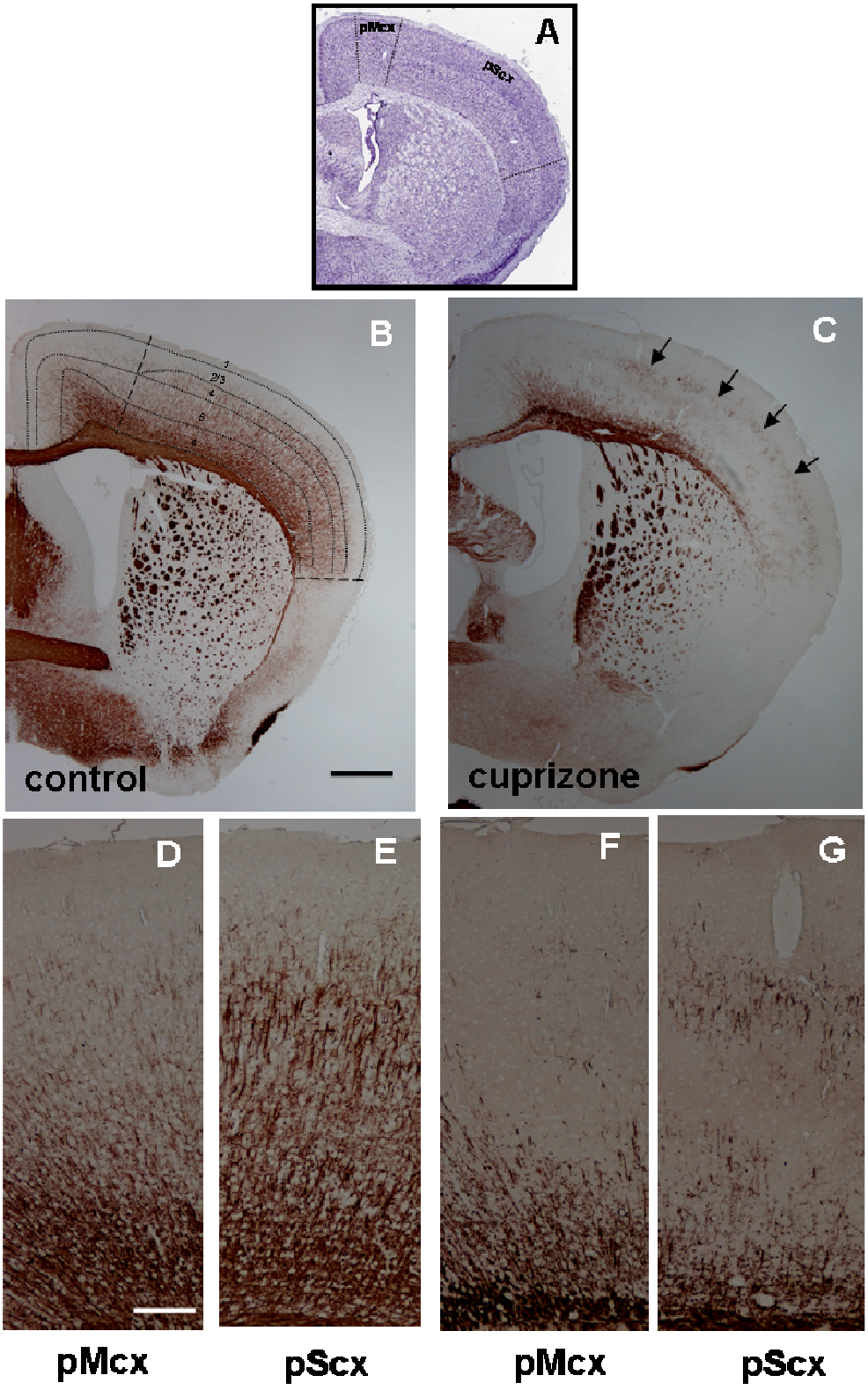


Figure 7

Effect of cuprizone (5wks, 0.2%) on rodent cortical grey matter myelination is presented by anti-PLP IHC. (A): Nissl-stained overview of the principal regions included in the study, i.e. the primary somato-motor (pMcx) and somato-sensory (pScx) area. (B/C): Overview of anti-PLP stained mouse sections of a control and cuprizone treated animal, respectively. Dashed lines in (B) delineate the different cortical layers 1-6. Arrows in (C) mark the internal granular layer 4. Note that PLP-immunoreactivity can be detected in cortical layers 4 and 6 after 5 wks cuprizone treatment. (D/E): Higher magnification views of respective cortical regions in control animals. (F/G): Higher magnification views of respective cortical regions after 5 wks cuprizone treatment (all anti-PLP staining). Scale bars: 350 µm (B/C); 50 µm (D-G).

Evaluation was separately performed for layer1, layers 2/3, layer 4 and layer 6. Quantification of PLP staining intensity revealed a reduction in all pScx layers included in the analysis. Due to low PLP levels in superficial cortical layers under control conditions with a gradual increase towards layer 6 (compare fig. 8A), extend of cortical myelin loss was greatest in layer 6 and lowest in layer 1.

To compare extend of myelin loss in the myelin-rich layer 6 with the white matter, the CC was included in the analysis. As demonstrated in fig. 8A, PLP staining intensity in layer 6 was ~50% compared to the myelinated CC (midline) in control animals. After 5 wks cuprizone exposure, PLP staining intensity was comparable in both regions. Thus, extend of myelin loss in layer 6 is still lower compared to the affected CC. We further performed semi-quantitative gene expression of PLP (fig. 8B) and MBP (fig. 8C) mRNAs as markers for myelinating oligodendrocytes in entire cortex samples. As shown, both oligodendrocyte marker mRNAs were already decreased after one week and remained at this low level. Reduction in PLP mRNA transcript levels was more pronounced (5% at week 1 compared to controls; $p<0.001$) compared to the reduction in MBP mRNA levels (47% at week 2 compared to controls; $p<0.05$).

3.3 Demyelination is paralleled by oligodendrocyte loss

We next quantified the number of $Olig2^+$ oligodendrocytes in different pScx layers. Under control conditions, oligodendrocyte numbers gradually increase from layer 1 towards layer 6. As shown in fig. 8D, a reduction of oligodendrocyte cell number could be observed in all layers after 5 wks cuprizone exposure. In layer 1, mean numbers of Olig2-expressing cells declined from 154±17 cells/mm^2 (control) to 119±11 (5wks; not significant), in layers 2/3 from 199±18 to 134±8, in layer 4 from 401±29 to 103±12, and in layer 6 from 773±40 to 211±29, respectively.

Furthermore, numbers of $Olig2^+$ cells in perineuronal and non-perineuronal position (i.e. satellite and myelinating oligodendrocytes, respectively) were quantified in layer 6. As shown in fig. 8E, numbers of satellite (illustrated in fig. 8F) as well as myelinating cortical oligodendrocytes significantly decreased during a 5 wks cuprizone treatment period. Remarkably, percentage decline of either $Olig2^+$ cell population was comparable (-75% for satellite and -73% for myelinating oligodendrocytes, respectively).

3.4 Microglia and astrocyte response are mainly determined by myelin debris

As already pointed out above, astrocytosis and microglia cell invasion and/or proliferation are well-known phenomena during cuprizone-induced demyelination [12, 29, 52, 66, 81]. To asses whether the activation of both cell types depends on the extend of myelin loss, number of $GFAP^+$ astrocytes and $Iba1^+$ microglia were quantified in cortical layers 1 (low extend of demyelination), 4 (intermediate extend of demyelination), and 6 (high extend of demyelination). As shown in figs. 9A/B, IHC for Iba1 to detect microglia/macrophages demonstrated that microglia is uniformly distributed in the pScx in control animals. During cuprizone-induced demyelination, pronounced accumulation of microglia

cells was observed. Microglia accumulation was most severe within the multiform layer 6 next to the demyelinated CC after 5 wks cuprizone treatment (4th column in fig. 9B). A moderate increase in microglia numbers was evident in layer 4 whereas no increase was evident in layer 1 (2nd and 3rd columns in fig. 9B, respectively). Extend of microgliosis was most pronounced in the CC (5th row in fig. 9B).

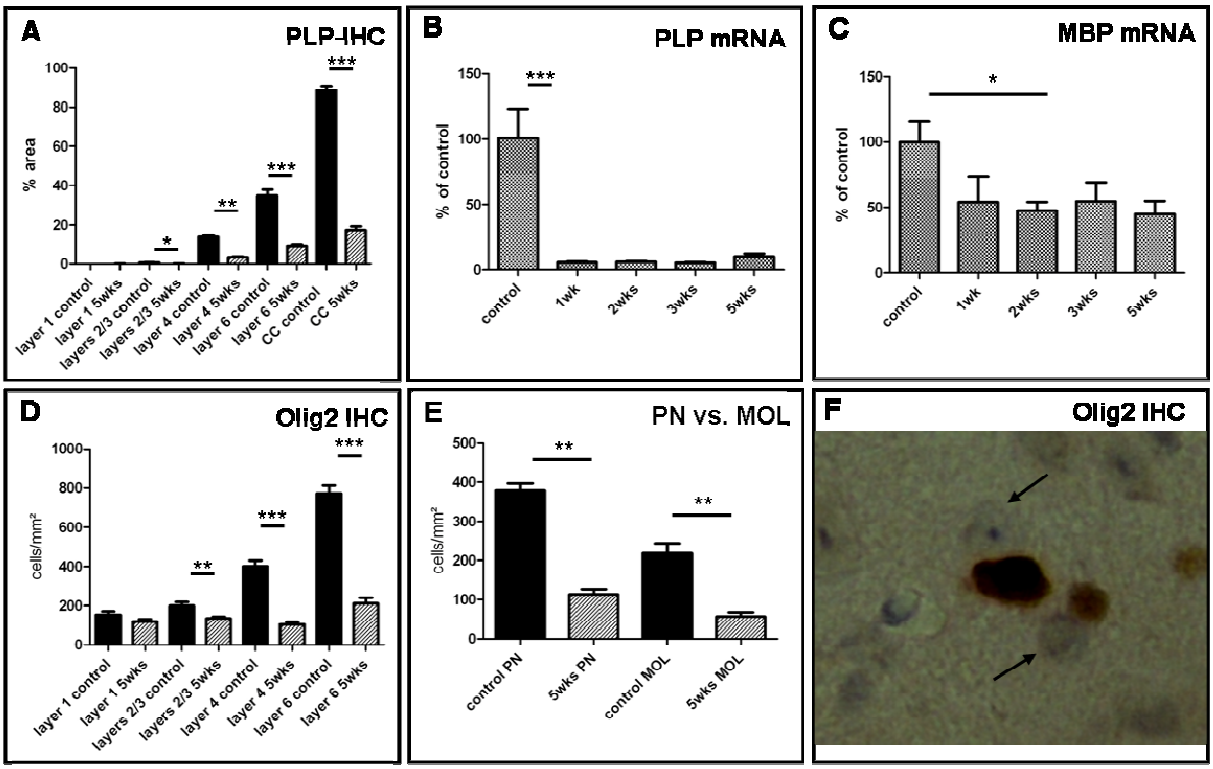


Figure 8

*Effect of cuprizone (up to 5wks, 0.2%) on cortical myelination (anti-PLP staining), myelin-related transcript levels (PLP and MBP mRNA), oligodendrocyte cell numbers (anti-Olig2) and perineuronal vs. satellite oligodendrocytes is presented. (A): Densitometric quantification of PLP-staining intensity in different primary somato-sensory areas (pScx) and the corpus callosum (CC). (B/C): PCR expression analysis of PLP and MBP within the entire cortex, respectively. Each bar represents the averaged fold reduction over untreated control mice of at least six mice per time point (±SEM). Values were normalized against a housekeeping gene (HPRT) and expressed as % of controls. (D): Results of Olig2$^+$ cell number quantification in different primary somato-sensory areas. (E): Results of perineuronal (PN) satellite and myelinating (MOL) oligodendrocyte quantification in layer 6 of the primary somato-sensory cortex of control animals and animals treated 5wks cuprizone. Two satellite oligodendrocytes are illustrated in (F) where oligodendrocytes are visualized by anti-Olig2 staining. Arrows in (F) mark HE-stained neuronal nuclei. Scale bar: 30 µm (F); *p<0.05, **p<0.01, and ***p<0.001.*

To study the time course of microglia activation within the entire telencephalic cortex, CD11b expression analysis was performed after 1, 2, 3 and 5 wks cuprizone treatment and compared to control animals. As shown in fig. 9C, quantification of CD11b mRNA expression in the total cortex without the adjacent CC supports the above observation. CD11b mRNAs were significantly increased after one week of cuprizone exposure (234% compared to controls, p<0.001). Expression remained stable till week 5.

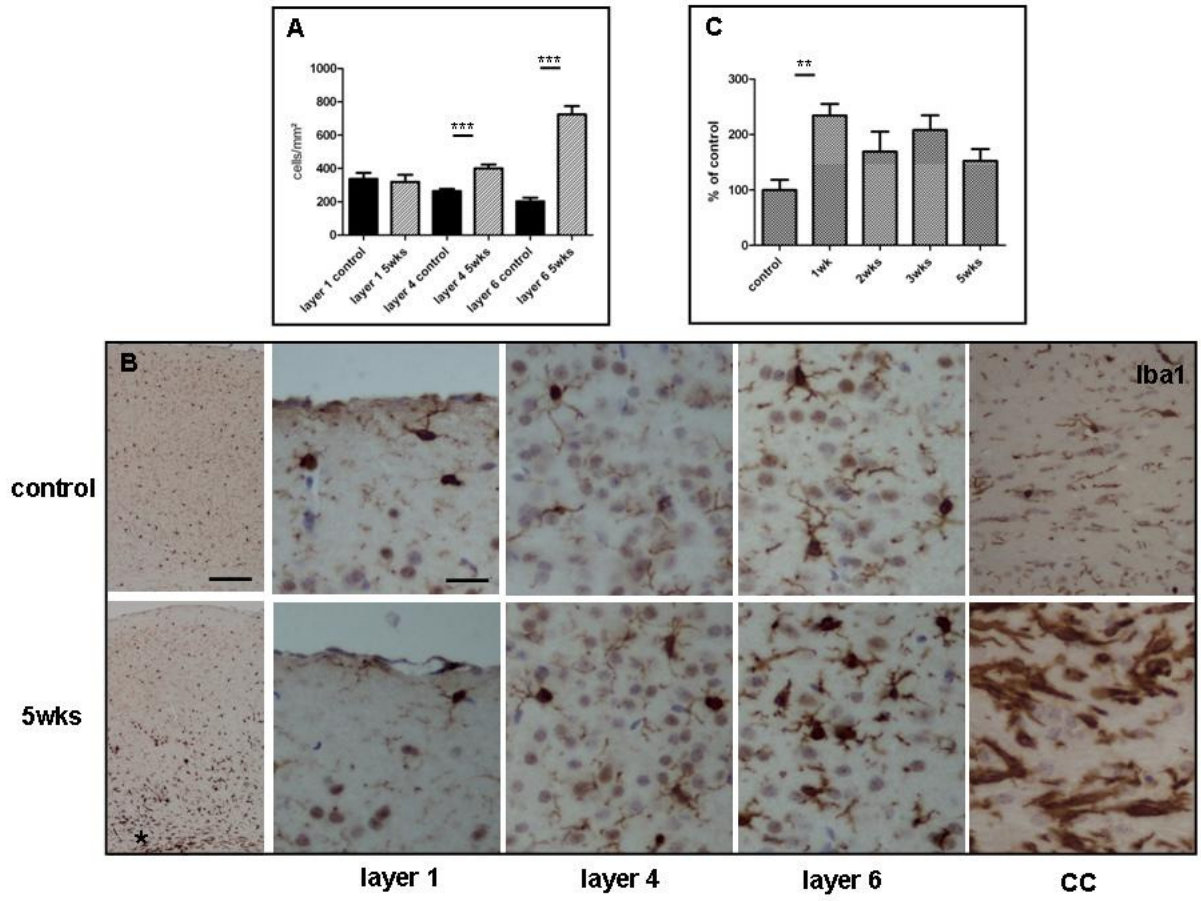


Figure 9

*Effect of cuprizone (up to 5wks, 0.2%) on cortical microgliosis (anti-Iba1 staining) is presented. (A): Results of Iba1$^+$ cell number quantification in different primary somato-sensory areas. (B): Representative anti-Iba1 stained mouse sections of respective primary somato-sensory cortical layers and the corpus callosum (CC). The upper row in (B) shows representative pictures of control animals whereas the lower row shows representative pictures of animals treated 5wks cuprizone. The 1st column in (B) shows an overview of the entire primary somato-sensory area. Respective layers are presented in columns 2-4 in higher magnification. Anti-Iba1 stained corpus callosum sections are presented in the 5th column. Star in the 1st column indicates microglia-rich layer 6 after cuprizone treatment. Note that microglia cells have several processes in the cortex whereas they are amoeboid-shaped in the affected corpus callosum after 5 wks cuprizone-induced demyelination. Real-time RT-PCR expression analysis for CD11b of the entire cortex is presented in (C). Each bar represents the averaged fold induction over untreated control mice of at least six mice per time point (±SEM). Values were normalized against a housekeeping gene (HPRT) and expressed as % of controls. Scale bars: 50 µm (B, 1st column); 20 µm (B, other columns); *p<0.05, **p<0.01, and ***p<0.001.*

Under control conditions, only few GFAP$^+$ cells were present. Within layer 1, GFAP$^+$ cells were regularly detectable within the subpial compartment and build up the glial limiting membrane (arrowheads in fig. 10B). Within layers 2-5, GFAP-expressing cells were usually found around blood vessels (arrow in fig. 10B). Rarely, GFAP$^+$ cells can be found within cortical layers 2-5 apart from blood vessels. In contrast, several GFAP-expressing astrocytes are visible in layer 6 next to the CC (star in fig. 10B). The morphological appearance of astrocytes revealed thin cells with few short processes under control conditions. After cuprizone treatment, astrocytes become hypertrophic and multipolar. As demonstrated in figs. 10A/B, number of GFAP$^+$ cells increased in all layers. However, astrocyte hypertrophy displayed striking regional differences. Superficial layers displayed moderate astrocyte hypertrophy (2nd row in fig. 10B), whereas most severe astrocyte hypertrophy was evident at the border of layer 6 to the white matter tract CC (4th row in fig. 10B). Moderate astrocyte hypertrophy was evident in layer 4 (3rd row in fig. 10B). Extend of astrocytosis (both increase in cell numbers and cell size) was most pronounced in the CC (5th row in fig. 10B). To study the time course of astrocyte activation within the entire telencephalic cortex, GFAP expression analysis was performed after 1, 2, 3 and 5 wks cuprizone treatment and compared to control animals. As shown in fig. 10C, quantification of GFAP mRNA expression in the total cortex without the adjacent CC supports the above observation. GFAP mRNAs were significantly increased after two wks of cuprizone exposure (471% compared to controls, $p<0.001$). Expression gradually increased till week 5 (612%).

3.5 Magnitude of microglia activation in Type 1 multiple sclerosis lesions depends on lesion activity

The results from the cuprizone model implicate that extend of microgliosis depends on the amount of myelin loss and, thus, on myelin debris present in the lesion. Whether the same holds true for MS is, however, not easy to investigate. While white matter lesions can clearly be classified to be active or inactive, most grey matter lesions lack microglia activation making them somehow difficult to stage. Thus, the lack of activated microglia cells in a given grey matter lesion might be because the lesion is already inactive (in other words old) or grey matter lesions do not display microgliosis *per se*. It appears obvious that mixed white-grey matter Type 1 lesions develop at the same time. Thus, the lesion stage of Type 1 lesions can be determined in the respective white matter part of the lesion. Following this attractive strategy, we determined the inflammatory infiltrate in different Type 1 lesions separately for the white and grey matter part. This enables us to analyze the inflammatory infiltrate within the myelin rich white matter and the myelin poor grey matter part. Furthermore, we included the visual cortex in our analysis. This region contains a myelin rich island, the so called "Gennari stripe". If our hypothesis that myelin debris is the major predictor for microgliosis is correct, one would expect more pronounced microglia activation within the demyelinated Gennari stripe compared to the surrounding sparse-myelinated grey matter areas.

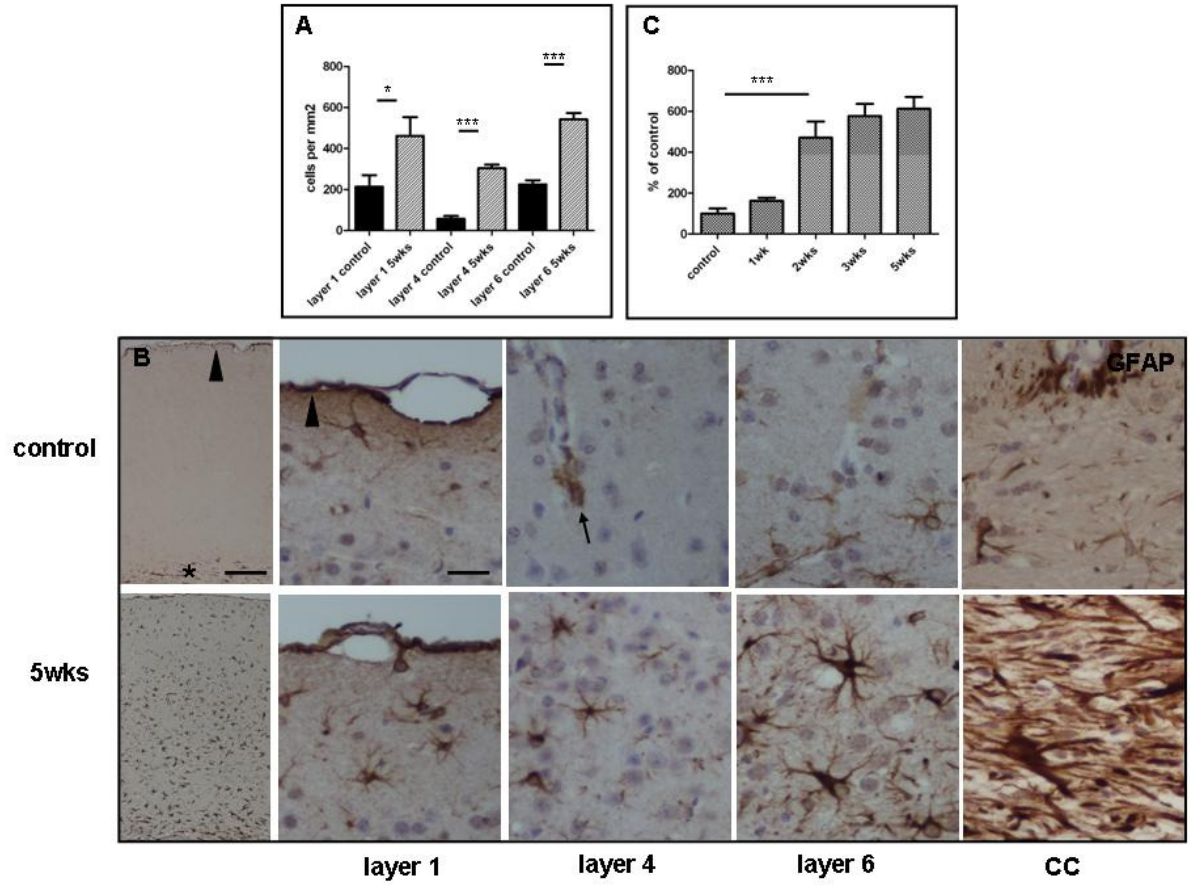


Figure 10

*Effect of cuprizone (up to 5wks, 0.2%) on cortical astrocytosis (anti-GFAP staining) is presented. (A): Results of GFAP$^+$ cell number quantification in different primary somato-sensory areas. (B): Representative anti-GFAP stained mouse sections of respective primary somato-sensory cortical layers and the corpus callosum (CC). The upper row in (B) shows control animals whereas the lower row animals treated 5wks cuprizone. The 1st column in (B) shows an overview of the entire primary somato-sensory area. Respective layers are presented in columns 2-4 in higher magnification. Anti-GFAP stained corpus callosum sections are presented in the 5th column. Star in the 1st column indicates the white-grey matter junction whereas arrowhead indicates the glia limitans. Note the pronounced increase in cell number (hyperplasia) and cell volume (hypertrophy) especially in layer 6 and the corpus callosum after 5 wks cuprizone exposure. Real-time RT-PCR expression analysis for GFAP of the entire cortex is presented in (C). Each bar represents the averaged fold induction over untreated control mice of at least six mice per time point (±SEM). Values were normalized against a housekeeping gene (HPRT) and expressed as % of controls. Scale bars: 50 µm (B, 1st column); 20 µm (B, other columns); *p<0.05, **p<0.01, and ***p<0.001.*

We screened paraffin-embedded *post-mortem* CNS tissues for the presence of cortical Type 1 lesions. From the 167 tissue blocks, we identified and analyzed 26 blocks from 9 MS brains, which contained Type 1 lesions. 13 blocks contained chronic-active, 8 chronic-inactive and 5 active Type 1 lesions. One representative chronic active Type 1 grey matter lesion is shown in fig. 11. As indicated in figs. 11B-D, both parts of the lesion display an almost complete loss of PLP staining intensity. Within the white and grey matter part of (chronic)-active Type 1 lesions, the difference in morphology of LN3$^+$ cells was striking. Within the cortical part, most cells projected processes and retained the morphology of activated microglia (see arrow in fig. 11G). In contrast, regularly amoeboid-shaped LN3$^+$ cells were

present in the white matter part (see arrowheads in fig. 11F). Quantification of microglia/macrophages in different Type 1 lesions is presented in fig. 11A. As expected, $LN3^+$ cell numbers were significantly higher in (chronic)-active white matter lesions compared to (i) NAWM or (ii) chronic inactive white matter lesions (black columns). As demonstrated in fig. 11A, number of LN3-expressing cells was significantly higher in (chronic)-active grey matter lesions compared to (i) NAGM or (ii) chronic inactive grey matter lesions (grey columns). The (chronic)-active grey matter parts contained ~ five times fewer $LN3^+$ cells compared to the respective white matter parts.

To further elaborate extend of $LN3^+$ cell accumulation in the demyelinated cortex as a function of myelin loss, tissue blocks were screened for visual cortex lesions. This region contains a myelin rich cortical layer, i.e. the line of Gennari (layer 4). As shown in figs. 11H-M, the inflammatory infiltrate was found to be more pronounced in the demyelinated myelin rich cortical layer 4 compared to the other affected layers. Within the line of Gennari, LN3-expressing cells were found to be swollen and have just few, short and thick processes. In contrast, $LN3^+$ cells display a more ramified morphology in the other demyelinated layers (compare figs. 11J/M).

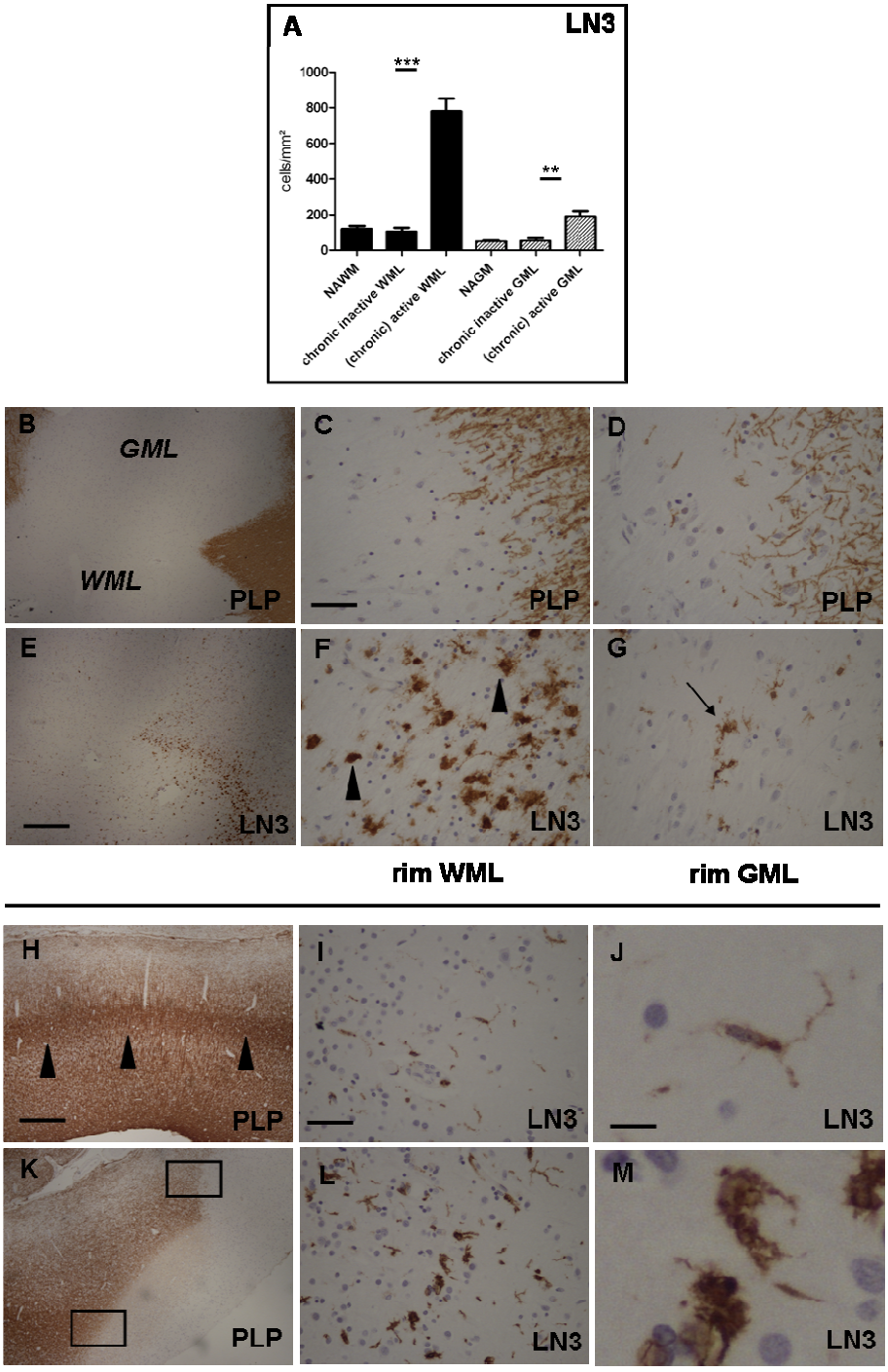


Figure 11

*Myelination and microglia/macrophage response in mixed white-grey matter Type 1 and transcortical Type 4 MS lesions is presented by anti-PLP and anti-LN3 (MHC class-II) IHC, respectively. (A): Results of MHC class II (LN3)$^+$ cell number quantification in grey and white matter parts of different Type 1 cortical lesions (active, chronic active, inactive), normal appearing white matter (NAWM) and normal appearing grey matter (NAGM). (B/E): Overview of a representative anti-PLP (B) or anti-LN3 (E) stained chronic-active Type 1 lesion. As indicated in (B), the lower part represents the demyelinated white matter part (WML), the upper part the demyelinated grey matter part (GML), respectively. (C/D and F/G): Higher magnification view at the lesion rim of anti-PLP and anti-LN3 stained sections, respectively. Arrowheads in (F) indicate amoeboid shaped macrophages. Arrow in (G) indicates a microglia cell with several thin processes. (H-M): Type 4 grey matter lesion of the primary visual cortex (anti-PLP and anti-LN3 IHC, respectively). Arrowheads in (H) indicate the myelin-rich Gennari stripe (layer 4) within the normal appearing grey matter. The upper box in (K) marks demyelinated grey matter in myelin-poor layers 1-2, shown in (I/J) in higher magnification. The lower box in (K) marks demyelinated grey matter in the myelin-rich Gennarri stripe, shown in (L/M) in higher magnification. Note that macrophages within the affected myelin-rich Gennari stripe are amoeboid whereas they are lank with several thin processes in affected myelin-poor superficial cortical layer. Scale bars: 800 µm (B/E/H/K); 20 µm (C/D/F/G/I/L), 10 µm (J/M); *p<0.05, **p<0.01, and ***p<0.001.*

Chapter 4: Brain lipid binding protein expression in activated astrocytes: potential target for remyelination therapy

Parts of this work have been published in Brain Behav Immun. 2011 May 1

Remyelination represents one of the most effective mechanisms to achieve axonal protection in demyelinating disorders. Remyelination is believed to restore the structural integrity of the axon-myelin unit and axonal conduction properties that are lost following demyelination [41, 82]. It is unresolved why in some patients remyelination is widespread while in others, it is sparse. The increasing importance of axonal damage and loss as the pathological basis for progressive loss of function in MS demands a better understanding of the remyelination processes in MS and possible reasons for its failure. Several mechanisms have been suggested that may result in a blockade of remyelination. The loss and destruction of oligodendrocyte progenitor cells within the lesions in the course of repeated de- and remyelination might play an important role [83]. In some lesions, however, progenitor cells are present [44-47], but remyelination still fails either because axons are not permissive for remyelination [48] or the maturation of progenitor cells is inhibited [49].

Glial cells, and particularly astrocytes, were found to be highly abnormal early in the course of MS. They undergo several morphological and biochemical changes referred to as reactive astrogliosis. The hallmarks of astrogliosis are hypertrophy of cellular processes, up-regulation of GFAP and vimentin, and re-expression of developmentally-related proteins such as nestin [84]. Astrogliosis varies quantitatively and qualitatively depending on the nature of injury and its micro-environment. It is likely that reactive astrocytes represent a heterogeneous population [59]. Consequently, activated astrocytes have been described as either beneficial or detrimental in CNS recovery after injury [84]. Factors responsible for the biochemical heterogeneity of reactive astrocytes are not known and nor are their different functions *in vivo* well understood. Regional differences in astrocytes, their activation state and the timing after injury may determine their function and their capability to aid or inhibit remyelination. Benefit may be gained from reactive astrocytes during early demyelination events, whereas later after demyelination, the net effect may be inhibitory for remyelination.

The cuprizone model is well-suited to study brain intrinsic events during demyelination and remyelination [3]. In this animal model, extensive remyelination is evident after acute demyelination whereas remyelination is impaired after prolonged cuprizone exposure.

Brain lipid binding protein (BLBP) belongs to the family of fatty acid-binding proteins (FABPs). FABPs are cytoplasmic 14-15 kDa proteins which are supposed to be involved in fatty acid uptake, transport, and targeting. Ten FABP genes have been identified showing a specific tissue distribution [85]. Brain FABP, also called FABP7 or BLBP, is widely used as a radial glia cell marker [5, 86-88] and expressed in cells of the astrocyte lineage [63, 89].

The aim of this study was to elucidate differences in brain intrinsic gene expression during an early and late demyelinating event and to relate gene expression profiles to remyelination and its failure. To

this end, we performed Affymetrix GeneChip® analysis from RNA of dissected CC after acute (5 wks) and chronic (13 wks) cuprizone-induced demyelination. Our findings clearly show a correlation between inflammatory gene transcripts and remyelination. Furthermore, BLBP expression by activated astrocytes is highly up-regulated during early disease courses but declines as disease progresses. Expression of BLBP in activated astrocytes was further corroborated in the EAE model and early vs. late human MS disease stages. The number of BLBP-expressing astrocytes declines with MS disease duration. *In vitro* studies demonstrated that the induced expression of BLBP in BLBP-negative human malignant glioma cell lines (U87) enhances the expression of fibroblast growth factor 2 (FGF2), platelet-derived growth factor alpha polypeptide (PDGF-AA), and osteopontin (SPP1).

4.1 Remyelination is limited after prolonged cuprizone exposure despite the presence of oligodendrocyte progenitor cells

We first reassessed the remyelination capacity of brains after acute and chronic cuprizone-induced demyelination. Remyelination capacity was tested after a 4-wk remyelination period after acute (5 wk) and chronic (13 wk) cuprizone-induced demyelination. Under these conditions, the CC is severely demyelinated after 5 and 13 wks of cuprizone treatment as demonstrated by anti-PLP IHC (figs. 12A-C; medial part of CC shown in higher magnification in figs. 12D-F). The myelin status of the CC significantly improves after acute demyelination during a 4 wk follow-up period as demonstrated by definite recovery of PLP immunoreactivity. In contrast, endogenous remyelination almost completely fails after chronic cuprizone exposure (figs. 12G/H). Within the acutely and chronically demyelinated lesions APC-positive oligodendrocytes can be found (figs. 12I/J). Additionally, we quantified $Olig2^{strong+}$ oligodendrocyte progenitor cell (OPC) numbers (figs. 12K/L). No significant difference was observed between the acutely and chronically demyelinated CC. Mean numbers were 345 ± 42.7 after acute vs. 427 ± 8 after chronic demyelination with $p = 0.21$. These findings clearly demonstrate that in the chronically demyelinated CC, remyelination is highly impaired despite the presence of pre-mature oligodendrocytes.

4.2 Remyelination appears to be limited due to the absence of pro-myelination factors

To identify genes which are differentially regulated after acute and chronic demyelination and, therefore, might be involved in endogenous remyelination, we used Affymetrix GeneChip® arrays as previously published [60]. Two different analytical approaches were performed. The first approach assumes that potential pro-myelination factors display an abundant expression after acute demyelination, whereas expression of these factors is reduced, when remyelination fails (fig. 13A, pattern I).

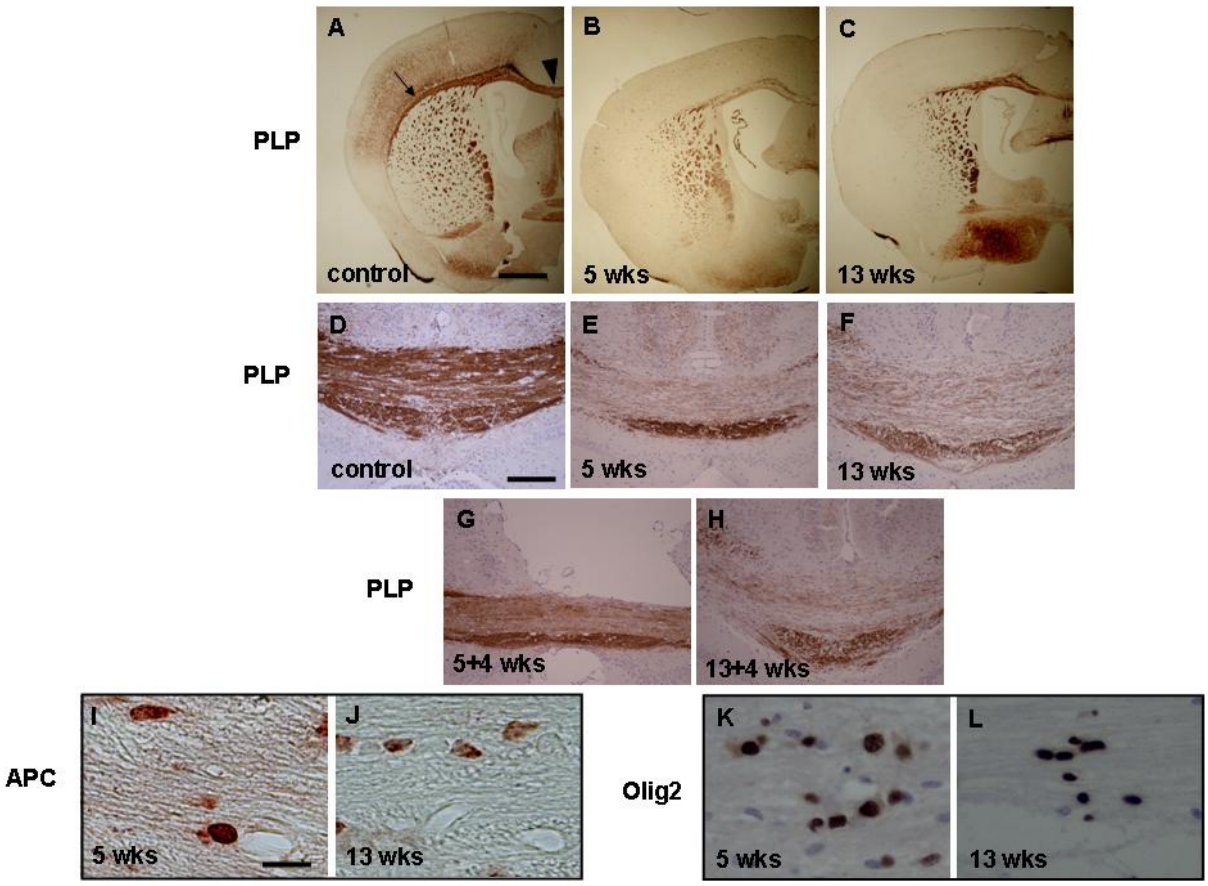


Figure 12

Remyelination capacity after cuprizone-induced acute (5 wks) and chronic (13 wks) demyelination is presented. (A-H): Myelination of the midline of corpus callosum after different cuprizone treatment periods (anti-PLP IHC). In control animals, the medial (arrowhead in A) and lateral (arrow in B) part of the corpus callosum are well myelinated. (B/C) show by an overview that both parts of the corpus callosum are severely demyelinated after 5 and 13 wks cuprizone treatment. (D-H): Higher magnification views (anti-PLP IHC). Note that significant remyelination occurs after acute demyelination (G), indicated by recovery of PLP immunoreactivity within the medial part of the corpus callosum whereas this region is almost devoid of any PLP^{+} fibres in the chronically demyelinated group (H). (I/J): Visualization of late-stage oligodendrocytes (anti-APC IHC). Note that both lesions contain several APC^{+} oligodendrocytes. However, oligodendrocytes display a shrunken morphology in the chronically but not acutely demyelinated corpus callosum. (K/L): Visualization of oligodendrocyte progenitor cells (anti-Olig2 IHC). Note the presence of $olig2^{strong+}$ oligodendrocyte progenitor cells after acute and chronic demyelination. Scale bars: 1 mm (A-C); 30 µm (D-H); 10 µm (I-L).

The second approach assumes that potential anti-myelination factors display an expression down-regulation after acute demyelination, whereas suppression of these factors is not present in the chronically demyelinated brain (fig. 13A, pattern II). Evaluation of Affymetrix GeneChip® analysis revealed that many genes followed pattern I whereas far less genes followed pattern II. The number of genes following pattern I depending on the strictness of criteria applied is presented in fig. 13C (strictness increases with y value, see fig. 13B). Eight genes followed pattern I with y = 0.8, 20 genes

with y = 0.7, 44 genes with y = 0.6, 74 genes with y = 0.5, 118 genes with y = 0.4, and 168 genes with y = 0.3, respectively. For y = 0.5, just 5 genes followed pattern II (see table 1).

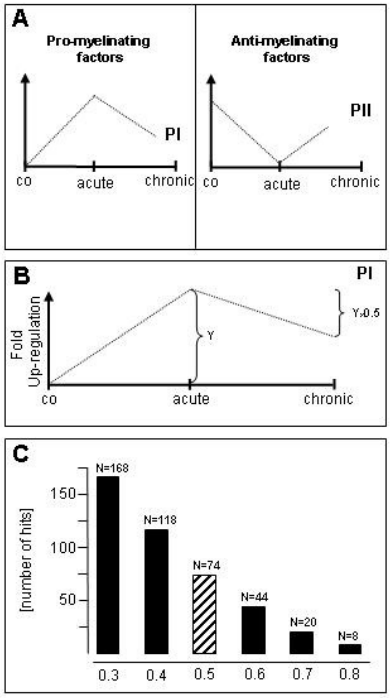


Figure 13

Applied strategy for gene-array evaluation is presented. (A): Anticipated expression patterns of pro-myelinating and anti-myelinating factors. (B): Mathematical formula used as inclusion criteria depending on the strictness of the applied criteria. (C): Number of genes following pattern I depending on strictness of inclusion criteria applied. Note that strictness of inclusion criteria increases with y value. Hatched column in (C) indicates that 74 genes follow pattern I for y = 0.5 which are listed in table 3.

4.3 Inflammatory response is critical for endogenous remyelination

Genes detected to follow pattern I (for y = 0.5, see hatched column in fig. 13C) were grossly categorized according to their biological function given by the Gene Ontology database (*http://www.geneontology.org*). One should note that the relatively strict standards applied (see materials and methods section) are likely to generate false-negative signals but less likely to produce false-positive signals. The most impressive finding is the predominance of immune and stress-response factors of genes following pattern I (see table 1). Many of the discovered genes are related to microglia/macrophages activation. Such genes include dedicator of cytokinesis 2 (Dock2) [90], or integrin alpha M (Itgam, CD11b) [91]. Others which are implicated to be involved in oligodendrocyte

maturation, such as insulin-like growth factor 1 (IGF1) [92], or secreted phosphoprotein 1 (SPP1, osteopontin) [93] also followed pattern I.

Pattern I genes

Phagocytosis
GO:0042116; GO:0050766; GO:0006909

Gene symbol	***Gene name***	Alternative
Slc11a1	natural resistance-associated macrophage protein 1	Nramp1
Fcgr2b	Fc receptor, IgG, low affinity IIb	CD32
Fcgr3	Fc receptor, IgG, low affinity III	CD16
Vav1	vav 1 oncogene	

Cell adhesion
GO:0007155

F11r	Junctional adhesion molecule 1	Jam1
Ly9	lymphocyte antigen 9	CD229
Itgb2	integrin beta 2	CD18, Mac1b
Lgals3bp	lectin, galactoside-binding, soluble, 3 binding protein	Cycap
Itgb5	integrin beta 5	
Csf3r	colony stimulating factor 3 receptor (granulocyte)	CD114; G-CSFR
Spp1	secreted phosphoprotein 1; osteopontin	Opn
Itgam	integrin alpha M	cd11b
Itgax	integrin alpha X	cd11c

Chemotaxis
GO:0006935; GO:0030593

Fcgr3	Fc receptor, IgG, low affinity III	CD16
Itgb2	integrin beta 2	CD18, Mac1b
Dock2	dedicator of cyto-kinesis 2	MBC
Ccl6	chemokine (C-C motif) ligand 6	C10
Csf3r	colony stimulating factor 3 receptor (granulocyte)	CD114; G-CSFR
Cxcl10	chemokine (C-X-C motif) ligand 10	IP10
C3ar1	complement component 3a receptor 1	

Inflammatory response
GO:0006955; GO:0006954

Slc11a1	natural resistance-associated macrophage protein 1	Nramp1
Fcgr2b	Fc receptor, IgG, low affinity IIb	CD32
Lilrb4	leukocyte immunoglobulin-like receptor, subfamily B, member 4	CD85K
Irgm1	immunity-related GTPase family M member 1	Lrg-47
Ccl6	chemokine (C-C motif) ligand 6	C10
Ly86	lymphocyte antigen 86	MD1
S1pr3	sphingosine-1-phosphate receptor 3	Edg3
Cd180	Lymphocyte antigen 78	Ly78
H2-D1	histocompatibility 2, D region locus 1	
Vav1	vav 1 oncogene	
Serping1	serine (or cysteine) peptidase inhibitor, clade G, member 1	C1-inhibiting factor
C1qb	complement component 1, q subcomponent, beta polypeptide	
C1qc	complement component 1, q subcomponent, C chain	
Oasl2	2'-5' oligoadenylate synthetase-like 2	

Cxcl10	chemokine (C-X-C motif) ligand 10	IP10
Clec7a	C-type lectin domain family 7, member a	BGR

Cell proliferation and differentiation
GO:0021846; GO:0050679; GO:0042127; GO:0030154; GO:0008283

Fabp7	fatty acid binding protein 7, brain	BLBP
Grn	granulin	PCDGF
Plau	plasminogen activator, urokinase	uPA
Lgals3	lectin, galactose binding, soluble 3	Mac2
Lipa	lysosomal acid lipase A	
Ifitm3	interferon induced transmembrane protein 3	Cd225

Regulation of apoptosis
GO:0043065; GO:0006916; GO:0006917;

Ptprc	protein tyrosine phosphatase, receptor type, C	CD45
Igf1	insulin-like growth factor 1	
Tgfbr1	transforming growth factor, beta receptor I	
Spp1	secreted phosphoprotein 1; osteopontin	Opn

Lipid metabolism
GO:0016042; GO:0006631; GO:0016042

Pld4	phospholipase D family, member 4	
Adfp	adipose differentiation related protein	
Hpgd	hydroxyprostaglandin dehydrogenase 15 (NAD)	pgdh1
Lpl	lipoprotein lipase	

Others

Cd48		BCM1
Gas2l3	growth arrest-specific 2 like 3	
Ramp3	receptor (calcitonin) activity modifying protein 3	
Havcr2	hepatitis A virus cellular receptor 2	Tim3
Cd68	macrosialin	Scard1
Hist1h1c	histone cluster 1, H1c	
Drd1a	dopamine receptor D1A	gpcr15
Lcp1	lymphocyte cytosolic protein 1	l-plastin
Prkcd	protein kinase C, delta	pkcd
Cyth4	cytohesin 4	pscd4
Nckap1l	NCK associated protein 1 like	hem1
Osmr	oncostatin M receptor	
Klhl6	kelch-like 6 (Drosophila)	
Trem2	triggering receptor expressed on myeloid cells 2	
Csf1r	colony stimulating factor 1 receptor	CD 115; M-CSFR
Slc15a3	solute carrier family 15, member 3	
Ms4a6c	membrane-spanning 4-domains, subfamily A, member 6C	
Ifit3	interferon-induced protein with tetratricopeptide repeats 3	garg49
Cst7	cystatin F (leukocystatin)	
Gbp3	nterferon-inducible guanylate binding protein 3	
Gbp2	Interferon-inducible guanylate binding protein 2	
Cd53	CD53 antigen	Tspan25
Lyn	Yamaguchi sarcoma viral (v-yes-1) oncogene homolog	
Cd52	CD52 antigen	CAMPATH-1
Gusb	glucuronidase, beta	
Capg	capping protein (actin filament), gelsolin-like	mbh1
A2m	alpha-2-macroglobulin	

Lag3	lymphocyte-activation gene 3	CD223
Tyrobp	TYRO protein tyrosine kinase binding protein	dap12
Trim30	tripartite motif-containing 30	rpt1

Pattern II genes

Nova1	neuro-oncological ventral antigen 1	
Ndst3	deacetylase/N-sulfotransferase (heparan glucosaminyl) 3	Hsst3
Cux2	cut-like homeobox 2	Cutl2
Neurod6	neurogenic differentiation 6	Ath2
Oscar	osteoclast associated receptor	

Table 1

Transcripts altered in remyelination and non-remyelination lesions. Genes are grouped according to their biological function given by the Gene Ontology (GO) project. Respective GO numbers are given.

4.4 Validation of Affymetrix GeneChip® analysis

To test the validity of Affymetrix GeneChip® analysis, two different strategies were followed. First, we measured the expression of genes reported in the literature to be repressed or induced under cuprizone challenge by rtPCR and compared these results with data from the Affymetrix GeneChip® evaluation. As expected, rtPCR revealed that demyelination and oligodendrocyte apoptosis lead to the rapid down-regulation of oligodendrocyte- and myelin-related genes after acute and chronic demyelination. These include myelin oligodendrocyte glycoprotein (MOG), PLP, myelin-associated oligodendrocyte basic protein (MOBP), or myelin-associated glycoprotein (MAG). On the other hand, expression of inflammatory and stress-response genes, such as GFAP, chemokine (C-C motif) ligand 3 (CCL3, Mip1α), or chemokine (C-C motif) ligand 6 (CCL6) were dramatically increased. Affymetrix GeneChip® evaluation displayed the same regulation pattern (data not shown). Expression of those genes being up-regulated in rtPCR analysis were induced in Affymetrix GeneChip® evaluation as well and *vice versa*.

Secondly, we verified the expression of 6 randomly selected genes following the pro-myelination pattern I for Y=20/15 (50%) as indicated in fig. 14. rtPCR expression analysis revealed that 5 out of 6 genes display the suggested pro-myelination expression pattern I, i.e. abundant expression after acute demyelination but low expression after chronic demyelination and in control samples. Genes included were adipose differentiation related protein (Adfp), cystatin F (leukocystatin; Cst7), yamaguchi sarcoma viral oncogene homolog (Lyn), interferon-induced protein with tetratricopeptide repeats 3 (Ifit3) and insulin-like growth factor-1 (IGF1) (see fig. 14). rtPCR analysis revealed that protein kinase C, delta (Prkcd) did not follow pattern I expression. Taken together, these results show that the applied Affymetrix GeneChip® approach is a valid method to estimate changes in gene expression after acute and chronic demyelination. If stricter criteria were applied (Y>20/15), all genes analyzed by rtPCR followed pattern I suggesting that this analysis would result in many false negative genes. In

contrast, rtPCR analysis revealed increasing numbers of false positive results if weaker criteria (Y<20/15) were applied. Therefore, the 50% subgroup is presented.

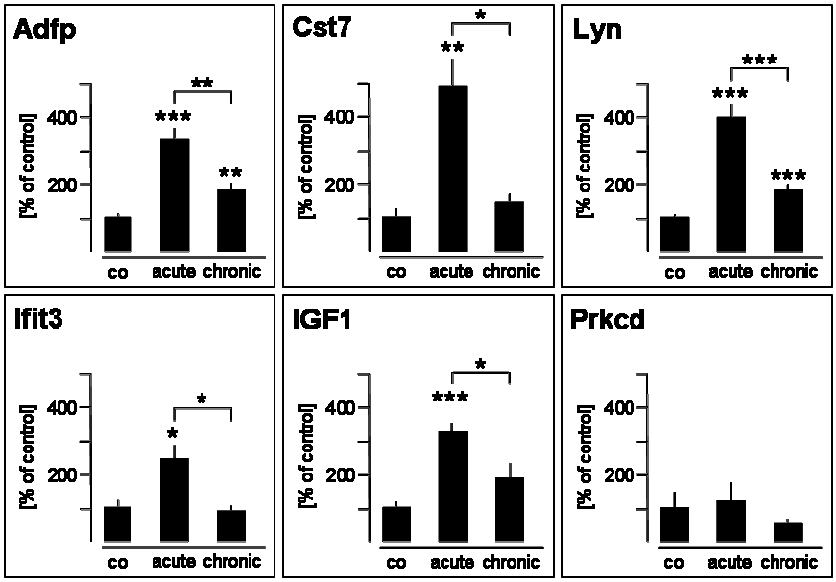


Figure 14

*Quantitative real-time RT-PCR expression analysis of 6 randomly chosen genes following the pro-myelination pattern I as indicated by the array analysis is presented. Each bar represents the averaged fold induction over untreated control mice of at least six mice per time point (±SEM). Values were normalized against a housekeeping gene (HPRT) and expressed as % of controls (*p<0.05, **p<0.01, and ***p<0.001). Note that 5 out of 6 genes follow the anticipated expression pattern I as indicated by the array analysis.*

4.5 Inflammatory cell composition differs between acute and chronic lesions

Since most genes following pattern I are related to microglia/macrophages activity, we speculated that the acutely demyelinated CC contains more microglia cells compared to the chronically demyelinated CC. Therefore, we aimed to characterize lesions used for the array analysis in detail using IHC. As shown in fig. 15A, cuprizone exposure induced a severe loss of PLP-reactive fibres and myelinated axons (as demonstrated by semi-thin sections) within the CC. The quantitative evaluation of APC^+ cells within the midline of CC is presented in fig. 15C and shows a significant loss of APC^+ oligodendrocytes after both acute ($p<0.01$) and chronic ($p<0.001$) cuprizone-induced demyelination. There is also a trend towards lower numbers of APC^+ cells in the chronically demyelinated compared to the acutely demyelinated CC, although no significant difference was detectable (fig. 15C). These results correspond well with mRNA expression levels of PLP obtained by rtPCR (data not shown). During cuprizone-induced demyelination, higher numbers of $GFAP^+$ astrocytes are seen within the CC compared to controls (fig. 15A, left column).

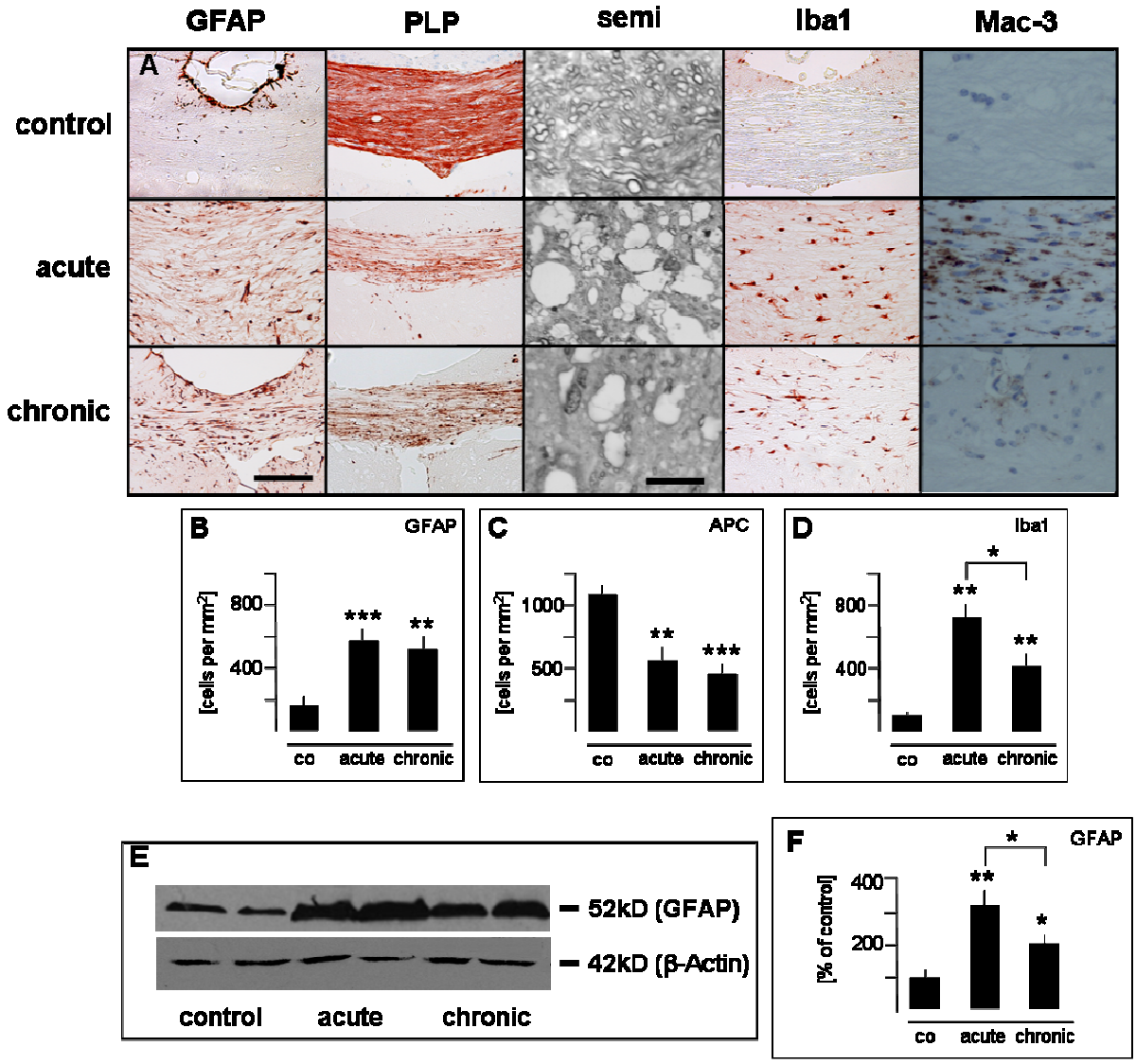


Figure 15

*Myelination and inflammatory cell composition in the medial corpus callosum (CC) of control (upper row in a), acutely (middle row in a), and chronically demyelinated brains (lower row in a) is presented. Brains were fixed at the same time-point as tissue was dissected for array analysis (i.e. control, 5/13 wks cuprizone followed by 2 days recovery as described in materials and methods). Anti-GFAP antibodies were used to visualize astrocytes (1st column in a), anti-PLP antibodies and semi-thin sections were used to visualize myelin (2nd and 3rd column in a, respectively), anti-Iba1 antibodies to visualize microglia/macrophages (4th column in a), and anti-Mac-3 antibodies to visualize activated microglia/macrophages (5th column in a). (B/C/D): Quantification of astrocytes, oligodendrocytes, and microglia cell number is shown, respectively. (E): Representative Western-blot analysis of GFAP levels within the entire corpus callosum. (F): Quantification of GFAP protein levels. Note that a normal myelination structure in the corpus callosum of control animals can be seen whereas after acute and chronic demyelination the midline of corpus callosum is almost completely demyelinated. Large vacuoles within the myelin sheaths can be observed in acutely and chronically demyelinated lesions. No difference exists in the number of APC^+ oligodendrocytes between the acute and chronic lesion as does not for the marked increase in $GFAP^+$ astrocytes. In contrast, accumulation of (activated) microglia/macrophages is less extensive after chronic compared to acute demyelination. Scale bars: 100 µm in IHC pictures; 2.5 µm in semi-thin sections; *p<0.05, **p<0.01, and ***p<0.001.*

Number of GFAP$^+$ astrocytes did not differ between the 5 and 13 wk group (fig. 15B). Interestingly, rt RT-PCR expression analysis revealed that mRNA transcript levels are significantly higher after acute compared to chronic demyelination despite the same number of GFAP$^+$ cells (data not shown). Due to the discrepancy of GFAP mRNA levels and GFAP$^+$ cell number, we performed western blotting analysis of protein samples isolated from the acutely and chronically demyelinated CC. As shown in figs. 15E/F, levels of GFAP protein are higher after acute (~300% induction compared to controls) compared to chronic demyelination (~200% induction compared to controls). Microglia/macrophages, as detected by Iba1 antibodies, were uniformly distributed in the CC of control animals while a sustained increase in Iba1$^+$ cells was present in the demyelinated CC of both treatment groups (fig. 15A). Quantification of Iba1$^+$ cells showed an increase in both groups, however, the remyelinating CC contains a higher number of Iba1$^+$ cells compared to the chronically demyelinated, non-remyelinating CC (fig. 15D). Anti-Mac-3 IHC revealed that much more activated microglia cells were present in the CC after acute (675 cells per mm^2 ± 94) compared to chronic (239 ± 36) cuprizone-induced demyelination (right column in fig. 15A). In control animals only a few Mac-3$^+$ cells were visible. In summary, it appeared that the active inflammatory infiltrate is more pronounced after acute demyelination compared to the chronically demyelinated CC.

4.6 GFAP$^+$ astrocytes strongly express the radial glia cell marker BLBP in acutely but not chronically demyelinated lesions

Some pro-myelination factors cannot be related to differences in microglia activation but are rather implicated in astrocyte function such as BLBP/FABP7. We focused on BLBP because it is a highly conserved protein in mammals and appears to modulate astrocyte function [63, 94]. We confirmed expression pattern of BLBP obtained by Affymetrix GeneChip® array analysis using rt RT-PCR. As shown in fig. 16A, expression of BLBP is ~2.5-fold higher after acute but not chronic demyelination compared to controls. Next we performed IHC to examine expression of BLBP in acutely and chronically demyelinated lesions at the protein level. As shown in figs. 16C/D, few round shaped BLBP$^+$ cells were observed within the myelinated CC of control animals. In contrast, numerous BLBP$^+$ cells are visible after acute demyelination (fig. 16E/F). Strong BLBP immunoreactivity was detected in the cytoplasm and cellular processes. Furthermore, in some cells, BLBP is also expressed within the nuclear compartment (arrow in fig. 16F). Those cells were PCNA positive as well, indicating proliferation (not shown). In striking contrast, BLBP immunoreactivity is diminished in the chronically demyelinated brain despite the abundant presence of GFAP$^+$ cells (figs. 16G/H and compare fig. 15A). In those lesions, BLBP protein is mainly located within the cellular processes sparing the cytoplasm and nucleus. Immunofluorescence double-labelling revealed that virtually all BLBP-expressing cells also express the astrocyte marker GFAP (fig. 16I).

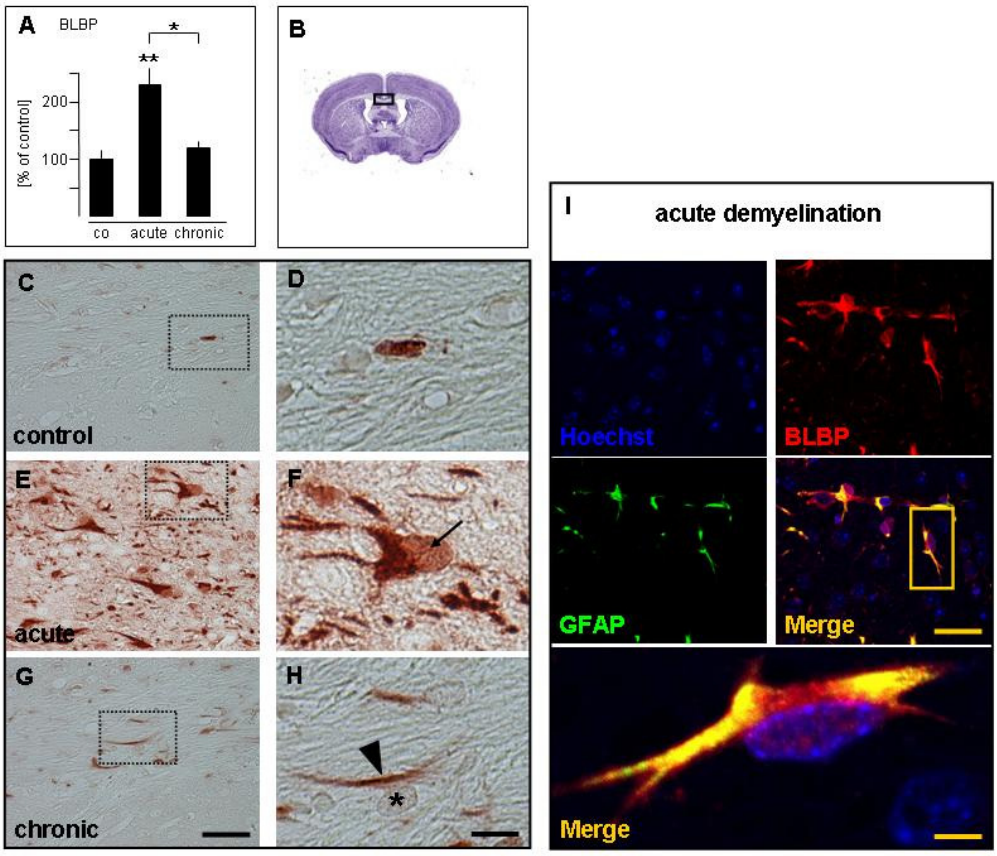


Figure 16

*Analysis of BLBP gene and protein expression after acute and chronic demyelination is presented. (A): Analysis of BLBP mRNA levels. Each bar represents the averaged fold induction over untreated control mice of at least six mice per time point (±SEM). Values were normalized against a housekeeping gene (HPRT) and expressed as % of controls. (B): The medial part of the corpus callosum is indicated. (C-H): Effect of acute and chronic cuprizone exposure on distribution of BLBP-positive cells within the medial corpus callosum. Cells marked by boxes in (C/E/G) are shown in a higher magnification in (D/F/H). Immunofluorescence double-labelling after acute demyelination within the corpus callosum is shown in (I). Appropriate secondary antibodies were used to detect the expression of BLBP (red) after acute demyelination and to co-localize it to astrocytes (GFAP, green). Yellow indicates co-localization of the red and green fluorochromes in the merged pictures. Expression of BLBP is significantly increased after acute demyelination whereas its expression is not induced after chronic demyelination compared to controls. Note that BLBP immunoreactivity can be detected within the cytoplasm, cellular processes, and nucleus (arrow in F) after acute demyelination. In contrast, BLBP protein is mainly located within the cellular processes (arrowhead in H) sparing the cytoplasm and nucleus (star in H) in chronic lesions. Further note that virtually all BLBP-expressing cells are also positive for GFAP. Scale bars: 30 µm (C/E/G); 15 µm (D/F/H); 20 µm and 7.5 µm (I); *p<0.05, **p<0.01, and ***p<0.001.*

4.7 Expression of BLBP in activated GFAP^{+} astrocytes strongly correlates with the presence of Olig2$^{strong+}$ oligodendrocyte progenitor cells in the cuprizone model

We next performed longitudinal studies (control, 1 wk, 2 wks, 4 wks, and 5 wks of cuprizone exposure) and analyzed the occurrence of BLBP^{+} astrocytes during the course of cuprizone-induced demyelination. Furthermore, we determined the correlation of BLBP^{+} astrocytes with (i) the presence of mature oligodendrocytes and oligodendrocyte progenitors, and (ii) the magnitude of microglia cell accumulation in the medial part of the CC. As shown in figs. 17A-E, number of BLBP^{+} astrocytes is still low after 2 wks cuprizone exposure. However, as expected, number of BLBP^{+} cells distinctively increases till week 5. Mean numbers were 112.9 ± SEM 9.8 cells/mm^2 in controls, 295 ± 53.4 at week 1, 267 ± 42.3 at week 2, 721 ± 78.1 at week 4, and 983 ± 125 at week 5, respectively.

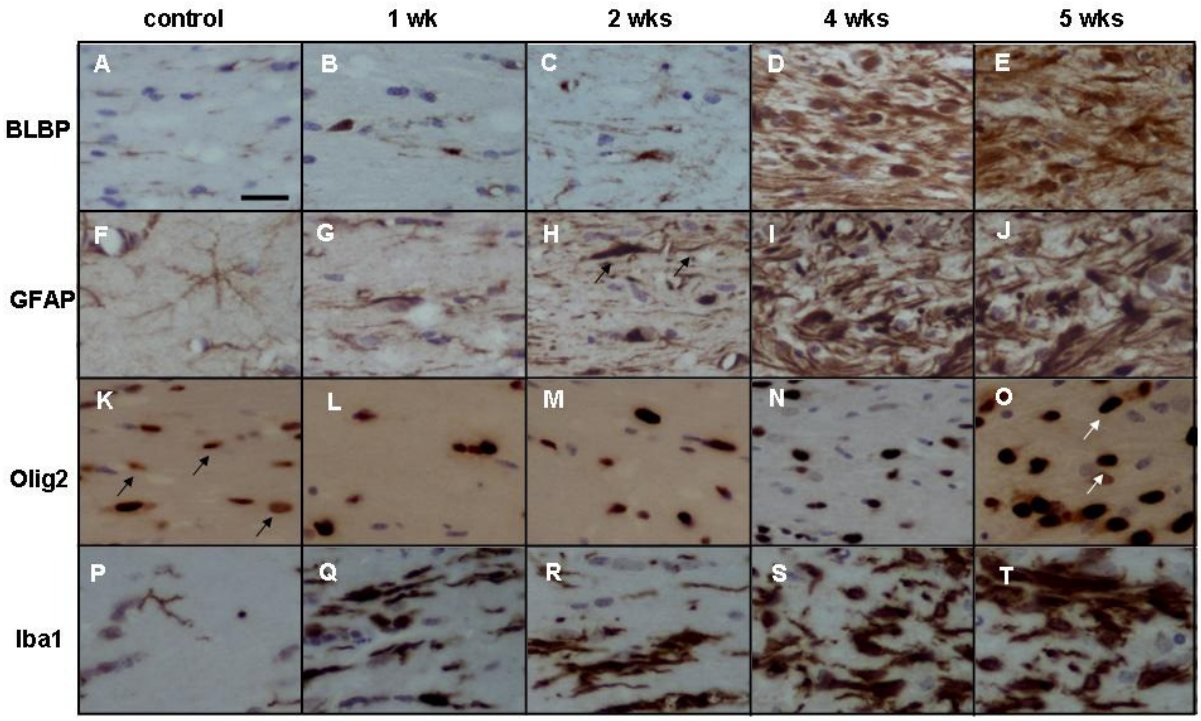


Figure 17

*Time dependent changes (control, 1 week, 2 wks, 4 wks and 5 wks cuprizone feeding) of the cellular composition within the medial corpus callosum are presented by anti-BLBP, anti-GFAP, anti-Olig2 and anti-Iba1 IHC. Significant accumulation of BLBP^{+}- and GFAP^{+} astrocytes can be detected between week 2 and 4 of cuprizone exposure. More GFAP^{+} cell processes can be seen at week 2 (arrows in H). Severe reduction in Olig2^{+} cell number is evident at week 1 and 2. Note the predominance of Olig2^{weak+} cells in the corpus callosum of control animals (arrows in K) whereas most oligodendrocytes are Olig2$^{strong+}$ after 5 wks cuprizone exposure (arrows in O). Further note that significant microglia activation can be detected already at week 1 as demonstrated by increase in Iba1-positive cell numbers (Q). For quantification of cell parameters see Results section. Scale bars: 20 µm; *p<0.05, **p<0.01, and ***p<0.001.*

The numbers of GFAP$^+$ astrocytes follow the same trend as observed for BLBP-positive astrocytes (figs. 17F-J). Already at week 2, more GFAP$^+$ cell processes are visible indicating astrocyte hypertrophy (see arrows in fig. 17H). Number of Olig2$^+$ cells are significantly ($p<0.001$) decreased at week 1 and 2, however, recover till week 5 (figs. 4K-O, $p<0.001$ week 2 vs. week 5). Mean numbers were 2014±168 cells/mm^2 in controls, 958±98 at week 1, 927±83 at week 2, 1215±76 at week 4, and 2249±182 at week 5. Notably, the CC of control animals comprises many Olig2^{weak+} mature oligodendrocytes (arrows in fig. 17K). In contrast, many Olig2$^{strong+}$ oligodendrocyte progenitor cells are present after 5 wks of cuprizone exposure (arrows in fig. 17O). Microglia/macrophages, as detected by Iba1 antibodies are uniformly distributed in the CC of control animals while a sustained increase in Iba1$^+$ cells is present at week 1 and progresses till week 5 (fig. 17P-T).

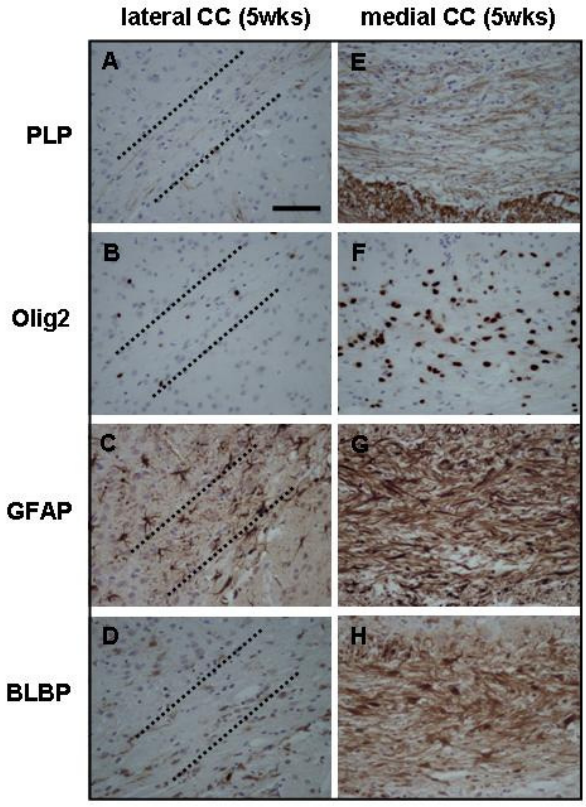


Figure 18

Regional differences in cellular composition and myelin status between the lateral (left side) and medial (right side) part of corpus callosum after 5 wks cuprizone exposure is presented by anti-PLP, anti-Olig2, anti-GFAP and anti-BLBP staining. Note that in contrast to the medial part, the lateral part of the corpus callosum is almost completely devoid of any PLP$^+$ myelinated axons (A/E) and Olig2$^+$ oligodendrocytes (B/F). Severe astrocytosis can be seen in both parts (C/G). In contrast, accumulation of BLBP$^+$ cells is evident solely in the medial (D) but not lateral part (H). Scale bars: 50 µm (A-H).

Furthermore, we compared the medial and lateral part of the CC after 5 wks cuprizone exposure. The lateral part of the CC is almost devoid of PLP immunoreactivity (fig. 18A, outlined by dashed lines) and Olig2^{+} cells (fig. 18B), whereas the medial part contains some PLP^{+} axons (fig. 18E) and, as already pointed out above, many Olig2$^{strong+}$ oligodendrocyte progenitor cells (fig. 18F). Distinctive astrocytosis, as detected by anti-GFAP IHC, is evident in both parts (fig. 18C/G). In contrast, anti-BLBP immunoreactivity is just observed in the medial part (fig. 18D/H).

4.8 Expression of BLBP in activated astrocytes appears not to be directly related to the inflammatory infiltrate

To compare accumulation of BLBP-expressing astrocytes in a toxic and an autoimmune-animal model of MS spinal cord tissue of SJL mice with PLP-induced relapsing-remitting EAE at different disease stages were examined. Clinical signs of relapsing-remitting EAE were first evident on day 9 post-immunization, and disease symptoms rapidly increased, peaking on day 10 (acute phase). Characteristic of relapsing-remitting EAE, this acute phase was followed by a remission (reduction of clinical signs). Anti-PLP IHC revealed significant, yet compared to the cuprizone model moderate demyelination in spinal cord of animals analyzed during the peak phase (8.91 % of area ± 1.71 given in arbitrary units; $p<0.05$ remission vs. peak) whereas no significant difference of PLP staining intensity was observed during the remission phase (17.48 % of area ± 2.15) nor compared to control animals (19.12 % of area ± 1.68). Lumbar spinal cord sections were analyzed for GFAP- and BLBP-expressing cells during the peak phase, remission phase, and in control animals. In the spinal cord white matter of complete freud's adjuvans control mice some GFAP^{+} cells with radially oriented processes towards the pia surface and/or the grey-white matter interface were visible. Occasionally, small stellate BLBP^{+} cells with an astrocyte-like morphology were present in the white matter (mean 1 cell/visual field±0.2). No inflammatory infiltrate (H&E staining) and only a few Iba1^{+} cells (8 cells/visual field ± 1) were seen in control animals (fig. 19A). During the peak phase of EAE, prominent foci of spinal cord inflammatory cells (arrow in fig. 19B) and accumulation of Iba1^{+} microglia/macrophages (29 cells/visual field ± 2) were observed in the spinal cord. In these inflamed regions, many GFAP^{+} cells were visible, indicating commencing astrocytosis (fig. 19B). The number of BLBP^{+} cells with an astrocyte-like morphology did not differ compared to controls (2 cells/visual field ± 0.7). In sharp contrast, accumulation of BLBP^{+} astrocytic cells was clearly evident during the remission phase of the disease (11 cells/visual field ± 2; $p<0.01$ compared to controls) besides significantly less prominent foci of inflammatory cells (fig. 19C). The number of Iba1^{+} cells in remission phase did not significantly differ compared to the lesions analyzed at the peak of disease (24 cells/visual field ± 2). Immunofluorescence double-labelling revealed that most BLBP^{+} cells with an astrocyte-like morphology also expressed the astrocytes marker GFAP (data not shown).

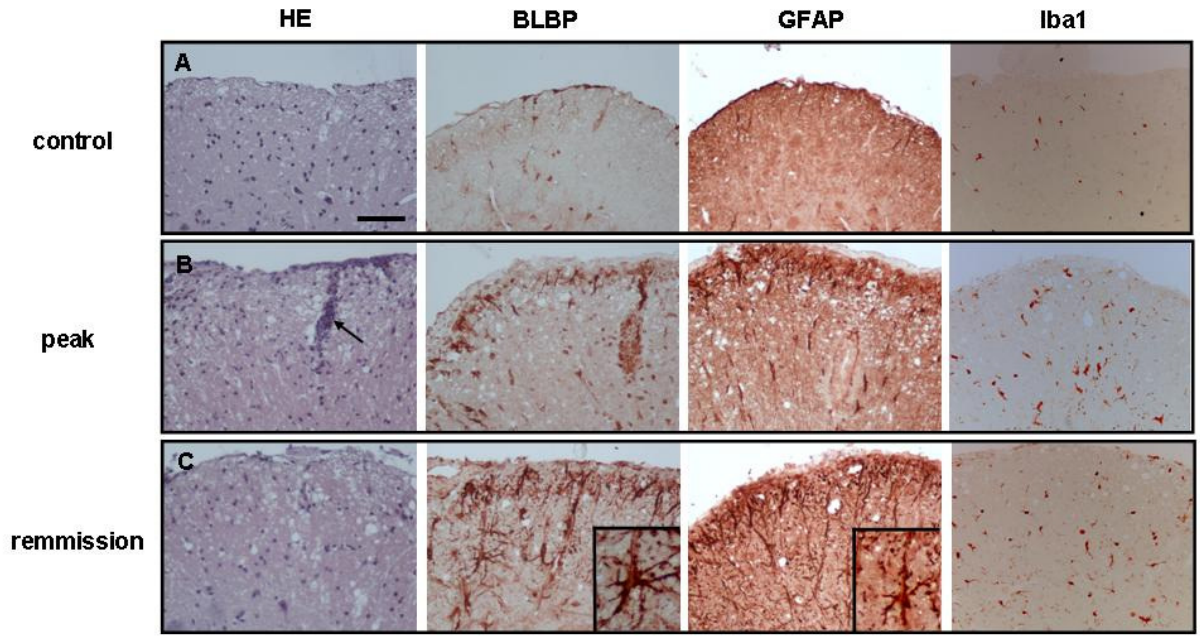


Figure 19

Hematoxylin-eosin (H&E) and immunohistochemistry (anti-BLBP, anti-GFAP, and anti-Iba1) from the lumbar anterior spinal cord white matter of PLP-induced EAE (SJL) animals is presented. (A): control animal. (B): Animal sacrificed during the peak phase of the disease. (C): Animal sacrificed during the remission phase of the disease. The arrow in (B) indicates a perivascular inflammatory infiltrate. In control animals, few BLBP$^+$ or GFAP$^+$ cells are visible, whereas several BLBP$^+$ and GFAP$^+$ cells are characteristic at the region of pronounced inflammatory infiltrate. However, most pronounced accumulation of BLBP$^+$ or GFAP$^+$ cells can be seen during the remission phase with star-shaped BLBP$^+$ and GFAP$^+$ cells (inserts in C). Both lesion types (peak and remission) contain numerous Iba1$^+$ microglia/macrophages. Scale bars: 100 µm.

4.9 Number of BLBP-expressing astrocytes in human MS lesions declines with disease duration

To examine if our findings in mouse models were relevant to human disease, we examined human MS samples from early and late disease stages. Since the efficiency of remyelination decreases with age and disease duration [95-98], selected *post-mortem* material of older patients with long disease duration (mean age = 67 years; mean disease duration = 24 years) was compared with early MS biopsy lesions of younger patients with short disease duration (mean age = 39 years; mean disease duration = 2.3 months). Furthermore, we compared number of BLBP$^+$ cells between (i) the rim of active and chronic active lesion and (ii) the centre of chronic lesions and the NAWM. One representative chronic active lesion is presented in fig. 20 although the NAWM is not shown in the overview since tissue blocks distant from detectable lesions were examined. The lesion centre, indicated in fig. 20A by the upper-box, is devoid of any LFB or anti-PLP reactivity (figs. 20E and H). A few HLA-DR expressing cells can be found (fig. 20K). The rim of the lesion (indicated by the lower

box in fig. 20A) contains thin PLP$^+$ myelin sheaths (fig. 20G) and numerous activated microglia/macrophages (fig. 20J). Within the lesion centre (fig. 20N) as well as in the NAWM (fig. 20L), very few BLBP$^+$ cells are visible. In contrast, the lesion border contains numerous BLBP$^+$ cells with an astrocyte-like morphology (fig. 20M). Numerous cells positive for the oligodendrocyte marker Olig2 (both, strong and weak) were present within the NAWM and the lesion border. In contrast, only a few are detectable in the centre of chronic active and chronic inactive lesions (figs. 20O-Q). Double-staining revealed that BLBP-expressing cells are GFAP$^+$-astrocytes (fig. 20R).

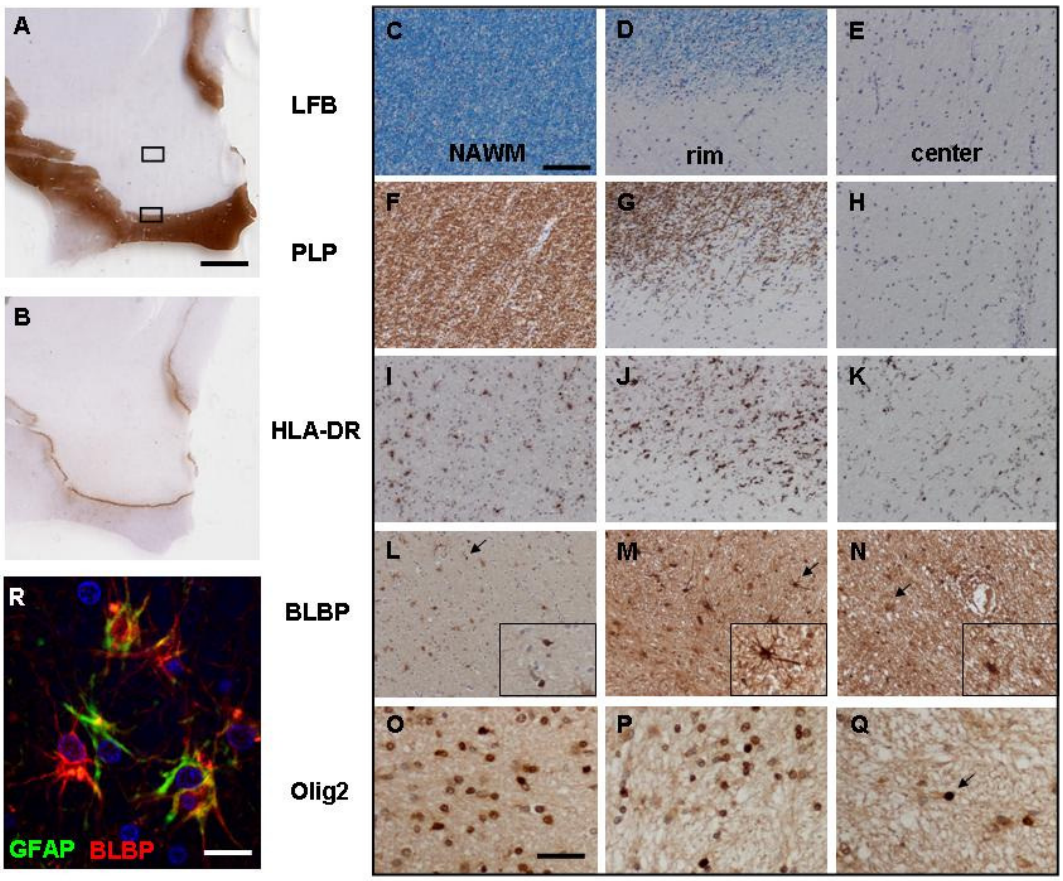


Figure 20

Photograph of an anti-PLP (A, F-H), Luxol fast blue (LFB)–stained (C-E), HLA-DR (B, I-K), BLBP (L-N), and Olig2-stained (O-Q) paraffin-embedded brain tissue section (chronic active lesion) is shown. Upper box in (A) indicates the lesion centre, lower box the lesion border, respectively. Number of HLA-DR positive cells is low in the NAWM and the centre of chronic-active lesions whereas numerous microglia/macrophages are located at the lesion rim. Within the lesion centre some round BLBP-positive cells are visible (arrows in l-n are presented in higher magnification as inserts). In contrast, the lesion border contains numerous BLBP-positive astrocytes. Numerous Olig2$^+$ cells can be found in the NAWM and at the rim of the lesion, whereas the centre of the lesion is almost devoid of Olig2$^+$ oligodendrocytes. Arrow in (Q) indicates an Olig2$^{strong+}$ oligodendrocyte progenitor cell. Co-localization of BLBP and GFAP is demonstrated by immunofluorescence double-labelling in (R). Scale bars: 3 mm (A/B); 30 µm (C-N), 50µm (O-Q), 2.5µm (R).

Representative pictures of biopsy cases are presented in fig. 21. The peri-plaque white matter (PPWM), indicated by the lower box in fig. 21A, contains densely-packed PLP^+ axons (fig. 21B), numerous GFAP-expressing astrocytes (fig. 21E) but only few $BLBP^+$ cells with an astrocyte-like morphology (fig. 21H). In contrast, many $BLBP^+$ cells are visible in the centre of the lesion (fig. 21I) paralleled by the presence of thin PLP-reactive fibres (fig. 21C) and $GFAP^+$ cells (fig. 21F). Quantification of $BLBP^+$ cell numbers are shown in fig. 21J. Since no significant differences in total number of BLBP-expressing astrocytes between (i) NAWM of *post-mortem* tissue and PPWM of brain biopsies, (ii) rim of active and chronic-active lesions, and (iii) centre of chronic inactive and chronic-active lesions could be observed, those data were pooled. No significant difference in total $BLBP^+$ astrocyte numbers was evident between PPWM/NAWM and the centre of chronic active/inactive lesions (16.7 ± 3.9 cells/mm^2).

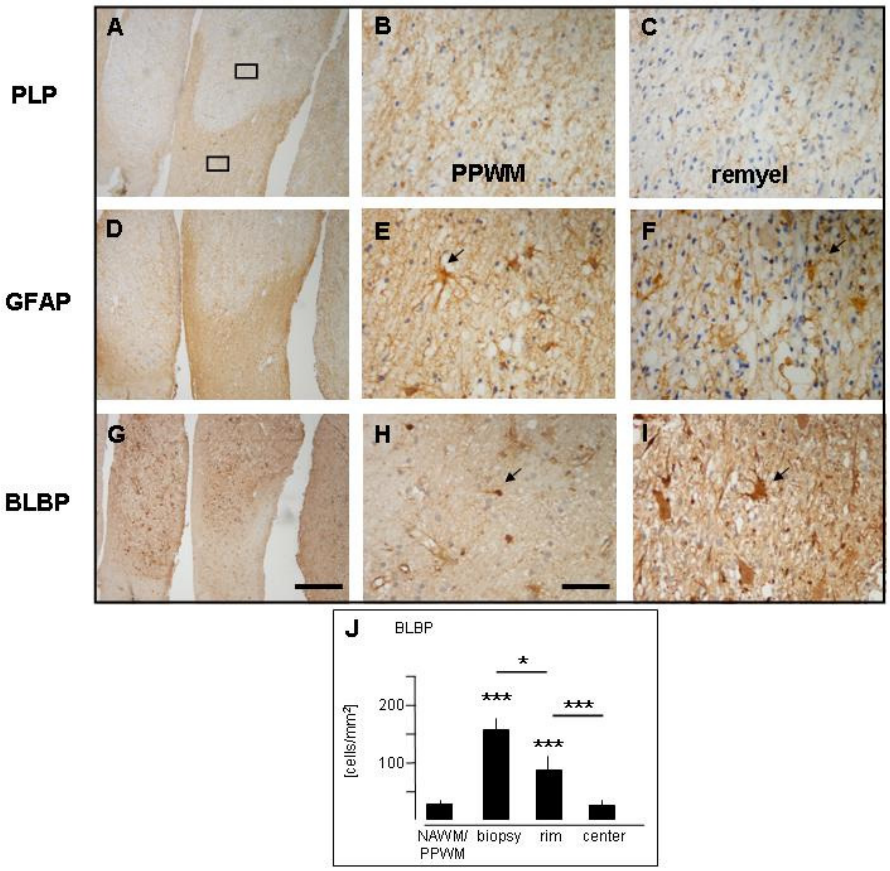


Figure 21

*Photograph of an anti-PLP (A-C), anti-GFAP (D-F) and anti-BLBP (G-I) stained, paraffin-embedded brain tissue section (acute lesion) is shown. Boxes in (A) indicate regions shown in (B/C, E/F and H/I) in higher magnification. The upper box indicates the region with intense remyelination, the lower the peri-plaque white matter (PPWM). In (J) quantification of $BLBP^+$ astrocytes in the normal appearing white matter (NAWM) and peri-plaque white mater (PPWM), the remyelination areas of biopsy human MS material (biopsy), the rim of active and chronic active lesions (rim), and the centre of chronic active and chronic inactive lesions (centre) is presented. Highest number of $BLBP^+$ astrocytes is found within remyelination areas of brain biopsies. Scale bar: 1 mm (A/D/G); 30 µm (B/C, E/F, H/I); *p<0.05, **p<0.01 and ***p<0.001.*

Most BLBP$^+$ astrocytes can be found in demyelinated tissue of biopsy samples (149.2 ± 20.28 cells/mm^2; compare figs. 21H/I), significantly more compared to the rim of (chronic)-active lesions (90.4 ± 20.2 cells/mm^2). BLBP-expressing astrocytes were hardly present within the centre of active lesions or in shadow-plaques in *post-mortem* tissue.

4.10 Expression of BLBP in U87 astrocytoma cells regulates FGF2, PDGF-AA and SPP1 but not IGF1 mRNA expression

It has been reported that BLBP might regulate gene expression [99]. We speculated that BLBP levels in astrocytes might influence expression of growth factors involved in oligodendrocyte maturation, such as IGF1, FGF2, PDGF-AA, or SPP1. To test this hypothesis, the BLBP-negative malignant glioma cell line U87 was stably transfected using a BLBP expression construct as reported previously [63] and expression of the four growth factors was analyzed using rt RT-PCR. As shown in fig. 9A, no expression of BLBP mRNA can be detected in control U87 cultures, whereas U87 cells, transfected using a human BLBP construct, express relevant levels of BLBP mRNA. As shown in fig. 22B, IGF-1 is not expressed in either controls or BLBP-transfected U87 cells. In contrast, levels of FGF2 (100 ± 3 vs. 187 ± 15; $p<0.01$), PDGF-AA (100 ± 17 vs. 172 ± 25; $p<0.05$) and SPP1 (100 ± 9 vs. 231 ± 15; $p<0.01$) mRNA are significantly higher in BLBP-transfected cells when compared to control cultures.

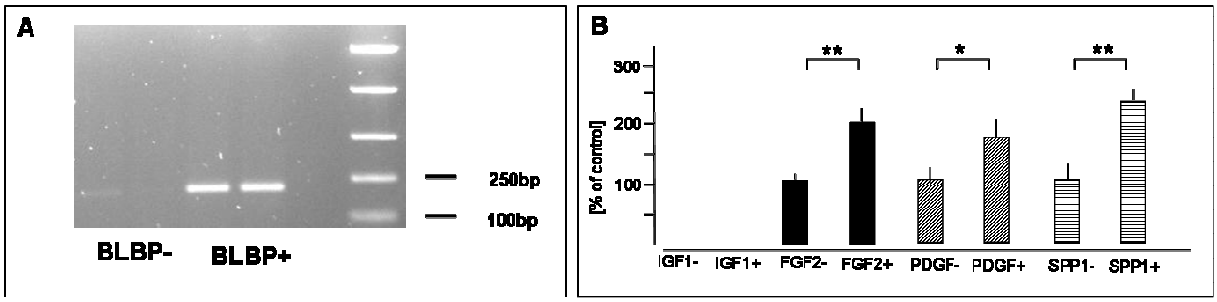


Figure 22

*Expression of growth factors IGF1, FGF2, PDGF-AA and SPP1 in BLBP$^+$ and BLBP$^-$ U87 malignant glioma cells is presented. Values were normalized against a housekeeping gene (18s) and expressed as % of non-transfected controls. (A) demonstrates high levels of BLBP mRNA in transfected cells (right side) compared to control cultures (left side). Note that mRNA levels for FGF2, PDGFAA and SPP1 are significantly higher in BLBP-transfected U87 cells when compared to controls; *p<0.05, **p<0.01 and ***p<0.001.*

Discussion

The results of my thesis can be summarized as follows:

i.) The cuprizone model reflects several features of multiple sclerosis histopathology and, maybe, pathogenesis, as well.
ii.) Brain region specific inflammatory responses are a critical link between oligodendrocyte stress and subsequent fulminant demyelination.
iii.) Myelin loss and, in consequence, myelin debris are important parameters for brain-intrinsic inflammatory responses.
iiii.) Brain lipid binding protein appears to be critically involved in endogenous remyelination processes.

In the following chapter, I would like to critically discuss our major findings and relate them to the current knowledge.

1. The cuprizone model as a tool to study demyelination

As pointed out already in the introduction, profound heterogeneity in the pattern of demyelination among MS patients exists [20, 100], at least in the initial disease stage. In respect of the cuprizone model, pattern III lesions are from great interest. Within these areas, myelin-forming oligodendrocytes show nuclear condensation and fragmentation which are typical signs of apoptosis. Some authors state that the histopathological pattern of cuprizone-induced demyelination resembles type III lesions [101]. Indeed, there are some similarities between both forms. MAG mRNA levels seem to be more down-regulated during early demyelination compared to other myelin protein markers [102], demyelination does not present in a perivenous distribution, borders are ill-defined, and pronounced oligodendrocyte apoptosis can be found in active demyelinating lesions [3]. However, other features of pattern III lesions, such as inflamed blood vessels and the presence of CD3+ T cells, are not observed in the cuprizone model. The later might be due to a direct suppression of cuprizone on T cell function [103, 104]. The question arises, whether cuprizone-induced demyelination models myelin loss observed in MS patients. This assumption is often challenged by experts in the field. The “perfect” MS animal model does not exist. We want to stress that MS is presently regarded as a disorder with many different features and facets. No current experimental animal model covers the entire complexity of MS in humans. Instead, the various animal models and intoxications can be applied to selectively investigate and uncover distinct pathological processes and repair mechanisms of MS [3]. Cuprizone intoxication is a straight forward model to investigate brain-intrinsic inflammatory responses, i.e. microgliosis and astrocyte activation. Furthermore, this model can be fruitful in deepening our understanding of remyelination and its failure, as shown by several groups [12, 105, 106].

In this study, we compared histopathological features of the cuprizone model with MS tissue samples. Cuprizone ingestion in mice induces a highly reproducible demyelination of distinct brain regions, among them the CC which represents the most frequently investigated white matter tract in this animal model [12, 52, 107]. After 5–6 wks of cuprizone treatment, the CC is almost completely demyelinated, a process called “acute demyelination”. Acute demyelination is followed by spontaneous

remyelination during subsequent weeks when mice are fed normal chow. In contrast, remyelination is highly restricted when cuprizone administration is prolonged (12 wks or longer), a process called "chronic demyelination". During late stages of acute demyelination, spontaneous remyelination occurs partially but fails under a continued cuprizone challenge [3]. Our group was able to show that other regions are affected as well. Norkute and colleagues reported that cuprizone treatment induces demyelination and astrocytosis in the mouse hippocampus [29]. However, no significant effect on microglia invasion was detected at any investigated time point (0, 3, 5, and 7 wks). In my thesis I was clearly able to show that distinct hippocampal subregions display significant microgliosis such as the medial alveus or fimbria region at week 5 (see chapter 1). As pointed out above, the magnitude of microgliosis progressed in the CC until week 5, whereas a reduction of microglia cell numbers could be observed in the fimbria after 2 wks cuprizone exposure (compare fig. 6). Furthermore, microgliosis is sparse in the affected grey matter. Due to the fact that A. Norkute mainly focused in her work on hippocampal grey matter structures and included a 3 wks cuprizone period as the earliest time point, early microgliosis might have been missed [29].

As already reported by Geurts and colleagues, hippocampal demyelination is frequent and extensive in MS [68]. We observed hippocampal demyelination to be a frequent phenomenon, as well. In the current study, we investigated the inflammatory response (i.e. microglia activation) within hippocampal white and grey matter regions of MS patients. Affected white matter regions displayed a more severe accumulation of LN3-expressing microglia/macrophages compared to demyelinated grey matter parts. One should note that in MS lesions, $LN3^+$ cells might originate either from brain resident microglia cells or recruited peripheral monocytes. Currently, no reliable marker can differentiate between both cell types. In cuprizone-induced demyelination it has recently been shown that peripheral monocytes are not recruited to the side of tissue injury [108], thus, $Iba1^+$ cells represent activated and/or recruited brain-resident microglia. Future studies have to show whether recruitment of peripheral monocytes differs between white and grey matter lesions in MS.

Pott and colleagues were able to demonstrate that cuprizone intoxication induces a severe demyelination of distinct cortical deep grey matter sub-regions. Striosomes, located within the caudate-putamen and the ventral part of the caudate nucleus displayed intense demyelination, whereas those within the globus pallidus and the head of the caudate nucleus were not affected. The matrix region was equally affected in the medial and lateral region [67]. My thesis shows for the first time to my knowledge that the two key findings in the cuprizone model (i.e. (i) preserved striosomes in regions distant to the ventricles and (ii) equal demyelination of the matrix region irrespective of their anatomical location) are relevant for MS. We were able to show that 8 out of 19 analyzed human basal ganglia lesions (i.e. striatal lesions) displayed a partial or complete preservation of myelinated axons within the striosomal compartment (figs. 5C/D). In contrast, the matrix is almost completely demyelinated (figs. 5G/H). Also not presented within the results section, combined striosome-matrix demyelination was another frequently observed phenomenon in MS. Future studies have to show

whether extend of striosome demyelination can be related to ventricular distance. If so, protective ingredients within the liquor might be considered being protective in MS.

2. Mechanism of cuprizone-induced demyelination

The underlying mechanisms of cuprizone-induced oligodendrocyte cell death are not fully understood. It has been assumed that a cuprizone-induced copper deficit might be detrimental to mitochondrial function in the brain [33] and that it is a disturbance of energy metabolism in oligodendroglia and cell function that leads to demyelination [3, 15]. Why oligodendroglia should be preferentially susceptible to copper deficit is not known, although an obvious hypothesis is that the perikaryon of this cell type has to maintain a vast expanse of myelin and this extraordinary metabolic demand places it in jeopardy if the demand cannot be met. Our data, however, do not support this hypothesis. We were clearly able to show that perineuronal satellite oligodendrocytes are equally vulnerable to cuprizone-induced demyelination compared to myelinating oligodendrocytes in the cortex. Reductions for both cell populations where approximately -75% (compare figs. 8E/F). Satelite oligodendrocytes are assumed to be non-myelinating cells in normal brains, but support adjacent neurons [109]. Our results suggest that oligodendrocyte specific toxicity of cuprizone is not linked to the metabolic demand of myelinating oligodendrocytes. Lack of detailed knowledge of the molecular details of the point of pathological action targeted by copper deficiency remains frustrating, as is our lack of knowledge as to the reason for preferential susceptibility of oligodendroglia in this model [15].

3. What determines microglia activation?

In the current study (chapter I and III) we investigated the relationship between amount of myelin debris (i.e. myelin loss) and microglia activation and astrocytosis in the cuprizone model. Furthermore, we determined microglia/macrophage activation in MS cortical lesions. We focused on Type 1 lesions since lesion “activity” can readily be determined by analyzing the white matter part. Our major finding was that extend of myelin loss is the major predictor for the degree of microglia/macrophage activation. Cortical layers with *a priori* sparse myelin content, such as layer 1 of the pScx displayed no significant increase in microglia cell numbers whereas cortical areas with an *a priori* high myelin content under control conditions, such as layer 6 of the pScx, displayed intense microgliosis. Microglia activation and accumulation was most pronounced in the white matter tract CC where the degree of myelin loss was highest. These observations are in line with results from others [110]. Furthermore, we were clearly able to demonstrate that both, grey and white matter areas in Type 1 MS lesions, display inflammatory activity. Comparable to our results using the cuprizone model, we found less pronounced microglia activation in the grey matter compared to the white matter part of Type 1 lesions. Thus, it appears that the degree of microgliosis in MS lesions is mainly dictated by the extend of myelin loss, at least in Type 1 lesions. The observation of higher local HLA-DR cell numbers within the demyelinated Gennari stripe strengthens our hypothesis.

Although MS has been classically thought of as a white matter disorder, the involvement of grey matter regions was acknowledged in early pathology studies [35]. Since the introduction of myelin IHC, such as anti-PLP or anti-MBP, demyelination of grey matter regions as an important feature in MS pathology has received new impetus. Clinically, grey matter demyelination is of importance. For example, MS patients with cognitive decline have more cortical damage than patients who are cognitively preserved. In one study, there were positive correlations between cortical volume values and performance in verbal memory, verbal fluency and attention/concentration testing in cognitively impaired MS patients [111]. In a later published study, the same group was not able to find any correlation between brain volume changes, deep grey matter volume or changes in lesion load on T2-weighted magnetic resonance imagings (MRIs) and cognitive impaired MS patients. However, patients with cognitive impairment displayed less cortical volume compared to cognitively preserved MS patients [112]. Thus, progressive neocortical grey matter loss is likely to be relevant for MS-associated cognitive impairment.

Based on their location, cortical grey matter lesions are named either Type 1 lesions (mixed white matter-grey matter lesions), Type 2 lesions (purely intracortical lesions), or Type 3 lesions (subpial lesions) [23-26]. Type 3 lesions are most common and can extend over several gyri to involve almost all sampled cortical areas [22, 23, 113]. Furthermore, it has been reported that cortical demyelination is a characteristic feature of progressive MS and is rare or absent in patients with acute or relapsing disease [22].

In our study, 26 out of 167 tissue blocks (~15%) contained cortical Type 1 lesions. Following the autopsy procedure at the VU University Medical Center, tissue blocks were selected on the basis of signal intensity changes in the white matter at post-mortem T2-weighted MRI [113, 114]. Thus, our sampling protocol is biased towards myelin abnormalities and, therefore, might overestimate the actual extend of Type 1 lesions in progressive MS cases. An even higher frequency of cortical Type 1 lesions has been reported by another group [24]. In their study, 38 of 110 tissue blocks (~34.5%) contained cortical Type 1 lesions [24]. In summary, breakthrough of white matter lesions into the grey matter is, obviously, a frequent phenomenon, at least during the progressive disease stage. Several studies investigated a possible correlation between cortical demyelination and white matter changes in MS. It was suggested that cortical lesions are independent of the presence of white matter lesions [22, 113]. However, the emergence of cortical Type 1 lesions appears to be closely associated with white matter pathology. It remains to be clarified whether cortical Type 1 lesions emerge in the grey matter and spread into the white matter or *vice versa*. However, several observations suggest that the later is true. First, the white matter part of most lesions included in this study was by far greater compared to the grey matter part. Second, in some tissue blocks we observed demyelination of deep cortical layers nearby active white matter lesions. Since those lesions do not fulfil the criteria of a “classical” Type 1 lesion, i.e. continuous demyelination of white and grey matter parts, they were not included in the current study. Third, we observed that several so called cortical “Type 4” lesions, extending

throughout the full width of the cerebral cortex, end at the white-grey matter junctions. Although a mild inflammatory reaction was observed within the nearby white matter, demyelination was not evident. This suggests that inflammatory white matter affects grey matter integrity. Findings from Peterson and colleagues [24] highlight the clinical importance of this "white matter attack" at cortical grey matter being evident in Type 1 lesions. They reported transacted axons, transacted dendrites and apoptotic neurons in demyelinated cortical grey matter and observed that the numbers of transsected neurites correlated with the inflammatory activity of the lesions. Further studies have to show whether Type 1 lesions correlate with clinical disability in MS.

Studies on the pathogenesis of grey matter lesions suggest that its underlying disease mechanisms differ between grey and white matter lesion. It has been reported that lymphocyte infiltration is a feature of white but not grey matter lesions. The highest density of $CD3^+$ T cells was found in MS white matter lesions. Fewer T cells were detected in cortical lesions that extended through both white and grey matter (i.e. Type 1 lesions). The lowest number of T cells was detected in intracortical demyelinated lesions (i.e. Type 2 lesions). A similar distribution was found using the CD4, CD8, and CD45RO markers [25]. Brink and colleagues investigated complement deposition in white and grey matter MS lesions. Whereas complement deposition was abundant in white matter lesions, significantly less was observed within the affected grey matter. In purely cortical lesions, the extent of complement deposition in general was lowest [21]. Van Horssen and colleagues recently reported that although blood-brain barrier (BBB) dysfunction is a common feature of white matter MS lesions, cortical MS lesions lack markers for BBB disruption [26]. However, some Type 1 lesions displayed BBB deficits such as serum protein leakage. Taken together, the higher inflammatory phenotype of active Type 1 grey matter lesions is paralleled by a close overlap with the pathology of white matter lesions. However, those tissue alterations are less severe in the grey compared to the white matter. Microglia cells can modulate all of the described parameters. It has been reported that microglia can potentiate damage to the BBB [115-117] and can modulate, together with astrocytes, lymphocyte trafficking [92, 118]. One might speculate that described differences in white and grey matter pathology might be due to the deficiency of myelin-driven microglia response.

In summary, our data demonstrate the importance of myelin loss for microglia activation in both, the white and grey matter. It appears that lack of inflammation in grey matter lesions might be either due to lesion inactivity (i.e. chronic lesions) or low myelin loss, especially in superficial cortical layers. Further studies have to show whether activated microglia actively regulate white matter features in the grey matter, such as lymphocyte infiltration or BBB damage.

4. The cuprizone model as a tool to study remyelination

In this study, we took advantage of the toxic de- and remyelination cuprizone model. In this model, feeding of cuprizone to young adult mice induces oligodendrocyte cell death which is closely followed by microglia and astrocytes activation [3]. Due to an intact BBB, peripheral cell recruitment does not occur [108]. It has been postulated that remyelination completely fails after a chronic demyelination

(13 wks) event [53, 119], whereas other reports suggest that remyelination does not completely fail but is delayed [120]. In our study, we did not observe any recovery in myelin staining intensity after a 4 wks recovery period. We cannot exclude that remyelination would have been evident after a longer recovery period or using more sensitive techniques such as electron-microscopy. However, it is obvious that remyelination is at least impaired after prolonged cuprizone exposure.

Remyelination can be classified as four consecutive steps: (i) proliferation of oligodendrocyte progenitor cells, (ii) migration towards the demyelinated axons, (iii) differentiation and, finally (iv) interaction of the premature oligodendrocyte with the axon (i.e. axon wrapping) [95]. There are likely to be many factors contributing to the eventual failure of remyelination in MS and the essential processes of progenitor recruitment, differentiation, axon-oligodendrocyte interaction and myelination itself may all be adversely affected albeit to differing extents by a changing lesion environment and increasing levels of axonal compromise. After 5 wks cuprizone treatment several features of remyelination are evident on the histological level. This is best demonstrated by our finding that many $Olig2^{strong+}$ OPCs have already been recruited to the midline of the CC at week 5, indicating that proliferation of OPCs and migration of those towards demyelinated areas is already in progress (compare figs. 17O and 18F). This observation is in line with findings from other groups [75, 110, 121, 122]. We can, therefore, not exclude that our experimental approach is biased towards those factors regulating differentiation rather than proliferation and migration of progenitor cells. Nevertheless, in light of findings that remyelination appears to be limited due to a disturbed differentiation of oligodendrocyte progenitor cells, findings of our Affymetrix®-analysis might identify new factors related to this differentiation block [45-47, 123].

5. Identification of ongoing remyelination

Remyelination areas are classified according to a set of histopathological criteria. In general, remyelination plaques are areas with reduced myelin staining intensity showing thin, irregularly formed myelin sheaths. According to Kuhlmann and colleagues [124] remyelinating lesions are infiltrated early on in MS by numerous macrophages and T cells, while remyelination plaques from chronic MS patients are characterized by a mild inflammatory reaction [124]. The presence of microglia or macrophages containing LFB or MOG-positive myelin breakdown products indicates persisting demyelination rather than remyelination. Patani et al. [125] highlight that neurofilaments should be visualized to ensure that reduced myelin staining intensity is not due to reduction of axonal density while Prineas and Connell [83] define a remyelinated plaque as a demyelinated area which (i) contains myelin and (ii) does not show macrophages containing LFB, MBP or CNPase-positive material although lipid-loaded PAS-positive foamy macrophages can be present [83]. Thus, it is almost impossible to identify ongoing remyelination in cross-sectional histological studies. The presence of remyelinated axons in for example so called “shadow-plaques” simply indicates that remyelination has occurred at a certain time point.

It is believed that remyelination is especially prominent at the early stages of MS and sparse after several years of disease duration [98]. Furthermore, several pathological studies have suggested that chronic lesions typically display limited remyelination that is restricted to the plaque periphery [83, 126]. To study expression of BLBP in early and late activated astrocytes in the context of remyelination capacity we followed two different strategies. First we compared BLBP expression levels and number of $BLBP^+$ astrocytes after acute and chronic cuprizone-induced demyelination. Recent astrocyte activation has occurred in the acutely demyelinated group (compare results from our longitudinal studies) whereas prolonged astrocyte activation is evident in the chronically demyelinated group. This is in line with observations from other groups [127]. Second, number of BLBP-expressing astrocytes was analyzed in patients with quite short (i.e. biopsy cases) and long (i.e. *post-mortem* tissue) disease duration, respectively. Furthermore, we compared BLBP expression between the rim and centre of chronic active lesions. Remarkably, numbers of $BLBP^+$ astrocytes are highest in lesions obtained from young patients with short disease duration where remyelination is thought to be most effective [95-98]. In line with this finding, numbers of $BLBP^+$ astrocytes are significantly higher after acute compared to chronic cuprizone-induced demyelination. One might speculate that BLBP expression simply marks activated astrocytes. While we can not completely rule out this possibility our data suggest that this is not the case. As shown in fig. 18, both parts of the CC contain activated astrocytes as indicated by anti-GFAP IHC. However, only astrocytes within the medial part of the CC express BLBP. Furthermore, activation of the astrocyte population is evident during the peak phase of PLP-induced EAE, whereas BLBP expression is still weak (compare fig. 19). A possible relevance of BLBP-expressing astrocytes for remyelination is highlighted by our observation that $Olig2^{strong+}$ OPCs are abundantly present in the medial part but almost absent in the lateral part of the CC at week 5. We rather suggest that BLBP expression by activated astrocytes occurs during the initial disease stages and declines as disease progresses. Thus, two astrocyte phenotypes can be distinguished: (1) GFAP positive astrocytes with high BLBP expression and (2) GFAP positive astrocytes with no/low BLBP expression. While regional differences of astrocyte function should be considered in this context [59] further studies are needed to show whether myelin debris directly induces expression of BLBP in activated astrocytes. This could be either by direct myelin debris-astrocyte interaction or indirectly by a modulation of microglia [128]. Several *in vitro* studies demonstrated that myelin phagocytosis by microglia and macrophages triggers release of proinflammatory cytokines and nitric oxide [129, 130]. Cytokines could subsequently induce or potentiate BLBP expression in astrocytes.

6. Relevance of inflammation for remyelination

The data from the gene expression studies and IHC findings indicate that the inflammatory response is critical for endogenous remyelination. The importance of inflammation for endogenous remyelination is well-documented [125]. The cytokines TNFα (mediated by the TNFα receptor 2) and interleukin 1β promote proliferation of OPCs and remyelination [50, 51]. Major histocompatibility complex-II-deficient mice display delayed remyelination and regeneration of oligodendrocytes compared to their

wild type littermates after cuprizone or Theiler's virus-induced demyelination [131, 132]. Furthermore, the activation of an inflammatory response by a combination of growth factors leads to myelin repair [133]. This shows a beneficial role for inflammatory responses in the CNS. Other factors related to inflammation, such as interferon-gamma [4, 134], however, might be detrimental for remyelination. The understanding of the dual role of inflammatory cytokines/factors represents a major goal for the development of new therapies. Abundant expression of factors being classified as potential pro-myelination factors (see fig. 13) might be related to myelin digestion by microglia at week 5 whereas phagocytic microglia are certainly less abundant in the chronically demyelinated brain. Further studies are necessary to elucidate whether phagocytosis of myelin by microglia is paralleled by release of growth factors from those cells.

7. Astroglia: general remarks

It is well-known that glial cells are more than "glue"-material between neurons, a "function" originally suggested by Rudolf Virchow in the mid 19th century. Astrocytes represent a subpopulation of macroglia in the peripheral and central nervous system. Since the late nineteenth century, astrocytes have been divided based on their morphology into two main subtypes: protoplasmic *(lat. astrocytus protoplasmaticus)* and fibrous astrocytes *(lat. astrocytus fibrosus)*. Protoplasmic astrocytes are present throughout the grey matter and exhibit morphological characteristics such as several stem branches that, in turn, give rise to finely branching processes in a uniform globoid distribution. In contrast fibrous astrocytes are found throughout the white matter and display many long fibre-like processes (*from Ramon Y, Cajal S; 1909: Histologie du systeme nerveux de l'homme et des vertebres*). Astroglia function exceeds by far a solely supportive role in neural tissue. These cells are dynamic, capable of communicating with neurons and other glial cells. Their processes extend to neuronal synapses, nodes of Ranvier, and to the BBB, and they are interconnected via gap junctions to each other as well as to oligodendrocytes [135, 136]. Astroglia are essential for the physical structuring of the brain, metabolism, and synaptic functioning in addition to their role in responding to pathological insults. Such insults provoke a graded cellular activation referred to as reactive gliosis [137, 138]. There is a growing body of evidence suggesting that the loss of normal astrocyte function or acquisition of non-physiological properties contribute to, or are even considered as, the primary cause of the genesis of human brain diseases. Alexander disease (AD) represents one of those disorders linking astrocyte dysfunction with disease pathogenesis [139-141]. AD is a progressive, usually fatal neurological disorder, and can be divided into an infantile, juvenile, and adult form. Although all three forms of AD can differ markedly in their clinical, para-clinical, and pathological presentation, they are united by the abundance of so-called "Rosenthal fibres" which are protein aggregates within astrocytes composed of GFAP, αB-crystallin, and heat shock protein 27 [142]. AD is a rare genetic disorder caused by mutations in the gene for GFAP - a type III intermediate filament protein transcribed from a 10 kb region located on chromosome 17 in humans and 11 in the mouse. Mice lacking this intermediate

filament protein still display normal development and reproduction [143]. In contrast, astrocytes of transgenic mice with an over-expression of the human GFAP gene, reveal inclusions resembling Rosenthal fibres [144]. Following these interesting findings, Brenner and colleagues showed that heterozygous miss-sense mutations of GFAP are associated with AD, establishing this rare disorder as the first example of a primary genetic disorder of astrocytes [145]. Another example of a dysfunction of astrocytes associated with brain pathology is neuromyelitis optica. Neuromyelitis optica (NMO or Devic's disease) is a severe autoimmune inflammatory and demyelinating disease of the CNS which predominantly affects the spinal cord and the optic nerve [146, 147]. Although previously referred to as a subtype of MS, the recent description of NMO-IgG, a highly disease-specific autoantibody found in NMO but absent in the classical form of MS, convincingly demonstrated that NMO is a specific disease and not just a subtype of MS. The target antigen of NMO-IgG was identified as aquaporin-4 (AQP4), the main water channel protein in the CNS, expressed on astrocyte end-feet at the BBB and brain-cerebrospinal fluid-barrier [148]. AQP4 plays a crucial role in the regulation of water fluxes from the extra- to the intracellular compartment in the CNS. A series of clinical and pathologic observations strongly suggest that auto-antibodies directed against astrocytic AQP4 play a central role in the physiopathology of NMO [149].

8. BLBP expression in astrocytes

Notwithstanding the importance of microglia/macrophages in the context of remyelination [55], we focused on the distribution of BLBP-expressing astrocytes. Schmid and colleagues [150] used fluorescence transgenic mice under the control of the BLBP promoter to study the cellular distribution and morphology of BLBP-expressing cells. They were able to show that during the early postnatal days, radial glia transform into $GFAP^+$ astrocytes in which the BLBP promoter remains active. Consistent with this, they observed BLBP expression in $GFAP^+$ astrocytes of the adult cerebral cortex and hippocampus. BLBP/GFAP double-positive cells were primarily found in the outer layers of the cortex to the pial surface and in cells distributed adjacent to the ventricles [150]. These observations are in good agreement with our results. Samples of control mice and NAWM in MS contain $GFAP^+/BLBP^+$ cells within the subpial compartment and next to the ventricular wall.

Recent reports suggest that BLBP might be involved in CNS pathology during adulthood. Studies of BLBP expression in neurological disorders reveal that expression is increased within different hippocampal sub-regions in response to cerebral ischemia [151]. In another study, three single nucleotide polymorphisms from BLBP showed an association with bipolar disorder [152]. Furthermore, it has been demonstrated that BLBP is expressed in astrocytoma and some malignant glioma cell lines. Cytoplasmic expression correlated with metastasis properties of those malignancies [63]. BLBP expression is found in pure glioblastoma histology and associated with reduced survival. Nuclear expression of BLBP was related to more invasive tumors [153, 154].

To our knowledge, only one other study investigated the distribution of BLBP-expressing astrocytes in MOG-induced EAE [89]. Here the authors recently demonstrated that BLBP/GFAP double-positive

cells accumulate within the spinal cord. During disease course, they observed large, multiprocess-bearing BLBP-expressing cells. It was suggested by the authors that migration of oligodendroglial lineage cells into the lesions is retarded by the intense peri-lesional gliosis. Our results, however, indicate a rather beneficial function of BLBP expression in astrocytes.

9. Possible role of BLBP for astrocyte-mediated oligodendrocyte maturation

To gain insight into underlying mechanisms of BLBP-mediated tissue repair, we stably transfected U87 malignant glioma cells with a human BLBP construct to investigate the relevance of BLBP-expression for growth factor expression. We selected IGF1, FGF2, PDGF-AA and SPP1 since all four peptides are well-known to modulate oligodendrocyte proliferation, maturation, or remyelination [93, 155, 156]. *In vitro* ligand binding studies have shown that the polyunsaturated fatty acid (PUFA), ω-3 docosahexaenoic acid (DHA; 22:6) is the preferred ligand of BLBP. BLBP also binds ω-6 arachidonic acid (AA; 20:4), albeit with a ~4-fold lower affinity [157]. Fatty acid binding proteins, among BLBP, are able to regulate intracellular levels and localization of fatty acids. Fatty acids, in particular PUFA are able to act as second messengers. They may substitute for the classical second messenger inositide phospholipid and the cyclic AMP signal transduction pathway. Furthermore, in mammals, the expression of many genes has been shown to be modulated by fatty acids in a positive or a negative manner. Several transcription factors, among peroxisome proliferator-activated receptor (PPAR) could mediate fatty acid effects [99, 158]. Whether BLBP stimulates growth factor expression by interfering with second messenger signalling cascades or by direct modulation of transcription factors, such as PPARs remains to be clarified.

Another attractive concept how BLBP expression in activated astrocytes might modulate tissue repair is by positively influencing cell migration and cell motility. Highly unsaturated long-chain fatty acids alter the structure and function of membranes, increasing their fluidity and elasticity [159-161]. Preferential localization of BLBP at the leading edges of astrocytes may result in increased PUFA content at these sites. Increased fluidity may directly promote cell motility or may activate cell signalling events associated with cell motility und thus further diminish the gap between oligodendrocyte progenitors and astrocytes processes. Mita and colleagues were able to demonstrate that expression of BLBP in $BLBP^-$ malignant glioma cells is accompanied by increased migration and extended cell processes. Conversely, BLBP depletion in $BLBP^+$ malignant glioma cells results in decreased migration, reduction in cell processes, and a more transformed phenotype [63].

In summary, we provide evidence that expression of BLBP negatively correlates with disease duration and in parallel with failure of remyelination. A direct contribution of BLBP-expression in activated astrocytes to myelin repair, however, remains to be verified.

References

[1] Kipp M, Beyer C. Impact of sex steroids on neuroinflammatory processes and experimental multiple sclerosis. Front Neuroendocrinol. 2009;30:188-200.
[2] Keegan BM, Noseworthy JH. Multiple sclerosis. Annu Rev Med. 2002;53:285-302.
[3] Kipp M, Clarner T, Dang J, Copray S, Beyer C. The cuprizone animal model: new insights into an old story. Acta Neuropathol. 2009;118:723-36.
[4] Barcellos LF, Sawcer S, Ramsay PP, Baranzini SE, Thomson G, Briggs F, et al. Heterogeneity at the HLA-DRB1 locus and risk for multiple sclerosis. Hum Mol Genet. 2006;15:2813-24.
[5] Gregory SG, Schmidt S, Seth P, Oksenberg JR, Hart J, Prokop A, et al. Interleukin 7 receptor alpha chain (IL7R) shows allelic and functional association with multiple sclerosis. Nat Genet. 2007;39:1083-91.
[6] Hafler DA, Compston A, Sawcer S, Lander ES, Daly MJ, De Jager PL, et al. Risk alleles for multiple sclerosis identified by a genomewide study. N Engl J Med. 2007;357:851-62.
[7] Illes Z, Safrany E, Peterfalvi A, Magyari L, Farago B, Pozsonyi E, et al. 3'UTR C2370A allele of the IL-23 receptor gene is associated with relapsing-remitting multiple sclerosis. Neurosci Lett. 2008;431:36-8.
[8] Islam T, Gauderman WJ, Cozen W, Mack TM. Childhood sun exposure influences risk of multiple sclerosis in monozygotic twins. Neurology. 2007;69:381-8.
[9] Munger KL, Levin LI, Hollis BW, Howard NS, Ascherio A. Serum 25-hydroxyvitamin D levels and risk of multiple sclerosis. Jama. 2006;296:2832-8.
[10] Grant WB. Epidemiology of disease risks in relation to vitamin D insufficiency. Prog Biophys Mol Biol. 2006;92:65-79.
[11] Ascherio A, Munger KL. Epstein-barr virus infection and multiple sclerosis: a review. J Neuroimmune Pharmacol.5:271-7.
[12] Clarner T, Parabucki A, Beyer C, Kipp M. Corticosteroids impair remyelination in the corpus callosum of cuprizone-treated mice. J Neuroendocrinol.
[13] Leary SM, Miller DH, Stevenson VL, Brex PA, Chard DT, Thompson AJ. Interferon beta-1a in primary progressive MS: an exploratory, randomized, controlled trial. Neurology. 2003;60:44-51.
[14] Oleszak EL, Chang JR, Friedman H, Katsetos CD, Platsoucas CD. Theiler's virus infection: a model for multiple sclerosis. Clin Microbiol Rev. 2004;17:174-207.
[15] Matsushima GK, Morell P. The neurotoxicant, cuprizone, as a model to study demyelination and remyelination in the central nervous system. Brain Pathol. 2001;11:107-16.
[16] Goverman J, Woods A, Larson L, Weiner LP, Hood L, Zaller DM. Transgenic mice that express a myelin basic protein-specific T cell receptor develop spontaneous autoimmunity. Cell. 1993;72:551-60.
[17] van der Valk P, De Groot CJ. Staging of multiple sclerosis (MS) lesions: pathology of the time frame of MS. Neuropathol Appl Neurobiol. 2000;26:2-10.
[18] Zeis T, Graumann U, Reynolds R, Schaeren-Wiemers N. Normal-appearing white matter in multiple sclerosis is in a subtle balance between inflammation and neuroprotection. Brain. 2008;131:288-303.
[19] Chard DT, Griffin CM, McLean MA, Kapeller P, Kapoor R, Thompson AJ, et al. Brain metabolite changes in cortical grey and normal-appearing white matter in clinically early relapsing-remitting multiple sclerosis. Brain. 2002;125:2342-52.
[20] Lucchinetti C, Bruck W, Parisi J, Scheithauer B, Rodriguez M, Lassmann H. Heterogeneity of multiple sclerosis lesions: implications for the pathogenesis of demyelination. Ann Neurol. 2000;47:707-17.
[21] Breij EC, Brink BP, Veerhuis R, van den Berg C, Vloet R, Yan R, et al. Homogeneity of active demyelinating lesions in established multiple sclerosis. Ann Neurol. 2008;63:16-25.
[22] Kutzelnigg A, Lucchinetti CF, Stadelmann C, Bruck W, Rauschka H, Bergmann M, et al. Cortical demyelination and diffuse white matter injury in multiple sclerosis. Brain. 2005;128:2705-12.
[23] Bo L, Vedeler CA, Nyland HI, Trapp BD, Mork SJ. Subpial demyelination in the cerebral cortex of multiple sclerosis patients. J Neuropathol Exp Neurol. 2003;62:723-32.
[24] Peterson JW, Bo L, Mork S, Chang A, Trapp BD. Transected neurites, apoptotic neurons, and reduced inflammation in cortical multiple sclerosis lesions. Ann Neurol. 2001;50:389-400.
[25] Bo L, Vedeler CA, Nyland H, Trapp BD, Mork SJ. Intracortical multiple sclerosis lesions are not associated with increased lymphocyte infiltration. Mult Scler. 2003;9:323-31.
[26] van Horssen J, Brink BP, de Vries HE, van der Valk P, Bo L. The blood-brain barrier in cortical multiple sclerosis lesions. J Neuropathol Exp Neurol. 2007;66:321-8.
[27] Carlton WW. Spongiform encephalopathy induced in rats and guinea pigs by cuprizone. Exp Mol Pathol. 1969;10:274-87.
[28] Kesterson JW, Carlton WW. Aqueductal stenosis as the cause of hydrocephalus in mice fed the substituted hydrazine, cuprizone. Exp Mol Pathol. 1970;13:281-94.
[29] Norkute A, Hieble A, Braun A, Johann S, Clarner T, Baumgartner W, et al. Cuprizone treatment induces demyelination and astrocytosis in the mouse hippocampus. J Neurosci Res. 2009;87:1343-55.
[30] Taylor LC, Gilmore W, Matsushima GK. SJL mice exposed to cuprizone intoxication reveal strain and gender pattern differences in demyelination. Brain Pathol. 2009;19:467-79.
[31] Messori L, Casini A, Gabbiani C, Sorace L, Muniz-Miranda M, Zatta P. Unravelling the chemical nature of copper cuprizone. Dalton Trans. 2007:2112-4.
[32] Cudd A, Nicolau C. Interaction of intravenously injected liposomes with mouse liver mitochondria. A fluorescence and electron microscopy study. Biochim Biophys Acta. 1986;860:201-14.
[33] Venturini G. Enzymic activities and sodium, potassium and copper concentrations in mouse brain and liver after cuprizone treatment in vivo. J Neurochem. 1973;21:1147-51.

[34] Geurts JJ, Stys PK, Minagar A, Amor S, Zivadinov R. Gray matter pathology in (chronic) MS: modern views on an early observation. J Neurol Sci. 2009;282:12-20.
[35] Geurts JJ, Barkhof F. Grey matter pathology in multiple sclerosis. Lancet Neurol. 2008;7:841-51.
[36] Behl C, Widmann M, Trapp T, Holsboer F. 17-beta estradiol protects neurons from oxidative stress-induced cell death in vitro. Biochem Biophys Res Commun. 1995;216:473-82.
[37] Patrikios P, Stadelmann C, Kutzelnigg A, Rauschka H, Schmidbauer M, Laursen H, et al. Remyelination is extensive in a subset of multiple sclerosis patients. Brain. 2006;129:3165-72.
[38] Franklin RJ, Ffrench-Constant C. Remyelination in the CNS: from biology to therapy. Nat Rev Neurosci. 2008;9:839-55.
[39] Irvine KA, Blakemore WF. Remyelination protects axons from demyelination-associated axon degeneration. Brain. 2008;131:1464-77.
[40] Smith EJ, Blakemore WF, McDonald WI. Central remyelination restores secure conduction. Nature. 1979;280:395-6.
[41] Halliday AM. Visual evoked potentials in demyelinating disease. Adv Neurol. 1981;31:201-15.
[42] Prineas JW, Barnard RO, Kwon EE, Sharer LR, Cho ES. Multiple sclerosis: remyelination of nascent lesions. Ann Neurol. 1993;33:137-51.
[43] Prineas JW, Barnard RO, Revesz T, Kwon EE, Sharer L, Cho ES. Multiple sclerosis. Pathology of recurrent lesions. Brain. 1993;116 (Pt 3):681-93.
[44] Scolding N, Franklin R, Stevens S, Heldin CH, Compston A, Newcombe J. Oligodendrocyte progenitors are present in the normal adult human CNS and in the lesions of multiple sclerosis. Brain. 1998;121 (Pt 12):2221-8.
[45] Chang A, Nishiyama A, Peterson J, Prineas J, Trapp BD. NG2-positive oligodendrocyte progenitor cells in adult human brain and multiple sclerosis lesions. J Neurosci. 2000;20:6404-12.
[46] Chang A, Tourtellotte WW, Rudick R, Trapp BD. Premyelinating oligodendrocytes in chronic lesions of multiple sclerosis. N Engl J Med. 2002;346:165-73.
[47] Wolswijk G. Chronic stage multiple sclerosis lesions contain a relatively quiescent population of oligodendrocyte precursor cells. J Neurosci. 1998;18:601-9.
[48] Charles P, Reynolds R, Seilhean D, Rougon G, Aigrot MS, Niezgoda A, et al. Re-expression of PSA-NCAM by demyelinated axons: an inhibitor of remyelination in multiple sclerosis? Brain. 2002;125:1972-9.
[49] John GR, Shankar SL, Shafit-Zagardo B, Massimi A, Lee SC, Raine CS, et al. Multiple sclerosis: re-expression of a developmental pathway that restricts oligodendrocyte maturation. Nat Med. 2002;8:1115-21.
[50] Arnett HA, Mason J, Marino M, Suzuki K, Matsushima GK, Ting JP. TNF alpha promotes proliferation of oligodendrocyte progenitors and remyelination. Nat Neurosci. 2001;4:1116-22.
[51] Mason JL, Suzuki K, Chaplin DD, Matsushima GK. Interleukin-1beta promotes repair of the CNS. J Neurosci. 2001;21:7046-52.
[52] Acs P, Kipp M, Norkute A, Johann S, Clarner T, Braun A, et al. 17beta-estradiol and progesterone prevent cuprizone provoked demyelination of corpus callosum in male mice. Glia. 2009;57:807-14.
[53] Harsan LA, Steibel J, Zaremba A, Agin A, Sapin R, Poulet P, et al. Recovery from chronic demyelination by thyroid hormone therapy: myelinogenesis induction and assessment by diffusion tensor magnetic resonance imaging. J Neurosci. 2008;28:14189-201.
[54] Mi S, Hu B, Hahm K, Luo Y, Kam Hui ES, Yuan Q, et al. LINGO-1 antagonist promotes spinal cord remyelination and axonal integrity in MOG-induced experimental autoimmune encephalomyelitis. Nat Med. 2007;13:1228-33.
[55] Kotter MR, Li WW, Zhao C, Franklin RJ. Myelin impairs CNS remyelination by inhibiting oligodendrocyte precursor cell differentiation. J Neurosci. 2006;26:328-32.
[56] Back SA, Tuohy TM, Chen H, Wallingford N, Craig A, Struve J, et al. Hyaluronan accumulates in demyelinated lesions and inhibits oligodendrocyte progenitor maturation. Nat Med. 2005;11:966-72.
[57] Hsu SM, Raine L, Fanger H. A comparative study of the peroxidase-antiperoxidase method and an avidin-biotin complex method for studying polypeptide hormones with radioimmunoassay antibodies. Am J Clin Pathol. 1981;75:734-8.
[58] Kooi EJ, van Horssen J, Witte ME, Amor S, Bo L, Dijkstra CD, et al. Abundant extracellular myelin in the meninges of patients with multiple sclerosis. Neuropathol Appl Neurobiol. 2009;35:283-95.
[59] Kipp M, Norkute A, Johann S, Lorenz L, Braun A, Hieble A, et al. Brain-region-specific astroglial responses in vitro after LPS exposure. J Mol Neurosci. 2008;35:235-43.
[60] Johann S, Kampmann E, Denecke B, Arnold S, Kipp M, Mey J, et al. Expression of enzymes involved in the prostanoid metabolism by cortical astrocytes after LPS-induced inflammation. J Mol Neurosci. 2008;34:177-85.
[61] Irizarry RA, Hobbs B, Collin F, Beazer-Barclay YD, Antonellis KJ, Scherf U, et al. Exploration, normalization, and summaries of high density oligonucleotide array probe level data. Biostatistics. 2003;4:249-64.
[62] Maere S, Heymans K, Kuiper M. BiNGO: a Cytoscape plugin to assess overrepresentation of gene ontology categories in biological networks. Bioinformatics. 2005;21:3448-9.
[63] Mita R, Coles JE, Glubrecht DD, Sung R, Sun X, Godbout R. B-FABP-expressing radial glial cells: the malignant glioma cell of origin? Neoplasia. 2007;9:734-44.
[64] Braun A, Dang J, Johann S, Beyer C, Kipp M. Selective regulation of growth factor expression in cultured cortical astrocytes by neuro-pathological toxins. Neurochem Int. 2009;55:610-8.
[65] Baertling F, Kokozidou M, Pufe T, Clarner T, Windoffer R, Wruck CJ, et al. ADAM12 is expressed by astrocytes during experimental demyelination. Brain Res.1326:1-14.
[66] Groebe A, Clarner T, Baumgartner W, Dang J, Beyer C, Kipp M. Cuprizone treatment induces distinct demyelination, astrocytosis, and microglia cell invasion or proliferation in the mouse cerebellum. Cerebellum. 2009;8:163-74.
[67] Pott F, Gingele S, Clarner T, Dang J, Baumgartner W, Beyer C, et al. Cuprizone effect on myelination, astrogliosis and microglia attraction in the mouse basal ganglia. Brain Res. 2009;1305:137-49.
[68] Geurts JJ, Bo L, Roosendaal SD, Hazes T, Daniels R, Barkhof F, et al. Extensive hippocampal demyelination in multiple sclerosis. J Neuropathol Exp Neurol. 2007;66:819-27.

[69] Geurts JJ, Reuling IE, Vrenken H, Uitdehaag BM, Polman CH, Castelijns JA, et al. MR spectroscopic evidence for thalamic and hippocampal, but not cortical, damage in multiple sclerosis. Magn Reson Med. 2006;55:478-83.
[70] Kiy G, Lehmann P, Hahn HK, Eling P, Kastrup A, Hildebrandt H. Decreased hippocampal volume, indirectly measured, is associated with depressive symptoms and consolidation deficits in multiple sclerosis. Mult Scler.
[71] Bird CM, Burgess N. The hippocampus and memory: insights from spatial processing. Nat Rev Neurosci. 2008;9:182-94.
[72] Brassington JC, Marsh NV. Neuropsychological aspects of multiple sclerosis. Neuropsychol Rev. 1998;8:43-77.
[73] Wishart H, Sharpe D. Neuropsychological aspects of multiple sclerosis: a quantitative review. J Clin Exp Neuropsychol. 1997;19:810-24.
[74] Coebergh JA, Roosendaal SD, Polman CH, Geurts JJ, van Woerkom TC. Acute severe memory impairment as a presenting symptom of multiple sclerosis: a clinical case study with 3D double inversion recovery MR imaging. Mult Scler.16:1521-4.
[75] Hesse A, Wagner M, Held J, Bruck W, Salinas-Riester G, Hao Z, et al. In toxic demyelination oligodendroglial cell death occurs early and is FAS independent. Neurobiol Dis. 2010;37:362-9.
[76] Heppner FL, Roth K, Nitsch R, Hailer NP. Vitamin E induces ramification and downregulation of adhesion molecules in cultured microglial cells. Glia. 1998;22:180-8.
[77] de Haas AH, Boddeke HW, Biber K. Region-specific expression of immunoregulatory proteins on microglia in the healthy CNS. Glia. 2008;56:888-94.
[78] Rivest S. Regulation of innate immune responses in the brain. Nat Rev Immunol. 2009;9:429-39.
[79] Gordon S. Alternative activation of macrophages. Nat Rev Immunol. 2003;3:23-35.
[80] Skripuletz T, Lindner M, Kotsiari A, Garde N, Fokuhl J, Linsmeier F, et al. Cortical demyelination is prominent in the murine cuprizone model and is strain-dependent. Am J Pathol. 2008;172:1053-61.
[81] Clarner T, Buschmann JP, Beyer C, Kipp M. Glial amyloid precursor protein expression is restricted to astrocytes in an experimental toxic model of multiple sclerosis. J Mol Neurosci.43:268-74.
[82] Fawcett JW, Housden E, Smith-Thomas L, Meyer RL. The growth of axons in three-dimensional astrocyte cultures. Dev Biol. 1989;135:449-58.
[83] Prineas JW, Connell F. Remyelination in multiple sclerosis. Ann Neurol. 1979;5:22-31.
[84] Williams A, Piaton G, Lubetzki C. Astrocytes--friends or foes in multiple sclerosis? Glia. 2007;55:1300-12.
[85] Veerkamp JH, Zimmerman AW. Fatty acid-binding proteins of nervous tissue. J Mol Neurosci. 2001;16:133-42; discussion 51-7.
[86] Sibbe M, Forster E, Basak O, Taylor V, Frotscher M. Reelin and Notch1 cooperate in the development of the dentate gyrus. J Neurosci. 2009;29:8578-85.
[87] Barry D, McDermott K. Differentiation of radial glia from radial precursor cells and transformation into astrocytes in the developing rat spinal cord. Glia. 2005;50:187-97.
[88] Bibel M, Richter J, Schrenk K, Tucker KL, Staiger V, Korte M, et al. Differentiation of mouse embryonic stem cells into a defined neuronal lineage. Nat Neurosci. 2004;7:1003-9.
[89] Bannerman P, Hahn A, Soulika A, Gallo V, Pleasure D. Astrogliosis in EAE spinal cord: derivation from radial glia, and relationships to oligodendroglia. Glia. 2007;55:57-64.
[90] Cimino PJ, Sokal I, Leverenz J, Fukui Y, Montine TJ. DOCK2 is a microglial specific regulator of central nervous system innate immunity found in normal and Alzheimer's disease brain. Am J Pathol. 2009;175:1622-30.
[91] Stegbauer J, Lee DH, Seubert S, Ellrichmann G, Manzel A, Kvakan H, et al. Role of the renin-angiotensin system in autoimmune inflammation of the central nervous system. Proc Natl Acad Sci U S A. 2009;106:14942-7.
[92] Komoly S, Hudson LD, Webster HD, Bondy CA. Insulin-like growth factor I gene expression is induced in astrocytes during experimental demyelination. Proc Natl Acad Sci U S A. 1992;89:1894-8.
[93] Selvaraju R, Bernasconi L, Losberger C, Graber P, Kadi L, Avellana-Adalid V, et al. Osteopontin is upregulated during in vivo demyelination and remyelination and enhances myelin formation in vitro. Mol Cell Neurosci. 2004;25:707-21.
[94] Mita R, Beaulieu MJ, Field C, Godbout R. Brain fatty acid-binding protein and omega-3/omega-6 fatty acids: mechanistic insight into malignant glioma cell migration. J Biol Chem. 2010;285:37005-15.
[95] Shen S, Sandoval J, Swiss VA, Li J, Dupree J, Franklin RJ, et al. Age-dependent epigenetic control of differentiation inhibitors is critical for remyelination efficiency. Nat Neurosci. 2008;11:1024-34.
[96] Shields SA, Gilson JM, Blakemore WF, Franklin RJ. Remyelination occurs as extensively but more slowly in old rats compared to young rats following gliotoxin-induced CNS demyelination. Glia. 1999;28:77-83.
[97] Rist JM, Franklin RJ. Taking ageing into account in remyelination-based therapies for multiple sclerosis. J Neurol Sci. 2008;274:64-7.
[98] Goldschmidt T, Antel J, Konig FB, Bruck W, Kuhlmann T. Remyelination capacity of the MS brain decreases with disease chronicity. Neurology. 2009;72:1914-21.
[99] Zimmerman AW, Veerkamp JH. New insights into the structure and function of fatty acid-binding proteins. Cell Mol Life Sci. 2002;59:1096-116.
[100] Lucchinetti CF, Bruck W, Rodriguez M, Lassmann H. Distinct patterns of multiple sclerosis pathology indicates heterogeneity on pathogenesis. Brain Pathol. 1996;6:259-74.
[101] Veto S, Acs P, Bauer J, Lassmann H, Berente Z, Setalo G, Jr., et al. Inhibiting poly(ADP-ribose) polymerase: a potential therapy against oligodendrocyte death. Brain.133:822-34.
[102] Morell P, Barrett CV, Mason JL, Toews AD, Hostettler JD, Knapp GW, et al. Gene expression in brain during cuprizone-induced demyelination and remyelination. Mol Cell Neurosci. 1998;12:220-7.
[103] Emerson MR, Biswas S, LeVine SM. Cuprizone and piperonyl butoxide, proposed inhibitors of T-cell function, attenuate experimental allergic encephalomyelitis in SJL mice. J Neuroimmunol. 2001;119:205-13.
[104] Mana P, Fordham SA, Staykova MA, Correcha M, Silva D, Willenborg DO, et al. Demyelination caused by the copper chelator cuprizone halts T cell mediated autoimmune neuroinflammation. J Neuroimmunol. 2009;210:13-21.

[105] Liu L, Belkadi A, Darnall L, Hu T, Drescher C, Cotleur AC, et al. CXCR2-positive neutrophils are essential for cuprizone-induced demyelination: relevance to multiple sclerosis. Nat Neurosci.13:319-26.
[106] Patel JR, McCandless EE, Dorsey D, Klein RS. CXCR4 promotes differentiation of oligodendrocyte progenitors and remyelination. Proc Natl Acad Sci U S A.107:11062-7.
[107] Clarner T, Buschmann JP, Beyer C, Kipp M. Glial amyloid precursor protein expression is restricted to astrocytes in an experimental toxic model of multiple sclerosis. J Mol Neurosci. 2011;43:268-74.
[108] Mildner A, Schmidt H, Nitsche M, Merkler D, Hanisch UK, Mack M, et al. Microglia in the adult brain arise from Ly-6ChiCCR2+ monocytes only under defined host conditions. Nat Neurosci. 2007;10:1544-53.
[109] Takasaki C, Yamasaki M, Uchigashima M, Konno K, Yanagawa Y, Watanabe M. Cytochemical and cytological properties of perineuronal oligodendrocytes in the mouse cortex. Eur J Neurosci.32:1326-36.
[110] Moharregh-Khiabani D, Blank A, Skripuletz T, Miller E, Kotsiari A, Gudi V, et al. Effects of fumaric acids on cuprizone induced central nervous system de- and remyelination in the mouse. PLoS One. 2010;5:e11769.
[111] Amato MP, Bartolozzi ML, Zipoli V, Portaccio E, Mortilla M, Guidi L, et al. Neocortical volume decrease in relapsing-remitting MS patients with mild cognitive impairment. Neurology. 2004;63:89-93.
[112] Amato MP, Portaccio E, Goretti B, Zipoli V, Battaglini M, Bartolozzi ML, et al. Association of neocortical volume changes with cognitive deterioration in relapsing-remitting multiple sclerosis. Arch Neurol. 2007;64:1157-61.
[113] Bo L, Geurts JJ, van der Valk P, Polman C, Barkhof F. Lack of correlation between cortical demyelination and white matter pathologic changes in multiple sclerosis. Arch Neurol. 2007;64:76-80.
[114] De Groot CJ, Bergers E, Kamphorst W, Ravid R, Polman CH, Barkhof F, et al. Post-mortem MRI-guided sampling of multiple sclerosis brain lesions: increased yield of active demyelinating and (p)reactive lesions. Brain. 2001;124:1635-45.
[115] Yenari MA, Xu L, Tang XN, Qiao Y, Giffard RG. Microglia potentiate damage to blood-brain barrier constituents: improvement by minocycline in vivo and in vitro. Stroke. 2006;37:1087-93.
[116] Kacimi R, Giffard RG, Yenari MA. Endotoxin-activated microglia injure brain derived endothelial cells via NF-kappaB, JAK-STAT and JNK stress kinase pathways. J Inflamm (Lond).8:7.
[117] Gehrmann J, Matsumoto Y, Kreutzberg GW. Microglia: intrinsic immuneffector cell of the brain. Brain Res Brain Res Rev. 1995;20:269-87.
[118] Babcock AA, Kuziel WA, Rivest S, Owens T. Chemokine expression by glial cells directs leukocytes to sites of axonal injury in the CNS. J Neurosci. 2003;23:7922-30.
[119] Vana AC, Flint NC, Harwood NE, Le TQ, Fruttiger M, Armstrong RC. Platelet-derived growth factor promotes repair of chronically demyelinated white matter. J Neuropathol Exp Neurol. 2007;66:975-88.
[120] Lindner M, Fokuhl J, Linsmeier F, Trebst C, Stangel M. Chronic toxic demyelination in the central nervous system leads to axonal damage despite remyelination. Neurosci Lett. 2009;453:120-5.
[121] Sabo JK, Aumann TD, Merlo D, Kilpatrick TJ, Cate HS. Remyelination is altered by bone morphogenic protein signaling in demyelinated lesions. J Neurosci. 2011;31:4504-10.
[122] Liu L, Darnall L, Hu T, Choi K, Lane TE, Ransohoff RM. Myelin repair is accelerated by inactivating CXCR2 on nonhematopoietic cells. J Neurosci. 2010;30:9074-83.
[123] Miron VE, Zehntner SP, Kuhlmann T, Ludwin SK, Owens T, Kennedy TE, et al. Statin therapy inhibits remyelination in the central nervous system. Am J Pathol. 2009;174:1880-90.
[124] Kuhlmann T, Miron V, Cui Q, Wegner C, Antel J, Bruck W. Differentiation block of oligodendroglial progenitor cells as a cause for remyelination failure in chronic multiple sclerosis. Brain. 2008;131:1749-58.
[125] Patani R, Balaratnam M, Vora A, Reynolds R. Remyelination can be extensive in multiple sclerosis despite a long disease course. Neuropathol Appl Neurobiol. 2007;33:277-87.
[126] Perier O, Gregoire A. Electron microscopic features of multiple sclerosis lesions. Brain. 1965;88:937-52.
[127] Ludwin SK. Central nervous system demyelination and remyelination in the mouse: an ultrastructural study of cuprizone toxicity. Lab Invest. 1978;39:597-612.
[128] Liu Y, Hao W, Letiembre M, Walter S, Kulanga M, Neumann H, et al. Suppression of microglial inflammatory activity by myelin phagocytosis: role of p47-PHOX-mediated generation of reactive oxygen species. J Neurosci. 2006;26:12904-13.
[129] Williams K, Ulvestad E, Waage A, Antel JP, McLaurin J. Activation of adult human derived microglia by myelin phagocytosis in vitro. J Neurosci Res. 1994;38:433-43.
[130] Mosley K, Cuzner ML. Receptor-mediated phagocytosis of myelin by macrophages and microglia: effect of opsonization and receptor blocking agents. Neurochem Res. 1996;21:481-7.
[131] Arnett HA, Wang Y, Matsushima GK, Suzuki K, Ting JP. Functional genomic analysis of remyelination reveals importance of inflammation in oligodendrocyte regeneration. J Neurosci. 2003;23:9824-32.
[132] Njenga MK, Murray PD, McGavern D, Lin X, Drescher KM, Rodriguez M. Absence of spontaneous central nervous system remyelination in class II-deficient mice infected with Theiler's virus. J Neuropathol Exp Neurol. 1999;58:78-91.
[133] Biancotti JC, Kumar S, de Vellis J. Activation of inflammatory response by a combination of growth factors in cuprizone-induced demyelinated brain leads to myelin repair. Neurochem Res. 2008;33:2615-28.
[134] Mana P, Linares D, Fordham S, Staykova M, Willenborg D. Deleterious role of IFNgamma in a toxic model of central nervous system demyelination. Am J Pathol. 2006;168:1464-73.
[135] Rash JE, Yasumura T, Dudek FE, Nagy JI. Cell-specific expression of connexins and evidence of restricted gap junctional coupling between glial cells and between neurons. J Neurosci. 2001;21:1983-2000.
[136] Venance L, Cordier J, Monge M, Zalc B, Glowinski J, Giaume C. Homotypic and heterotypic coupling mediated by gap junctions during glial cell differentiation in vitro. Eur J Neurosci. 1995;7:451-61.
[137] Faulkner JR, Herrmann JE, Woo MJ, Tansey KE, Doan NB, Sofroniew MV. Reactive astrocytes protect tissue and preserve function after spinal cord injury. J Neurosci. 2004;24:2143-55.
[138] Pekny M, Nilsson M. Astrocyte activation and reactive gliosis. Glia. 2005;50:427-34.
[139] Li R, Messing A, Goldman JE, Brenner M. GFAP mutations in Alexander disease. Int J Dev Neurosci. 2002;20:259-68.
[140] Sawaishi Y. Review of Alexander disease: beyond the classical concept of leukodystrophy. Brain Dev. 2009;31:493-8.

[141] Quinlan RA, Brenner M, Goldman JE, Messing A. GFAP and its role in Alexander disease. Exp Cell Res. 2007;313:2077-87.
[142] Ma CS, Nichols KE, Tangye SG. Regulation of cellular and humoral immune responses by the SLAM and SAP families of molecules. Annu Rev Immunol. 2007;25:337-79.
[143] Pekny M, Leveen P, Pekna M, Eliasson C, Berthold CH, Westermark B, et al. Mice lacking glial fibrillary acidic protein display astrocytes devoid of intermediate filaments but develop and reproduce normally. Embo J. 1995;14:1590-8.
[144] Messing A, Head MW, Galles K, Galbreath EJ, Goldman JE, Brenner M. Fatal encephalopathy with astrocyte inclusions in GFAP transgenic mice. Am J Pathol. 1998;152:391-8.
[145] Brenner M, Johnson AB, Boespflug-Tanguy O, Rodriguez D, Goldman JE, Messing A. Mutations in GFAP, encoding glial fibrillary acidic protein, are associated with Alexander disease. Nat Genet. 2001;27:117-20.
[146] Jarius S, Wildemann B. AQP4 antibodies in neuromyelitis optica: diagnostic and pathogenetic relevance. Nat Rev Neurol.6:383-92.
[147] Saikali P, Cayrol R, Vincent T. Anti-aquaporin-4 auto-antibodies orchestrate the pathogenesis in neuromyelitis optica. Autoimmun Rev. 2009;9:132-5.
[148] Lennon VA, Wingerchuk DM, Kryzer TJ, Pittock SJ, Lucchinetti CF, Fujihara K, et al. A serum autoantibody marker of neuromyelitis optica: distinction from multiple sclerosis. Lancet. 2004;364:2106-12.
[149] Jarius S, Paul F, Franciotta D, Waters P, Zipp F, Hohlfeld R, et al. Mechanisms of disease: aquaporin-4 antibodies in neuromyelitis optica. Nat Clin Pract Neurol. 2008;4:202-14.
[150] Schmid RS, Yokota Y, Anton ES. Generation and characterization of brain lipid-binding protein promoter-based transgenic mouse models for the study of radial glia. Glia. 2006;53:345-51.
[151] Ma D, Zhang M, Mori Y, Yao C, Larsen CP, Yamashima T, et al. Cellular localization of epidermal-type and brain-type fatty acid-binding proteins in adult hippocampus and their response to cerebral ischemia. Hippocampus. 2009.
[152] Watanabe A, Toyota T, Owada Y, Hayashi T, Iwayama Y, Matsumata M, et al. Fabp7 maps to a quantitative trait locus for a schizophrenia endophenotype. PLoS Biol. 2007;5:e297.
[153] Kaloshi G, Mokhtari K, Carpentier C, Taillibert S, Lejeune J, Marie Y, et al. FABP7 expression in glioblastomas: relation to prognosis, invasion and EGFR status. J Neurooncol. 2007;84:245-8.
[154] Liang Y, Bollen AW, Aldape KD, Gupta N. Nuclear FABP7 immunoreactivity is preferentially expressed in infiltrative glioma and is associated with poor prognosis in EGFR-overexpressing glioblastoma. BMC Cancer. 2006;6:97.
[155] Shum BO, Mackay CR, Gorgun CZ, Frost MJ, Kumar RK, Hotamisligil GS, et al. The adipocyte fatty acid-binding protein aP2 is required in allergic airway inflammation. J Clin Invest. 2006;116:2183-92.
[156] Mason JL, Xuan S, Dragatsis I, Efstratiadis A, Goldman JE. Insulin-like growth factor (IGF) signaling through type 1 IGF receptor plays an important role in remyelination. J Neurosci. 2003;23:7710-8.
[157] Balendiran GK, Schnutgen F, Scapin G, Borchers T, Xhong N, Lim K, et al. Crystal structure and thermodynamic analysis of human brain fatty acid-binding protein. J Biol Chem. 2000;275:27045-54.
[158] Duplus E, Glorian M, Forest C. Fatty acid regulation of gene transcription. J Biol Chem. 2000;275:30749-52.
[159] Stillwell W, Wassall SR. Docosahexaenoic acid: membrane properties of a unique fatty acid. Chem Phys Lipids. 2003;126:1-27.
[160] Hashimoto M, Hossain S, Yamasaki H, Yazawa K, Masumura S. Effects of eicosapentaenoic acid and docosahexaenoic acid on plasma membrane fluidity of aortic endothelial cells. Lipids. 1999;34:1297-304.
[161] Rojas CV, Martinez JI, Flores I, Hoffman DR, Uauy R. Gene expression analysis in human fetal retinal explants treated with docosahexaenoic acid. Invest Ophthalmol Vis Sci. 2003;44:3170-7.

List of publications

List of publications

PD Dr. med. Markus Kipp, Institut für Neuronatomie, RWTH Aachen
Publications: 30 First-/last-author: 13 / 10

Research articles

Kipp M, Gingele S, Pott F, Clarner T, van der Valk P, Denecke B, Gan L, Siffrin V, Zipp F, Dreher W, Baumgartner W, Pfeifenbring S, Godbout R, Amor S, Beyer C. BLBP-expression in astrocytes during experimental demyelination and in human multiple sclerosis lesions. *Brain Behav Immun, 2011 Jan 28;* **IP 5,1**

Kipp M#, Norkus A#, Krauspe B, Clarner T, Berger K, van der Valk P, Amor S, Beyer C. The hippocampal fimbria of cuprizone-treated animals as a structure for studying neuroprotection in multiple sclerosis. *Inflamm Res. 2011 Apr 24;* **IP 1,58**

Clarner T, Parabucki A, Beyer C, **Kipp M**. Corticosteroids impair remyelination in the corpus callosum of cuprizone-treated mice. *J Neuroendocrinol, 2010;* **IP 3,70**

Dang J, Mitkari B, **Kipp M**[#], Beyer C[#]. Gonadal steroids prevent cell damage and stimulate behavioral recovery after transient middle cerebral artery occlusion in male and female rats. *Brain Behav Immun, 2011 Jan 28;* **IP 5,1**

Fahlenkamp AV, Coburn M, Czaplik M, Ryang YM, **Kipp M**, Rossaint R, Beyer C. Expression analysis of the early chemokine response 4 h after in vitro traumatic brain injury. *Inflamm Res, 2010 Nov 23;* **IP 1,58**

Fahlenkamp AV, Coburn M, Haase H, **Kipp M**, Ryang YM, Rossaint R, Beyer C. Xenon Enhances LPS-Induced IL-1beta Expression in Microglia via the Extracellular Signal Regulated Kinase 1/2 Pathway. *J Mol Neurosci, 2010*; **IP 2,72**

Clarner T, Beyer C, **Kipp M.** Amyloid precursor protein expression is restricted to astrocytes in an experimental toxic model of multiple sclerosis. *J Mol Neurosci, 2010;* **IP 2,72**

Johann S, Dahm M, **Kipp M**, Beyer C, Arnold S. Oestrogen regulates mitochondrial respiratory chain enzyme transcription in the mouse spinal cord. *J Neuroendocrinol. 2010* **IP 3,70**

Baertling F[#], Kokozidou M[#], Pufe T, Clarner T, Windoffer R, Wruck CJ, Brandenburg LO, Beyer C, **Kipp M**. ADAM12 is expressed by astrocytes during experimental demyelination. *Brain Res, 2010; 1326:1-14.* **IP 2,46**

Kramer M, Dang J, Baertling F, Denecke B, Clarner T, Kirsch C, Beyer C, **Kipp M**. TTC staining of damaged brain areas after MCA occlusion in the rat does not constrict quantitative gene and protein analyses. *J Neurosci Methods, 2010; 187: 84-9.* **IP 2,29**

Brandenburg LO, **Kipp M**, Lucius R, Pufe T, Wruck CJ. Sulforaphane suppresses LPS-induced inflammation in primary rat microglia. *Inflamm Res, 2009; 59(6):443-50.* **IP 1,58**

Pott F, Gingele S, Clarner T, Dang J, Baumgartner W, Beyer C, **Kipp M**. Cuprizone effect on myelination, astrogliosis and microglia attraction in the mouse basal ganglia. *Brain Res, 2009; 1305: 137-49.* **IP 2,46**

Lorenz L, Dang J, Misiak M, Tameh Abolfazl A, Beyer C, **Kipp M**. Combined 17beta-oestradiol and progesterone treatment prevents neuronal cell injury in cortical but not midbrain neurones or neuroblastoma cells. *J Neuroendocrinol, 2009; 21: 841-9.* **IP 3,70**

Brandenburg LO, Lucius R, Tameh Abolfazl A, **Kipp M**, Wruck CJ, Koch T, Beyer C, Pufe T. Internalization and signal transduction of PrP(106-126) in neuronal cells. *Ann Anat, 2009; 191: 459-68.* **IP 0,87**

Braun A, Dang J, Johann S, Beyer C, **Kipp M**. Selective regulation of growth factor expression in cultured cortical astrocytes by neuro-pathological toxins. *Neurochem Int, 2009; 55: 610-8.* **IP 3,54**

Norkute A[#], **Kipp M[#]**, Dang J, von Keyserlingk DG, Valanciute A, Beyer C. Early formation of a GFAP-positive cell population in the ventricular zone during chicken brain development. *Cells Tissues Organs, 2009; 191: 57-65.* **IP 3,32**

Groebe A[#], Clarner T[#], Baumgartner W, Dang J, Beyer C, **Kipp M**. Cuprizone treatment induces distinct demyelination, astrocytosis, and microglia cell invasion or proliferation in the mouse cerebellum. *Cerebellum, 2009; 8: 163-74.* **IP 3,28**

Trotter A, Hilgendorff A, **Kipp M**, Beyer C, Kueppers E, Kiossis E, Stuplich J, Pohlandt F, Thome U. Gender-related effects of prenatal administration of estrogen and progesterone receptor antagonists on VEGF and surfactant-proteins and on alveolarisation in the developing piglet lung. *Early Hum Dev, 2009; 85: 353-9.* **IP 2,12**

Acs P[#], **Kipp M[#]**, Norkute A, Johann S, Clarner T, Braun A, Berente Z, Komoly S, Beyer C. 17beta-estradiol and progesterone prevent cuprizone provoked demyelination of corpus callosum in male mice. *Glia, 2009; 57: 807-14.* **IP 4,93**

Norkute A[#], Hieble A[#], Braun A, Johann S, Clarner T, Baumgartner W, Beyer C, **Kipp M**. Cuprizone treatment induces demyelination and astrocytosis in the mouse hippocampus. *J Neurosci Res, 2009; 87: 1343-55.* **IP 2,98**

Trotter A[#], **Kipp M[#]**, Schrader RM, Beyer C. Combined application of 17beta-estradiol and progesterone enhance vascular endothelial growth factor and surfactant protein expression in cultured embryonic lung cells of mice. *Int J Pediatr, 2009; 2009: 170491.*

Kipp M, Norkute A, Johann S, Lorenz L, Braun A, Hieble A, Gingele S, Pott F, Richter J, Beyer C. Brain-region-specific astroglial responses in vitro after LPS exposure. *J Mol Neurosci, 2008; 35: 235-43.* **IP 2,72**

Johann S, Kampmann E, Denecke B, Arnold S, **Kipp M**, Mey J, Beyer C. Expression of enzymes involved in the prostanoid metabolism by cortical astrocytes after LPS-induced inflammation. *J Mol Neurosci, 2008; 34: 177-85.* **IP 2,72**

Kipp M[#], Karakaya S[#], Johann S, Kampmann E, Mey J, Beyer C. Oestrogen and progesterone reduce lipopolysaccharide-induced expression of tumour necrosis factor-alpha and interleukin-18 in midbrain astrocytes. *J Neuroendocrinol, 2007; 19: 819-22.* **IP 3,70**

Karakaya S[#], **Kipp M**[#], Beyer C. Oestrogen regulates the expression and function of dopamine transporters in astrocytes of the nigrostriatal system. *J Neuroendocrinol, 2007; 19: 682-90.* **IP 3,70**

contribute equal

Review articles

Kipp M, Clarner T, Gingele S, Pott F, Amor S, van der Valk P, Beyer C. Brain lipid binding protein (FABP7) as modulator of astrocyte function. *Physiological Research, 2011.* **IP 1,43**

Kipp M, Berger K, Clarner T, Dang J, Beyer C. Sex steroids control neuroinflammatory processes in the brain: relevance for acute ischemia and degenerative demyelination. *J Neuroendocrinol, 2011.* **IP 3,70**

Kipp M, Clarner T, Dang J, Copray S, Beyer C. The cuprizone animal model: new insights into an old story. *Acta Neuropathol, 2009; 118: 723-36.* **IP 6,39**

Kipp M, Beyer C. Impact of sex steroids on neuroinflammatory processes and experimental multiple sclerosis. *Front Neuroendocrinol, 2009; 30: 188-200.* **IP 12,04**

Kipp M, Karakaya S, Pawlak J, Araujo-Wright G, Arnold S, Beyer C. Estrogen and the development and protection of nigrostriatal dopaminergic neurons: concerted action of a multitude of signals, protective molecules, and growth factors. *Front Neuroendocrinol, 2006; 27: 376-90.* **IP 12,04**

Curriculum Vitae (deutsch)

Persönliche Daten:

Name	Kipp
Vorname	Markus
Geburtstag	25. März 1978
Geburtsort	Oberndorf/Neckar
Staatsangehörigkeit	deutsch

Qualifikationen:

1997	Abitur, Albeckgymnasium Sulz/Neckar
ab 1999 bis 2007	Humanmedizin
2008	Promotion zum Dr. med. („summa cum laude"), Institut für Neuroanatomie, RWTH Aachen, Prof. Dr. C. Beyer
2010	Habilitation für das Fach Anatomie

Appendix

Appendix 1: Transcardial perfusion of mice

Fixative

- Boil 800 ml of bi-distilled water
- Dissolve 3.3 g $NaH_2PO_4xH_2O$ (Natriumdihydrogenphosphat-Monohydrat, Carl-Roth, Germany) and 45 g $Na_2HPO_4x12H_2O$ (di-Natriumhydrogenphosphat-Dodecahydrat, Carl-Roth, Germany)
- Dissolve 20 g paraformaldehyde (Sigma-Aldrich; Germany)
- Add 100 ml saturated picric acid (Sigma-Aldrich; Germany)
- Let cool to room temperature, set pH to 7.4 and add bi-distilled water to 1000 ml
- Filter and cool to 4 °C

Procedure

- 30 min prior to start, apply 10 µl Clexane-40mg (Sanofi-aventis, Germany) by intraperitoneal injection
- Deeply anaesthetise animals with Isolfuran (5%, Abbott, Germany)
- Fix the animal in supine position, open the thorax by using forceps and scissors and cut a small opening into the right atrium of the heart
- Insert a small needle into the left ventricle of the heart and perfuse 50 ml of ice-cold perfusion solution
- Cut the head and/or the trunk
- Incubate the tissue samples overnight at 4 °C in the same fixative
- Dissect the brain/spinal cord and store in one to five diluted fixative at 4 °C till the paraffin-embedding procedure

Appendix 2: Paraffin-embedding of mice tissue samples

Since paraffin is immiscible with water, the main constituent of most tissue blocks need to be dehydrated by progressively more concentrated ethanol baths. This is followed by a clearing agent, usually xylene or less toxic substitutes such as Histo-Clear, to get rid of the ethanol. Finally, molten paraffin wax infiltrates the sample and replaces the xylene/substitute.

Tissue samples were embedded in paraffin by immersing them under gentle agitation for the desired time in

- 70% Ethanol: 3 x 30 min
- 96% Ethanol 3 x 30 min
- 100% Ethanol 3 x 30 min
- Histo-Clear (Biozym, Germany) 3 x 60 min
- Parrafin (VWR, Germany) 3 x 120 min and then overnight at 60 °C

Thereafter, tissue samples were blocked in paraffin and processed following standard protocols.

Appendix 3: Immunohistochemistry

Immunohistochemistry is a method for demonstrating the presence and location of proteins in tissue sections. In our lab, we routinely use paraffin-embedded material for the detection of proteins in brain tissue. Immunohistochemical stainings are accomplished with primary antibodies that recognize the protein of interest. Since antibodies are highly specific, the antibody will bind only to the target protein in the tissue section. The antibody-antigen interaction is subsequently visualized using either a chromogenic detection system, in which an enzyme conjugated to the antibody cleaves a substrate to produce a colored precipitate at the location of the protein, or fluorescent detection, in which a fluorophore is conjugated to the antibody and can be visualized using fluorescence microscopy. The given protocol describes the first method, i.e. chromogenic detection.

- Deparaffinise and rehydrate sections in xylol (4 x 5 min), 100% Ethanol (3 x 2 min), 96% Ethanol (2 x 2 min), 70% Ethanol (2 x 2 min) and PBS (1 x 5 min)
- Perform heat-mediated antigen retrieval by boiling slides in the desired buffer. Either use Tris/EDTA (10 mM Tris Base, 1 mM EDTA Solution, 0.05% Tween 20, pH 9.0) or Sodium citrate buffer (10 mM Sodium citrate, 0.05% Tween 20, pH 6.0). Therefore, remove the slides from the PBS and place them in a microwaveable vessel. Place the vessel inside the microwave. Set microwave to full power and wait until the solution comes to the boil. Boil for 20 min from this point. If using a scientific microwave, program so that antigens are retrieved for 10 min once the temperature has reached approximately 98°C
- Let slides cool down till room temperature
- Wash in PBS (3 x 5 min)
- Block endogenous peroxidase activity by incubating slides for 30 min in 0.3% hydrogen peroxide (Carl-Roth, Germany) diluted in PBS
- Wash in PBS (3 x 5 min)
- If primary mouse antibodies are used on mouse tissue, block unspecific bindings of secondary anti-mouse antibodies by incubating the slides in blocking solution (Immunologic, Netherlands) for 3 h at room temperature
- Decant the blocking solution and apply the primary antibody over night at 4 °C diluted in blocking solution. Use a wet chamber to avoid drying-out of the slides
- The next day, decant the primary antibody and wash in PBS (3 x 5 min)
- VECTASTAIN® ABC (peroxidase) system (vectorlabs, USA) or EnVision® polymer secondary antibodies (Dako, Germany) are used to label primary antibody-antigen conjugates following the manufacturer recommendation
- Wash in PBS (3 x 5 min)
- Incubate the slides in either 3,3-Diaminobenzidine (Dako, Germany) or aminoethyl carbazole (Invitrogen, Germany) for 10 min in room temperature to visualize antibody-antigen conjugates
- Counterstain with haematoxylin to visualize cell nuclei if desired
- Dehydrate sections in 70% Ethanol (3 x 2 min), 96% Ethanol (3 x 2 min), 100% Ethanol (3 x 2 min), xylol (4 x 5 min)
- Mount slides

Appendix table 1: Clinical details of patients (chapter 3)

MS type	Gender	Age in years	Disease duration	Post mortem delay	Cause of death	A	CA	CI	blocks
Progressive	M	70	46 years	8h	Cardiac arrest		2	2	17
Secondary progressive	M	49	25 years	8h	Pneumonia		3		10
Secondary progressive	M	61	31 years	9h	Unknown	1	1	1	15
Relapsing-remitting	M	50	17 years	5h	Pulmonal cancer				4
Primary progressive	M	66	26 years	7h	Ileus		2		14
Primary progressive	M	71	26 years	7h	Pneumonia by aspiration				8
Primary progressive	M	41	14 years	7h	Urosepsis, Pneumonia	4	1	1	9
Progressive	F	75	28 years	5h	Cardio-pulmonary dysfunction				2
Progressive	F	81	64 years	5h	Unknown				5
Secondary progressive	F	43	23 years	11h	Subdural haematoma, pneumonia		3	2	8
Secondary progressive	F	67	42 years	9h	Cardio-pulmonary dysfunction				4
Secondary progressive	F	81	59 years	7h	Unknown				12
Secondary progressive	F	78	30 years	11h	CVA relapse, dehydration		1		5
Primary progressive	F	56	19 years	6h	Unknown			1	7
Primary progressive	F	88	25 years	8h	Unknown				9
Primary progressive	F	76	19 years	9h	Unknown				7
Primary progressive	F	77	41 years	9h	Euthanasia				4
Progressive	F	77	48 years	11h	Pneumonia, bleeding caused by duodenal ulcer			1	6
not determined	F	47	16 years	4h	Cardio-pulmonary dysfunction				7
not determined	F	74	16 years	7h	Shock, cause unknown				10
not determined	F	68	44 years	8h	Cerebral vascular problems				4

Abbreviations: male (M), female (F), hours (h); cerebrovascular accident (CVA)

Appendix table 2: Clinical details of patients (chapter 4)

MS type	Gender	Age in years	Disease duration	Post mortem delay	Cause of death
Autopsy					
Primary progressive	F	72	10 years	12h	Pneumonia
Progressive	F	84	35 years	1h	Euthanasia
Progressive	F	84	35 years	1h	Euthanasia
Progressive	F	70	30 years	7h	Urinary tract infection
Progressive	M	66	26 years	8h	Unknown
Secondary progressive	F	66	22 years	6h	Unknown
Primary progressive	M	44	13 years	12h	Unknown
Biopsy					
isolated syndrom	F	52	2 months	not applicable	not applicable
isolated syndrom	M	25	1.5 months	not applicable	not applicable
isolated syndrom	F	29	1 month	not applicable	not applicable
isolated syndrom	F	62	2 months	not applicable	not applicable
Relapsing-remitting	M	31	18 days	not applicable	not applicable
Relapsing-remitting	M	39	8 months	not applicable	not applicable

Appendix table 3: List of antibodies

Primary antibodies	Manufacturer	Host	IHC mouse	IHC human	WB	AGR
Adenomatus Polyposis Coli (APC)	Calbiochem; OP80	mouse	1:200			citrate
Beta-Actin	Sigma; A2066	rabbit			1:1000	
Glial fibrillary acidic protein (GFAP)	Encore; RPCA-GFAP	rabbit	1:1000		1:10.000	none
Ionized calcium binding protein 1 (Iba1)	Wako; 019-19741	rabbit	1:500			Tris/EDTA
Oligodendrocyte transcription factor 2 (Olig2)	Millipore; MABN50	rabbit	1:1000	1:1000		Tris/EDTA
Proteo Lipoprotein (PLP)	Serotec; MCA839G	mouse		1:1200		none
M3/84 antibody (MAC-3)	BD Pharmingen; 553323	rat	1:500			Tris/EDTA
Brain lipid binding protein (BLBP)	Abcam; ab32423	rabbit	1:500	1:250		none
Neuronal nuclei (Neu-N)	Millipore; MAB377	mouse	1:1000			
HLA-DR (LN3)	Abcam; ab49388	mouse		1:250		citrate
Secondary antibodies						
Alexa-Fluor 488	Invitrogen; A11034	donkey	1:500	1:500		
Alexa-Fluor 568	Invitrogen; A11004	goat	1:500	1:500		
Biotinilated secondary antibody anti mouse	Vector labs; BA-2000	horse	1:500			
Biotinilated secondary antibody anti rabbit	Vector labs; BA-1000	horse	1:500			
HRP-conjugated anti-mouse	Abcam; ab6728	rabbit			1:3000	
HRP-conjugated anti-rabbit	BioRad; 170-5046	goat			1:3000	

Abbreviations: Immunohistochemistry (IHC), western blot (WB), antigen retrieval (AGR)

Appendix table 4: List of primers

	sense	antisense	bp	AT
HPRT (m)	gct ggt gaa aag gac ctc t	cac agg act aga aca cct gc	249	62
PLP (m)	tgg cga cta caa gac cac ca	gac aca ccc gct cca aag aa	116	56
CD11b (m)	cca tga cct tcc aag aga atg c	acc ggc ttg tgc tgt agt c	147	60
GFAP (m)	gag atg atg gag ctc aat gac c	ctg gat ctc ctc ctc cag cga	381	60
ADFP (m)	gac ctt gtg tcc tcc gct tat	caa ccg caa ttt gtg gct c	157	60
CST7 (m)	gga gct gta ctt gcc gag c	cat ggg tgt cag aag tta ggc	108	60
LYN (m)	gtg aca ttg tgg tgg cct tat	acc att ccc cat gct ctt cta	105	61
IFIT3 (m)	agt gag gtc aac cgg gaa tct	tct agg tgc ttt atg tag gcc a	188	60
BLBP (m)	gga cac aat gca cat tca aga ac	ccg aac cac aga ctt aca gtt t	101	60
PRKCD (m)	cct cct gta cga aat gct cat c	gtt tcc tgt tac tcc cag cct	181	60
IGF1 (m)	cta cca aaa tga ccg cac ct	cac gaa ctg aag agc atc ca	155	60
18s (h)	caa ctt tcg atg gta gtc g	cct tcc ttg gat gtg gta	110	58
IGF1 (h)	atg tct ttc agt tcg tgt gtg	gca ctc cct cta ctt gcg ttc	258	62
FGF2 (h)	atc aaa gga gtg tgt gct aac a	cct gcc cag ttc gtt tca gtg	177	65
PDGF (h)	cca gcg act cct gga gat aga	cgt cct ggt ctt gca gac ag	168	62
SPP1 (h)	ctc cat tga ctc gaa cga ctc	cag gtc tgc gaa act tct tag at	229	65

Abbreviations: mosue (m), human (h), base pair (bp), annealing temperature (AT)